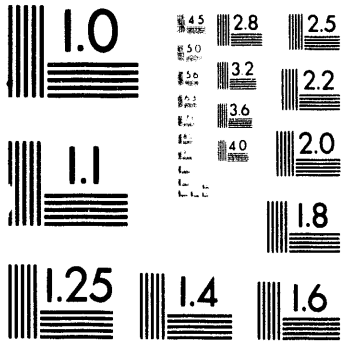
1.0
2.8
2.5
3.2
2.2
3.6
2.0
4.0
1.1
1.8
1.25
1.4
1.6

1 of 2

DOE/ER/40627-3

"ELEMENTARY PARTICLE INTERACTIONS"

PROGRESS REPORT TO DEPARTMENT OF ENERGY

DOE DE-FG05-91ER40627

(October 1, 1992 - September 30, 1993)

W. M. Bugg, G. T. Condo, T. Handler, E. L. Hart, K. Read, and B. F. L. Ward

October 1993

DISCLAIMER

This report was prepared as an account of work sponsored by an agency of the United States Government. Neither the United States Government nor any agency thereof, nor any of their employees, makes any warranty, express or implied, or assumes any legal liability or responsibility for the accuracy, completeness, or usefulness of any information, apparatus, product, or process disclosed, or represents that its use would not infringe privately owned rights. Reference herein to any specific commercial product, process, or service by trade name, trademark, manufacturer, or otherwise does not necessarily constitute or imply its endorsement, recommendation, or favoring by the United States Government or any agency thereof. The views and opinions of authors expressed herein do not necessarily state or reflect those of the United States Government or any agency thereof.

MASTER

DISTRIBUTION OF THIS DOCUMENT IS UNLIMITED

DOE/ER/40627-3

"ELEMENTARY PARTICLE INTERACTIONS"

Progress Report

October 1, 1992 - September 30, 1993

W. M. Bugg, G. T. Condo, T. Handler, E. L. Hart,
K. Read, and B. F. L. Ward

Department of Physics & Astronomy
University of Tennessee
Knoxville, Tennessee 37996-1200

October 1993

PREPARED FOR THE U.S. DEPARTMENT OF ENERGY
UNDER GRANT NUMBER DE-FG05-91ER40627

"Elementary Particle Interactions"

PROGRESS REPORT TO DEPARTMENT OF ENERGY

DOE DE-FG05-91ER40627

TASK A

W. M. Bugg, G. T. Condo, T. Handler,
E. L. Hart, and K. Read

TASK A

TABLE OF CONTENTS

Page

I. Fermilab E782 - E745 1

II. GEM

A. Calorimeter 2
B. GEM Tracker 3
C. GEM Software Activities 4

III. L3 6

A. Interlock Enhancement 7
B. Analysis Projects 9
C. Meetings and Shifts 12
D. LEP Developments 14
E. L3 Upgrades 15

IV. Fixed Target Photoproduction 17

A. E687: Vector, Charm and Exotic States 18
B. E831 at FNAL 29
C. BC72: Light Quark Spectroscopy 33
D. SDC Collaboration 36

V. SLD 45

VI. E144 at SLAC 51

VII. Silicon Detectors - Radiation Hardness Program

A. Model for Bulk Damage and Study of Surface Effects 59
B. Material Change in Silicon Through Gamma Exposure 93

VIII. List of Publications 103

I. Fermilab E782-745 [with Tohoku University, FNAL, and Jadavpur University (India)]

Film analysis, both at Tennessee and Tohoku, ended in the spring and summer of 1993, with most of the E-782 events of interest measured and on data summary tapes. Much of the final scanning was carried out by the Jadavpur group under an NSF contract. They continue to work on the remaining film. Physics analysis is proceeding. Several talks were given this summer by Professors Kitagaki and Hart at the "Bubbles" conference at CERN, 14-16 July, on the Tohoku chamber and some of the experimental results obtained from it.

II. GEM Detector

A. Calorimeter

The SSCL and to a lesser extent the TNRLC have for a period of over two years partially supported a calorimeter design team at Tennessee under the direction of Yuri Kamychkov of UTK and Mark Rennich of ORNL, chief engineer for GEM external calorimeter. The activities of this group have been extensive including R and D on BaF_2 electromagnetic calorimeter, spaghetti and scintillating tile with wave shifting fiber hadron calorimetry. Essentially all of the detector simulations for the GEM hadron calorimeter was carried out by this group. Since adoption of the scintillating tile techniques by GEM for the outer calorimeter in November 1992, the group has worked exclusively on R and D and engineering design for the GEM Technical Design Report. The results of this work are summarized in the GEM TDR. On completion of that report the team began to disband with three team members going to other Universities (two to the University of Mississippi and one to the University of Arizona). We are currently searching for suitable positions for the remaining team members in light of the fate of the SSC project. The team has served as the core of the GEM hadron calorimeter design effort throughout the GEM project.

B. Gem Tracker

Ken Read has concentrated his GEM efforts on the tracker. He coordinates the ORNL Instrumentation and Controls Division's efforts to develop a radiation hard analog memory unit (AMU) for the GEM Interpolating Pad Chamber (IPC). The IPC surrounds the central silicon microstrip tracker.

The IPC outer tracker is a multiwire proportional chamber whose cathode plane is a pad array. The pads are read out using geometrical charge division. The pad resolution is 50 μm. The electron collection time is 20 ns.

The front-end IPC electronic readout consists of a preamp followed by an AMU followed by a flash ADC. The AMU is a switched capacitor array. Due to its close proximity to the interaction point, it must be fabricated using a process resistant to 2 Mrad accumulated dose. The current choice is to use the Harris AVLSI-RA 1.2 μm CMOS process. A further challenge is that the electronic noise level must be less than 1% of the signal. The 16-channel AMU is 128 cells deep. The channel pitch is 200 μm and the cell length is 30 μm. The shaped output of each IPC pad signal is sampled every 16 ns. The dynamic range is 10 bits and the access time is 500 ns.

Read simulates the expected electronic readout performance and helps coordinate the activities of the electrical engineers involved on the project.

This summer the first rad hard prototypes of the AMU and preamp chips were received back from the foundry. Their performance was good and provides much useful information for optimizing the design as the R and D proceeds. Effort is underway to characterize and study these prototype chips. Recently ORNL has designed a reduced-power version of the IPC preamp which appears very promising. The power dissipation is one fourth that of the GEM baseline design developed elsewhere and described in the GEM TDR.

C. GEM Software Activities

As a member of the GEM central tracker group, Read performs Monte Carlo simulations for the proposed silicon central tracker and the surrounding IPC system. His software simulations are performed on a recently acquired Hewlett-Packard 9000/710 workstation. This workstation is one of the platforms supported by the GEM software group.

In addition to simulating overall tracking performance, Read has also run simulations to investigate the expected performance of the electronic readout itself. The CERN GARFIELD wire chamber program is used to simulate the chamber properties, including Landau fluctuations. This program generates current waveforms which are useful for detailed preamp optimization. These waveforms are then input to a subsequent program written by a colleague. The effects included in the simulation are charge

sharing, amplifier noise, shaping time differences, clock skew, and the effects of digitization. Read has worked with an engineer in the Instruments and Control Division to enhance the simulation to include the effects of charge injection and incomplete charge collection. The goal is to understand more fully the effects on resolution. One must balance the trade-offs of power, speed, and noise to optimize the capacitor cell size and switch resistance.

The chief electrical engineer involved on the project at ORNL, C. Britton, is pursuing a Ph.D. in electrical engineering at UTK. This project is a principal topic of his thesis research. Read is a member of C. Britton's doctoral thesis committee.

III. L3

UTK is involved in the L3 experiment at LEP through activities of K. Read, Hans Cohn and most recently Y. Kamychkov. Read shares a joint appointment as a Collaborating Scientist with Oak Ridge National Laboratory and Y. Kamychkov will soon be appointed to a similar position. Read has been a member of the L3 Collaboration since 1987. Read and Cohn worked extensively at the L3 experiment at CERN during summer 1993. During the rest of the year, L3 data analysis has been the primary focus of Read while Kamychkov concentrated exclusively on GEM.

Read's L3 data analysis concentrated in 1993 primarily on use of the electromagnetic calorimeter (BGO). He worked with an L3 colleague on reconstruction of J/ψ and χ_c mesons. In addition, he attended L3 meetings, both public and private, concerned with both hardware and software issues. He provided advice concerning the BGO level-1 power and temperature monitoring system which he had developed in previous years. He served as L3 shift leader during his shifts and fulfilled his L3 shift allotment for the year. He engaged in discussions to stay abreast of the status of developments of the proposed LHC collider and detectors at CERN and helped coordinate the L3 activities of H. Cohn and Y. Kamychkov this year.

A. Interlock Enhancement

The L3 electromagnetic calorimeter (BGO) has a hierarchical readout system. The level-1 readout is powered by 106 low-voltage power supplies controlled and monitored by an interlock system. The interlock software was in large part written by Read. The basic system consists of four IBM PC compatible computers at various locations which acquire safety-related data through CAMAC and communicate with other each many times per second. These PC's constitute a dedicated, stand-alone, slow-control local area DECNET network. The master PC transfers its information to the online VAX where it is summarized, logged, displayed to shift operators, and distributed to other interested parties (L3 slow control, BGO online monitoring).

Unwanted outside DECNET traffic from the online VAX cluster can hamper the operation of this system. Such traffic can cause a fatal communication error between the PC's at a rate of about once per week. Due to the fail-safe nature of the system this presents no danger to the electronics; however, such a failure cuts power and has the very undesirable effect of stopping any data collection run in progress. A graduate student from Lausanne University, A. Kasser, developed software for a new "gateway" PC to isolate the slow-control PC traffic from the outside world. All DECNET traffic from the PC's goes to the gateway. The gateway is connected to the VAX via TCP/IP and can properly deliver messages in either the direction between the PC's and the VAX.

Thus, in essence, the gateway serves an inexpensive DECNET bridge completely adapted to this application.

Read had an opportunity to observe routine operation of the gateway PC. The performance was excellent. The only glitch observed was a very infrequent need for the gateway itself to be rebooted after a communication problem with the VAX. This is quite innocuous and does not lead to a power cut or stopping a data collection run.

A related enhancement is now in routine operation. The level-1 power is no longer automatically cut during a PC reboot. (Of course, the power will be cut if the PC hangs too long.) Allowing power to survive across PC reboots frees the shift taker to consider rebooting PC's as needed to cure any rare communication problems without interfering with a data collection run. Read observed this new feature in routine operation for the first time.

Read is pleased that the system is finally free of any significant communication problems. That is not to say that the software can be frozen now. The new silicon luminosity monitor (discussed below) has its level-1 power monitored and controlled by this PC network now. A new PC is dedicated to monitoring the status of the pump and silicon oil system used to cool the BGO level-1 electronics. Software for this PC is being improved. Eventually, this PC will be integrated in to the existing network of PC's.

The system of PC's also measures and records the dew point at several locations around the detector. One of the readings is provided by a commercial dew point meter

outside the region of strong magnetic field. The other two readings are calculated based on temperature and humidity sensors located on either side of the detector (in a magnetic field region). It was demonstrated this summer that the temperature sensors are sensitive to whether the L3 magnet is on or not. Thus, two of the dew point readings are unreliable (a few degrees too high) when the magnet is on (i.e., when there is no access to the detector). The dew point is actually a critical issue for L3 at times during the summer. The cooling shield inlets for the level-1 electronics can be as cold as 14°C in order to maintain the detector at 18°C. Accurate, reliable remote dew point information provided by the PC system is required by experts to decide whether to take action because of a dangerously high dew point. This action consists of turning off the appropriate on-detector electronics and turning off the corresponding cooling system circulation. The air conditioning system for the experimental hall can usually maintain the dew point below 8°C unless the hall doors are opened (during an access period).

B. Analysis Projects

A principal purpose of Read's recent trip was to pursue data analysis and engage in discussions concerning a particular analysis topic of interest to him. During the past year, Read has been studying the process $b \to \chi_c X$ where $\chi_c \to J/\psi + \gamma$ and $J/\psi \to \mu^+\mu^-$. This is a reaction that L3 should be especially able to observe due to its excellent muon momentum and photon energy resolution.

A graduate student at L3, M. Wadhwa, from the University of Annecy originally performed this research starting last year. Read engaged in extensive discussions with M. Wadhwa, performed data analysis, and studied theoretical papers. There was some time pressure since two talks and a thesis on this topic were being produced this summer.

The analysis using 1990-92 data, corresponding to 1.1 million hadronic events, for the $J/\psi \rightarrow \mu^+\mu^-$ channel recently has been essentially completed by M. Wadhwa. The analysis begins by selecting $J/\psi \rightarrow \mu^+\mu^-$ candidates.[1] A sample of 87 ± 13 candidates is obtained. This corresponds to a branching ratio of $Br(Z \rightarrow J/\psi + X) = (3.6 \pm 0.5(stat) \pm 0.4(sys)) \times 10^{-3}$. It is expected that many of these J/ψ mesons arise from the decay $\chi_c \rightarrow J/\psi + \gamma$. Using the BGO to search for isolated photons in the J/ψ event sample and calculating the $J/\psi + \gamma$ invariant masses, a peak is observed at the known $\chi_{c1}(3510)$ mass corresponding to 19 ± 7 χ_c candidates. This yields a branching ratio of $Br(Z \rightarrow \chi_{c1} + X) = (7.5 \pm 2.9 \pm 0.6) \times 10^{-3}$. These results are consistent with the recent ARGUS measurement of the $B \rightarrow \chi_c + X$ branching ratio. This represents the first observation of the χ_c state at LEP. At the end of the summer, L3 submitted the results on this topic.[2]

---

[1] "Inclusive J Production in Z^0 Decays," (O. Adriani, *et al.*, L3 Collaboration), Phys. Lett. B288, 412 (1992).

[2] "χ_c Production in Hadronic Z Decays," (O. Adriani, *et al.*, L3 Collaboration), submitted to Phys. Lett. B.

This analysis topic is of interest because the χ_c production appears to be greater than theoretical predictions. Both the J = 1 and J = 2 states of the χ_c have appreciable, known branching ratios to $J/\psi + \gamma$; the J = 0 state does not. Thus, the observed χ_c signal probably is comprised of both χ_{c1} and χ_{c2} mesons. It remains to be determined whether L3 can resolve the two states and how large the J = 2 contribution is. Originally, the J = 2 contribution was expected to be suppressed in B decay. Recently, very preliminary speculation suggests that the higher than anticipated branching ratio could be explained by a smaller-than-expected suppression of production of the J = 2 χ_c state in *b*-quark decay.

Read recently has focussed his efforts on searching for χ_c candidates using the $J/\psi \rightarrow e^+e^-$ channel, which has not been done yet by L3. This was not dealt with in Wadhwa's thesis. Read adapted existing software to analyze data stored in an abbreviated format. L3 has a significant J/ψ signal in the e^+e^- channel. Many of these events also contain low energy photons. By forming $J/\psi + \gamma$ invariant mass combinations, one can search for χ_c candidates.

Due to electron identification and photon finding inefficiencies, it is expected that the signal using the $J/\psi \rightarrow e^+e^-$ channel will be quite weak. Still, Read believes it will be useful for completeness to pursue this analysis. Also, it will be very instructive for the future when the 1993 data is analyzed and the increased statistics are included.

Other recent analysis efforts within L3 have led to papers concerning improved measurement of electroweak parameters including $\sin^2\bar{\theta}_W$, measurement of the $Z \to b\bar{b}$ partial width, improved Higgs mass limits, searches for new narrow resonances, and a search for a possible additional heavy gauge boson, Z'.

C. Meetings and Shifts

Read was assigned seven shifts during his trip. He was appointed L3 shift leader for all of his shifts. The responsibilities of the shift leader include communicating with LEP control, authorizing subdetectors to take individual calibration and test runs as appropriate, quickly contacting appropriate experts in case of trouble, and communicating with the spokesman.

BGO shift procedures are similar to last year. The principal changes concern a new calibration run for the new silicon luminosity monitor (SLUM) discussed below and a generally more regimented schedule for taking pedestal runs and calibration runs for the xenon lamp flasher and LED calibration system.

In June there was a serious problem concerning the new silicon microstrip vertex detector (SMD). Apparently, the cooling system for the SMD on-detector electronics was somewhat inadequate. This resulted in heating of the inner portion of the existing, surrounding gas and wire tracking chamber (TEC) by several degrees. The net effect was to cause an unacceptable degradation in resolution for the inner TEC layers. LEP

commenced operation this year with sustained high luminosity. It is unfortunate that much of the early data from this year has degraded TEC data. L3 decided to cope with the problem by leaving the SMD off except for up to 12 hours per week of running. This cured the TEC problem, of course. However, this thwarted shaking down the newly installed SMD. The cooling problem was corrected after a scheduled extended access. The SMD and TEC are now functioning routinely.

The SMD-TEC problem and other incidents have led the L3 spokesman to be increasingly concerned with smooth operation of the detector. He recently has resumed spending a significant amount of time in the L3 control room to monitor operations.

In past years LEP collided four separated "bunches" of electrons with four counter-rotating bunches of positrons, thereby providing collisions at all four interaction points around the ring at the same time. Now, routine operation involves doubling the number of bunches to eight bunches of both electrons and positrons. This reduces the interval between collisions from 22 μsec to 11 μsec. Although, the appropriate electronics has been upgraded to allow both 4- and 8-bunch running, there are some remaining issues to be solved. The L3 dead time is as high as 9% during 8-bunch running. The BGO readout is the principal contributor to this dead time. A recently implemented buffered readout mode has significantly reduced the BGO dead time for 4-bunch running. However, such a solution does not yet exist for 8-bunch mode. Efforts

are underway, particularly by the BGO group, to reduce the dead time to a more acceptable level.

Read attended a B-physics meeting which served as a rehearsal for U. Becker's (MIT) upcoming talk concerning the χ_c (see analysis section above) at the Montreal Heavy Flavors Conference. This meeting was naturally of great interest to him since it was devoted to an analysis topic with which he is concerned. Also present at the meeting was G. Sauvage (U. Annecy) who was preparing to present the latest χ_c results at the June L3 general meeting in Amsterdam.

D. LEP Developments

LEP operations are now smoother than ever before. A total of 6 pb^{-1} had already been collected by July, corresponding to over 180,000 detected hadronic Z^0 decays. Instantaneous luminosities of near 10^{31} $cm^{-2}sec^{-1}$ are now routine. Fills often exceed 8 hours. Refilling can take less than an hour.

Advances have been made concerning improving the absolute energy calibration of LEP using a polarized beam. Unlike SLAC, LEP can not provide collisions using polarized beams. LEP does, however, use a single (or separated, non-colliding) polarized beam for energy calibration purposes. The polarization arises spontaneously via the Sokolov-Ternov effect. The time to achieve significant polarization is reduced by passing the beam through wiggler magnets. The amount of polarization is measured

using a laser polarimeter technique. Data gathered during resonant depolarization of the beam provides an absolute energy calibration of the machine. The beam energy uncertainty is significantly reduced below the previous value of 20 MeV.

At present, LEP often enters a brief period of machine development after each fill to improve the resonant depolarization beam energy calibration technique. It is anticipated that this will eventually become a routine beam energy calibration run after each fill, thereby allowing an extremely accurate, absolute energy calibration of the data over time.

It has been conclusively demonstrated that the LEP lattice is affected by lunar tidal forces. Software corrections for this effect have been implemented.

E. L3 Upgrades

A number of detector upgrades have taken place during the past year. The upgrades include an RFQ calibration system, a new silicon luminosity monitor (SLUM), and a new silicon microstrip vertex detector (SMD).

The RFQ BGO calibration system has been installed. This small accelerator and target system serves as a source of low energy photons used to calibrate the electromagnetic calorimeter *in situ*. The system is not ready for routine operation and is operated only by experts at present.

Two new silicon strip luminosity monitors have been installed on either side of L3 in front of the existing BGO luminosity monitors. The monitors are expected to reduce the experimental systematic error on the L3 luminosity measurement from 0.6% to about 0.2% which is comparable to the systematic error introduced by theoretical uncertainties. The new subsystem provides radial coverage between 76 and 154 mm from the beamline (28 to 57 mrad). The radial resolution is 0.14 mm and the azimuthal resolution is 0.2°.

A silicon microstrip vertex detector (SMD) similar to ALEPH's was installed inside L3's TEC chamber around the beam pipe during the last winter shutdown. The subdetector is coordinated by U. Perugia/INFN with major contributions from other institutes. The SMD greatly improves L3's tracking capabilities and physics potential. It consists of two double-sided layers of silicon microstrips providing polar angle coverage from 25° to 155°. The intrinsic design resolution is approximately 5 μm for the $r\phi$ coordinate and 10 μm for the z coordinate. This resolution is to be compared with the performance of the existing L3 central tracker (TEC). In the $r\phi$ plane, the TEC has a 55 μm single wire resolution. In the non-bending plane, the single track resolution is 500 μm.

IV. Fixed Target Photoproduction

Summary

Current efforts are in the physics analysis of FNAL E687 and the SLAC SHF experiments (BC72 - 75). We are re-skimming E687's entire 500 million event sample to investigate charge exchange processes (such as $\gamma p \rightarrow a_2^+(1320)n$), poorly understood mesons (especially the higher mass K states, such as the $K^*(1370) \rightarrow K\pi$)[1], possibly exotic states (such as $C(1480) \rightarrow \phi\pi$ which is a candidate $q^2\bar{q}^2$ state), and higher mass states.

We are also involved with detector development, namely E831 (the upgrade of E687) and the SDC detector for the SSC.

---

[1]This particular state, observed by LASS in K^-p scattering, deviates from the quark model prediction by ~150 MeV [1].

A. E687: Vector, Charm and Exotic States

Since the end of the data taking phase of the experiment, E687 has become one of the dominant sources of information on the decays of charmed mesons and baryons [2] – [11]. In addition, several papers have been contributed to: the XXVI International Conference on High Energy Physics (Dallas, Texas [12] – [15]), the Lepton-Photon '93, and the 1993 Heavy Flavors Conference (Pavia, Italy [16] – [18]). It is expected that at least five more papers devoted to charm physics will be submitted in the next year. In the past year the data available from this experiment has formed the bases for at least six Ph.D. theses.

The impact of E687 on charm physics can most readily be seen by the small errors associated with lifetime measurements or in the quantity of these events. The charmed baryon sector has evidence for the Ω_c^0 decaying into $\Omega^-\pi^+$ with 10.3 ± 3.9 events (the mass of $2705.9 \pm 3.3(stat) \pm 2.0(sys)$ MeV differs from ARGUS's value of $2719 \pm 7.0 \pm 2.5$ MeV which is based upon 12.2 ± 4.5 events). The Λ_c^+ decays are based on ~ 1340 $pK\pi$ events and represents roughly a factor of 10 increase in this channel over previous experiments. The large number of Λ_c^+'s available allow examination of Cabbibo suppressed decays, such as $\Lambda_c^+ \rightarrow pK^+K^-$, which E687 found to have a $BR_{\Lambda_c^+ \rightarrow pK^+K^-} = 0.096 \pm 0.029 \pm 0.010 \times BR_{\Lambda_c^+ \rightarrow pK\pi}$. Other Cabibbo suppressed baryon decays include the Ξ_c^0 with 42 ± 10 events (ACCMOR is the only other experiment to see this state, with 4 events) and the Ξ_c^+ with 29.7 ± 7.0 events. The D mesons provide more precision data, both in Vector – Pseudoscalar decays and in the semileptonic decays. The lifetime of the $D_s \rightarrow \phi\pi^\pm$ is based upon ~ 900 events (more than 4 times the number of events seen previously by any single experiment, as currently listed by the PDG [19]). The result of $\tau_{D_s \rightarrow \phi\pi^\pm} = 0.475 \pm 0.020 \pm 0.007$ ps raises the World average slightly, but decreases the World error. E687 has provided an absolute branching ratio for the D_s^+ (using our own measurement of $D_s \rightarrow \phi\mu\nu$), of $D_s^+ \rightarrow \phi\pi^+/D_s^+ \rightarrow all = 0.031 \pm 0.009(stat) \pm 0.005(sys) \pm 0.004(th)$ ps. Finally, the form factors in the D^+ semileptonic decay (based upon the Spectator model with the matrix elements factored into leptonic and hadronic components) provide tests of both theoretical predictions and

experimental measurements. The decay $D^+ \to \overline{K}^{*0}\mu^+\nu$ provides support for the E653 form factors R_v and R_2 versus those of E691. Finally, a precise measurement of the D^0 and D^+ lifetimes (based on a sample of $\sim 25,900$ fully reconstructed decays into $K\pi$, $K\pi\pi\pi$ and $K\pi\pi$) found $\tau_{D^0} = 0.4200 \pm 0.0045 \pm 0.0030$ ps and $\tau_{D^+} = 1.0420 \pm 0.0015 \pm 0.0011$ ps.

The two theses submitted to the University of Tennessee [20] – [21] have been devoted to the high energy photoproduction of (mostly) light quark (u,d,s) mesons. These data were obtained by selecting semi-inclusive final states based upon 2, 3, and 4 charged track topologies with the additional requirement that the event was free from electromagnetic energy. The data samples used to extract these states were taken from a subset (132 Exabyte 2.5 GByte tapes) of the entire data set[2]. The subskim of the data chosen for the UT theses did not select strange particle final states in an unbiased manner[3]. Thus, only the pionic modes and those modes containing a $\phi(1020)$ could be examined in a bias free fashion. In the future, a skim of the entire data set will be employed which will allow the study of any available light quark states.

1. Pionic Final States

The dipion final state ($\gamma N \to \pi^+\pi^- N$) is dominated by the production of the $\rho^0(770)$ as occurs at lower energies. Evidence was also found for the photoproduction of the $\rho'(1700)$ whose dipion decay has become well established in the past 10 years. The neutral four pion final state is also dominated by this latter state (see Figure 1).

---

[2]The entire raw data set is contained on roughly 600 Exabyte tapes. The reconstruction process (entailing 5 UNIX farms, partially managed by UT) roughly doubled this data size, and final subskims reduced the size to $\sim 200 - 400$ tapes.

[3]If the event contained a K^+K^- pair, this subskim accepted the event only if the K^+K^- mass was < 1.1 GeV.

(a) (b)

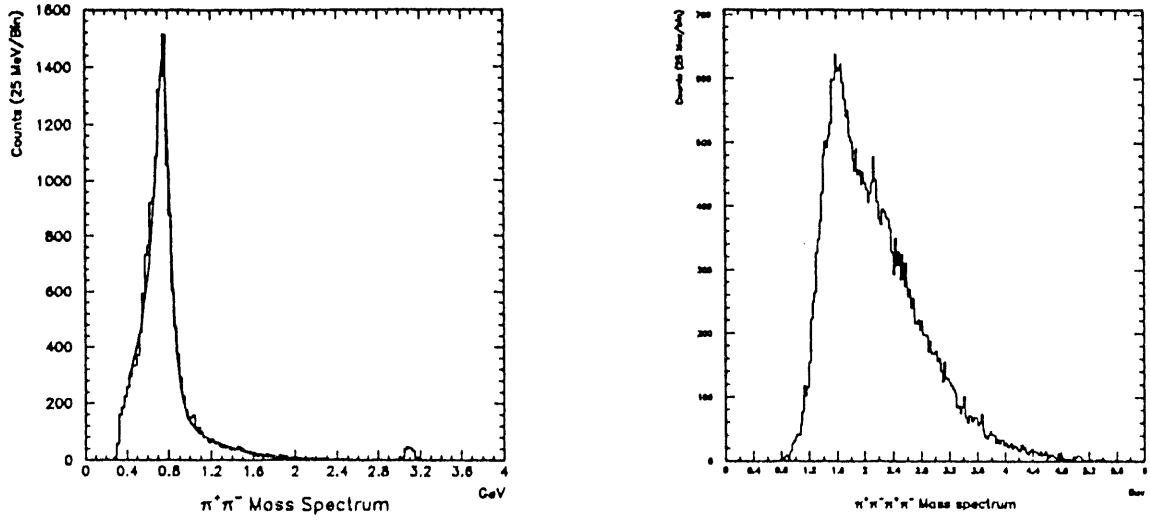

FIG. 1. (a) The $\pi^+\pi^-$ mass from the two track sample showing copious $\rho(770)$ production and some $J/\psi(3097)$ (presumably $\mu\mu$ misidentified as $\pi\pi$). (b) The $\pi^+\pi^-\pi^+\pi^-$ mass from the four track sample, showing the $\rho'(1700)$ signal.

The other fully pionic final state examined was $\pi^+\pi^-\pi^\pm$ which was available in the three prong event sample as well as in the four prongs. Aside from scale the charged 3π and neutral 2π spectra of the 3 and 4 prong events are quite similar. The neutral dipion spectrum shows statistically significant signals corresponding to the production of $\rho(770)$, $f_2(1270)$ and $\rho_3(1690)$ mesons (see Figure 2). We are aware of no other observations of the dipion decays of the $f_2(1270)$ and/or $\rho_3(1690)$ in forward photoproduction [22]. The 3π spectra from $\rho^0(770)\pi^\pm$, $f_2(1270)\pi^\pm$ and $\rho_3(770)\pi^\pm$ show enhancements which we interpret as $a_2^\pm(1320)$, $\pi_2^\pm(1670)$ and $a_3^\pm(2050)$ (see Figures 3 and 4). The $a_2^\pm(1320)$ which has been observed at 5 GeV and 20 GeV in charge exchange photoproduction occurs in our data with a cross section consistent with the expectations of one-pion exchange ($\sigma \sim E_\gamma^{-n}$ with $n \approx 1.5$).

(a) (b)

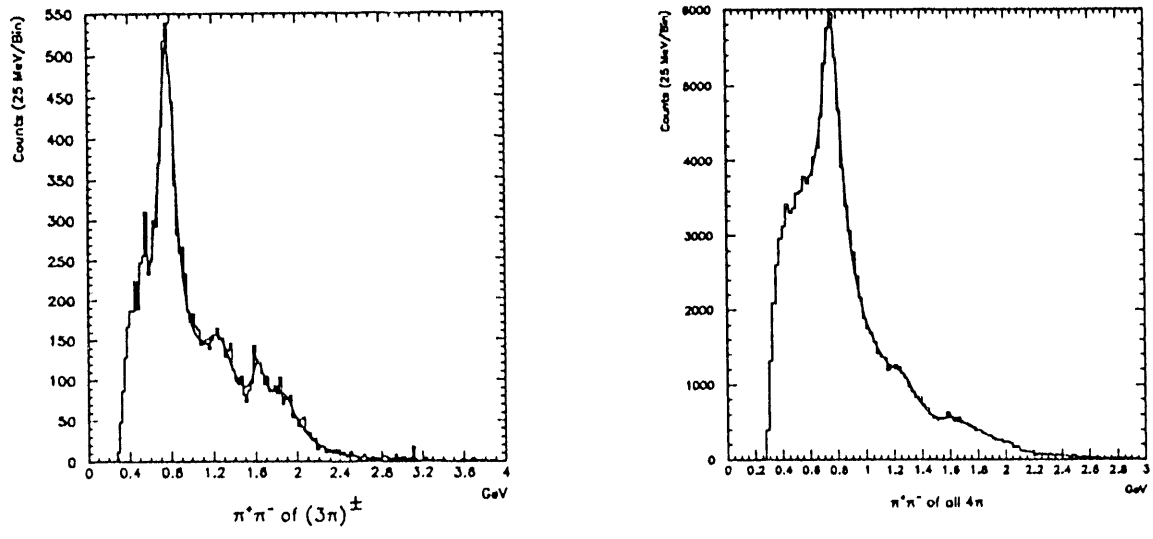

FIG. 2. The neutral dipion combinations from (a) the three track sample and (b) the four track sample.

(a) (b)

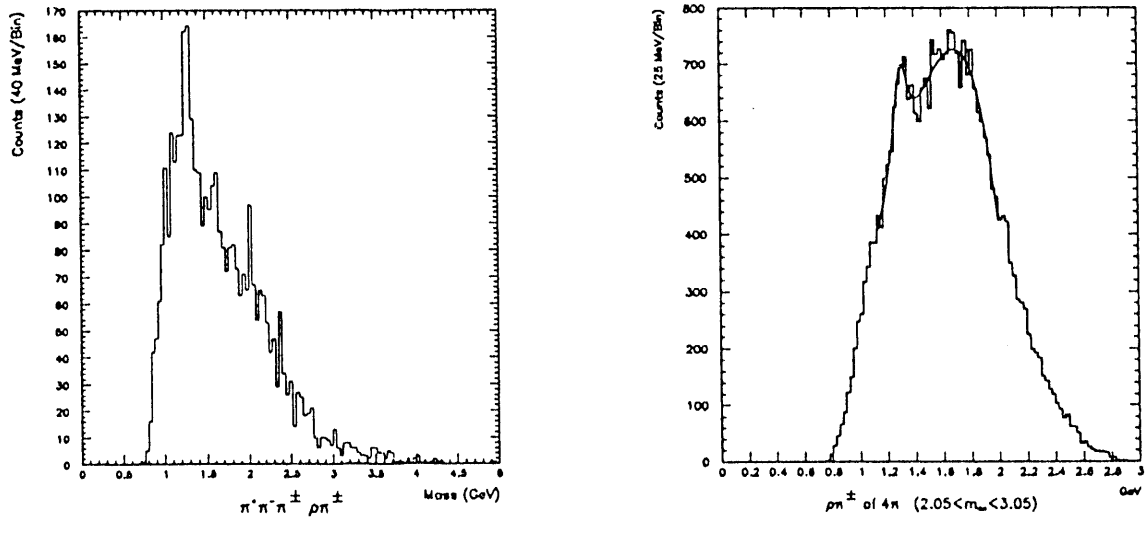

FIG. 3. The $\rho(770)\pi^\pm$ combinations from (a) the three track sample and (b) the four track sample.

(a) (b)

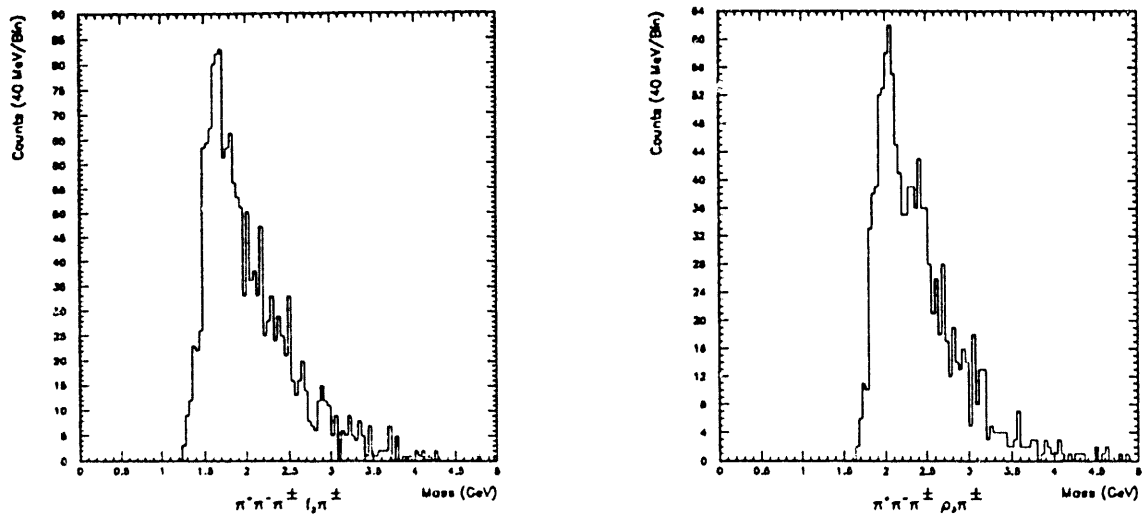

FIG. 4. (a) The $f_2(1270)\pi^{\pm}$ combinations and (b) the $\rho_3(1690)\pi^{\pm}$ combinations from the three track sample.

2. States Decaying to K^+K^-

Figure 5 shows the K^+K^- spectrum from the reaction $\gamma N \rightarrow K^+K^-N$ and $\gamma N \rightarrow K^+K^-\pi^{\pm}N'$ where an enormous $\phi(1020)$ signal is evident. The character of this spectrum indicates the quality of the resolution available from the (Čerenkov identified) K^+K^- sample. The magnitude of the $\phi(1020)$ signal from the $\gamma N \rightarrow K^+K^-N$ sample, when compared to the $\rho(770)$ signal, discussed in the previous section, is quite consistent with the expectation of the vector dominance model (VDM) model of photon interactions.

The $K^+K^-\pi^{\pm}$ ($\phi\pi^{\pm}$) spectra in both the 3 prong and the 4 prong events (see Figures 6(b) and 7(a)) contain a strong enhancement in the 1480 - 1500 MeV region.

(a) (b)

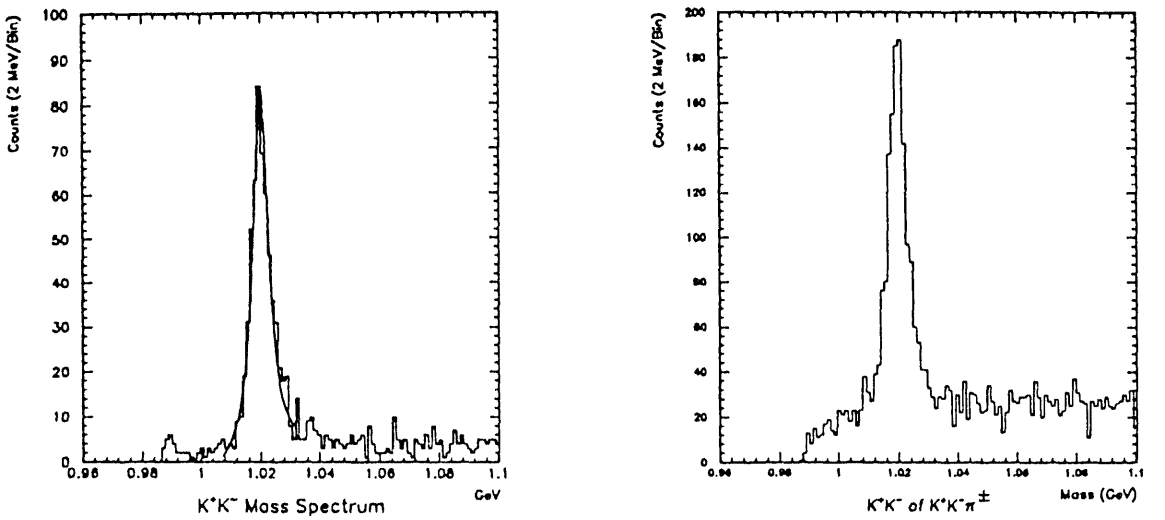

FIG. 5. (a) The K^+K^- mass from the two track sample, with tight Čerenkov identification of kaons and cuts similar to the $\pi^+\pi^-$ data. (b) The K^+K^- mass from the three track sample, again with tight Čerenkov identification. Note that both plots have *2* MeV bin-widths.

(a) (b)

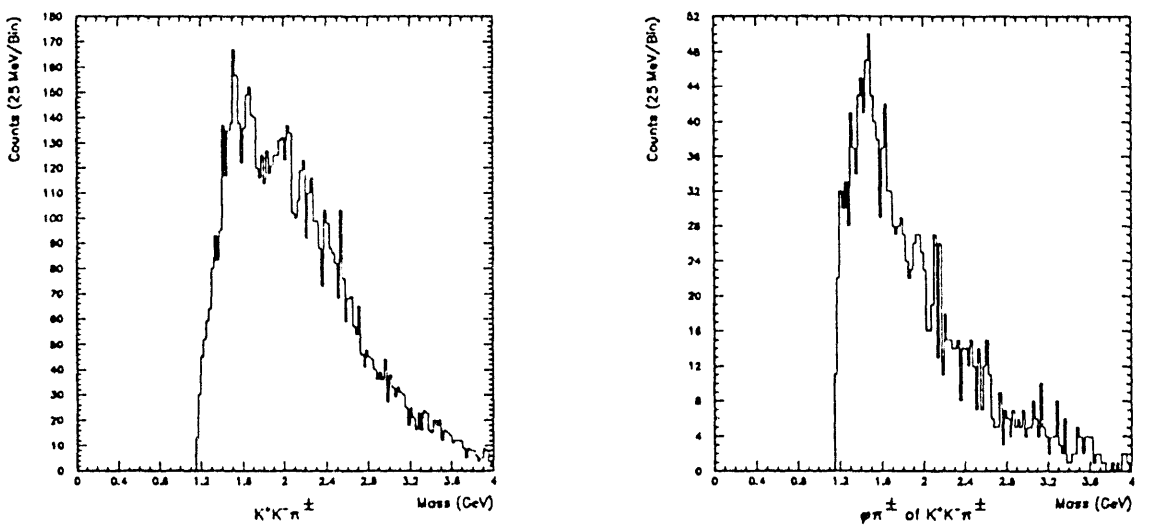

FIG. 6. (a) The $K^+K^-\pi^\pm$ mass spectrum from the three track data. (b) The $\phi(1020)\pi^\pm$ mass spectrum from (a), where the $\phi(1020)$ mass is taken as $1.005 \leq M_{KK} \leq 1.035$ GeV.

(a) (b)

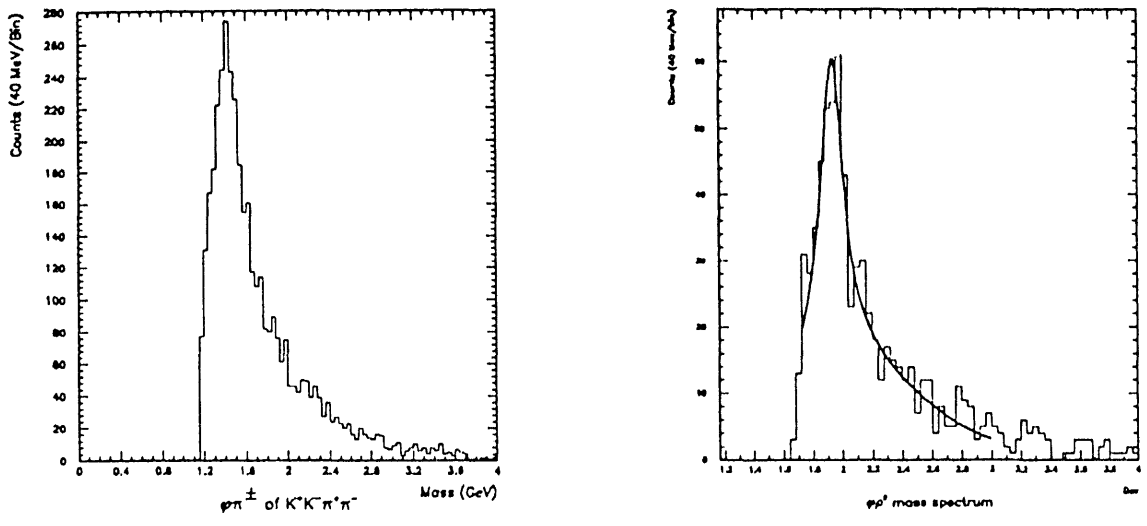

FIG. 7. (a) The $\phi(1020)\pi^{\pm}$ mass spectrum from the four track data. (b) The $\phi(1020)\rho(770)$ mass spectrum from $K^+K^-\pi^+\pi^-$ with tight Čerenkov cuts on the kaons.

Close and Lipkin [23] have suggested the existence of a $q^2\overline{q^2}$ state in this mass region which was subsequently reported by Bityukov [24] in the reaction $\pi^-p \rightarrow \phi\pi^0 n$. There is, so far, no independent confirmation of the existence of this state. We have an advantage in photoproducing this final state, due to the smaller backgrounds associated with photoproduction as compared to the backgrounds of hadroproduction. Although such a state is prominent in our data (see Figures 6 and 7(a)), this signal also appears to have a strong component which decays to $K^*(892)\overline{K} + \overline{K^*}(892)K$. Because of our subskim requirement (the presence of a $\phi(1020)$), our K^* sample will be biased, so that a more complete analysis of this state has been deferred until our current re-skim of this data is complete. Additionally, the $K^+K^-\pi^+\pi^-$ channel shows evidence for a (perhaps exotic) $\phi\rho$ state (see Figure 7(b)).

In order to avoid the K^+K^- mass bias, the complete E687 data set is currently being re-skimmed. This obviously opens the possibility for an analysis of a much broader scope. The previous examinations of the $K\pi$ and $K\pi\pi$ (see Figures 8 and 9) show several K^*, K_1 and K_2 states. LASS has provided most of the data to date on massive K states, and we will be able to provide a strong confirmation of these states, as well as a chance to explore

new states. The skim of the entire data set should enhance our ability to study these states. Table I shows the sets of (known) decays that should be available some of which may be preferentially produced in photon interactions.

(a) (b)

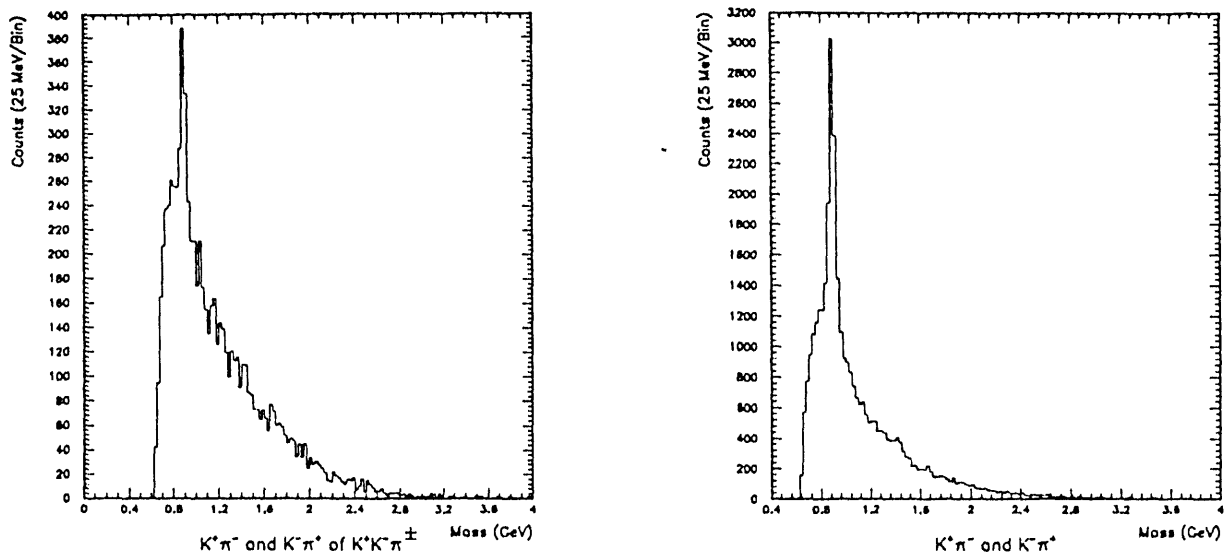

FIG. 8. The neutral $K\pi$ mass combinations from: (a) the $K^+K^-\pi^\pm$ data sample, and (b) the $K^+K^-\pi^+\pi^-$ (both combinations) data sample. The $K^*(892)$ dominates both sets of spectra, though the $K^*(1410)$ and the $K^*(1680)$ are seen.

TABLE I. The accessible states from $K^+K^-\pi^\pm$ and $K^+K^-\pi^+\pi^-$.

State	Decay Mode
$[\phi(1020),\ f_2(1750),\ \phi'(1680)]\pi^\pm$	$[K^+K^-]\pi^\pm$
$[K^*(892),\ K^*(1410),\ K_0^*(1430),\ K_2^*(1430),\ K^*(1680)]\overline{K}$ + c.c.	$[K^\pm\pi^\mp]K^\mp$
$[\phi(1020),\ f_2(1750),\ \phi'(1680)][\pi^+\pi^-,\ \rho^0(770)\ f_0(975),\ f_2(1270)]$	$[K^+K^-][\pi^+\pi^-]$
$[K^*(892),\ K^*(1410),\ K_0^*(1430),\ K_2^*(1430),\ K^*(1680)]\overline{K}\pi$ + c.c.	$[K^\pm\pi^\mp]K^\mp\pi^\pm$
$[K^*(892),\ K^*(1410),\ K_0^*(1430),\ K_2^*(1430),\ K^*(1680)][\overline{K^*}(892),\ \overline{K^*}(1410),\ \overline{K_0^*}(1430),\ \overline{K_2^*}(1430),\ \overline{K^*}(1680)]$	$[K^\pm\pi^\mp][K^\mp\pi^\pm]$
$[K_1(1270),\ K_1(1400),\ K(1460),\ K_2(1580),\ K_1(1650)]\overline{K}$ + c.c.	$[K^\pm\pi^+\pi^-]K^\mp$

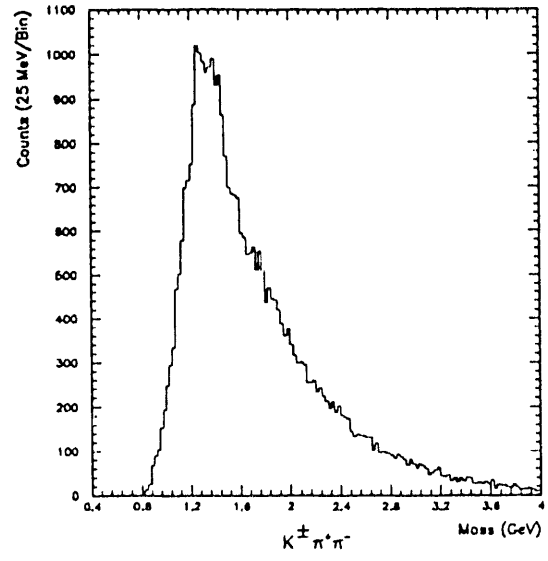

FIG. 9. The $K^{\pm}\pi^{+}\pi^{-}$ mass combinations from the $K^{+}K^{-}\pi^{+}\pi^{-}$ data sample. The $K_1(1270)$ and the $K_1(1400)$ are most readily seen, though indications of other higher mass K states are seen.

3. $\mu^+\mu^-$ and $\mu^+\mu^-\pi^+\pi^-$ States

The evidence for the production of $c\bar{c}$ states $J/\psi(3097)$ and $\psi(2s)$ has also been examined (see Figure 10) in E687. The $\psi(2s)$ enhancement may lead to another paper, comparing its $\mu^+\mu^-$ decay and $[J/\psi]\pi^+\pi^-$ decay modes. The possibility of $b\bar{b}$ photoproduction, primarily identified through $\Upsilon \rightarrow \mu^+\mu^-$ (the branching ratio is $\sim 2.5\%$) is waiting the final re-skim of the 1990–1991 data set. The possibility of finding the Υ, and hence the first photoproduced $b\bar{b}$ state, is quite real when higher interaction energies are included (there are a few events with an invariant mass of ~ 9 GeV).

(a) (b)

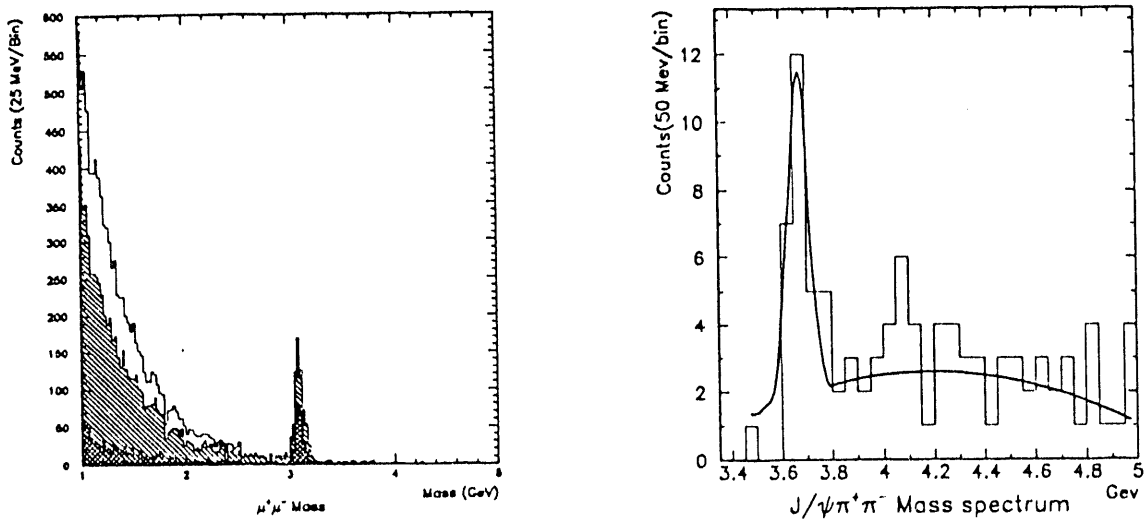

FIG. 10. (a) The decay $J/\psi \to \mu^+\mu^-$ from the two track sample. The unshaded histogram corresponds to *all* tracks assigned a $\mu^+\mu^-$ mass, regardless the Čerenkov assignments. The hatched histogram shows the $\mu^+\mu^-$ mass without kaons and protons, based upon Čerenkov information, and the fully hatched histogram shows those events based upon muon identification. (b) The radial excitation $\psi(2s) \to [J/\psi \to \mu^+\mu^-]\pi^+\pi^-$ from the four track sample (one neutral combination has a mass between 3.0 GeV and 3.2 GeV).

4. Charm States

We wish to look into the $\overline{K}a_1(1260)$ decays of the D, namely the $D^0 \to K^-a_1^+(1260)+c.c.$ and the $D^+ \to \overline{K}_S^0 a_1^+(1260) + c.c.$ Kamal and Verma have made specific predictions based upon the W emission decay terms in the Bauer, Stech, and Wirbel (BSW) model [25]. Kamal and Verma are able to determine more accurately the branching ratios in the $D \to \overline{K}a_1$, which favors either a more massive $a_1(1260)$ or a broader width [26]. Mark III has examined these decays[4] [27], and found the annihilation terms of Kamal and Verma are necessary

[4]Mark III has found the branching ratios to be: $BR(D^0 \to K^-a_1^+(1260)) = 9.0 \pm 0.9 \pm 1.7$ and $BR(D^+ \to \overline{K}_S^0 a_1^+(1260)) = 7.1 \pm 1.8 \pm 1.1$, based upon ~ 1500 reconstructed D's.

to explain the relative branching ratios of the D with an $a_1(1260)$ decay product. We are interested in this decay for two reasons: the confirmation of a wider $a_1(1260)$ would compliment our earlier work, and the fact that these branching ratios imply that our sample will be more statistically significant than the Mark III data. A sub-sample of these decays are shown in Figures 11 and 12.

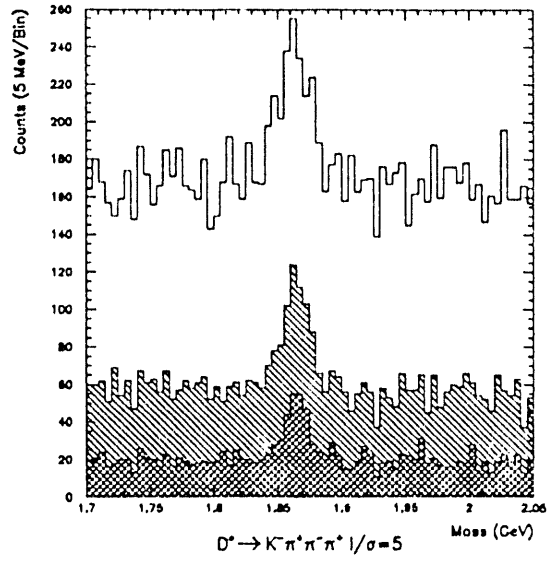

FIG. 11. A small subset of the $D^0 \rightarrow K^-\pi^+\pi^+\pi^- + c.c.$ decay (for various l/σ cuts, where l is the length of the secondary decay from the primary interaction, and σ is the error on the constrained vertex.). (c) the D^0 mass for values of $l/\sigma = 5$ (unhatched), 8 (hatched), and 14 (cross-hatched).

(a) (b)

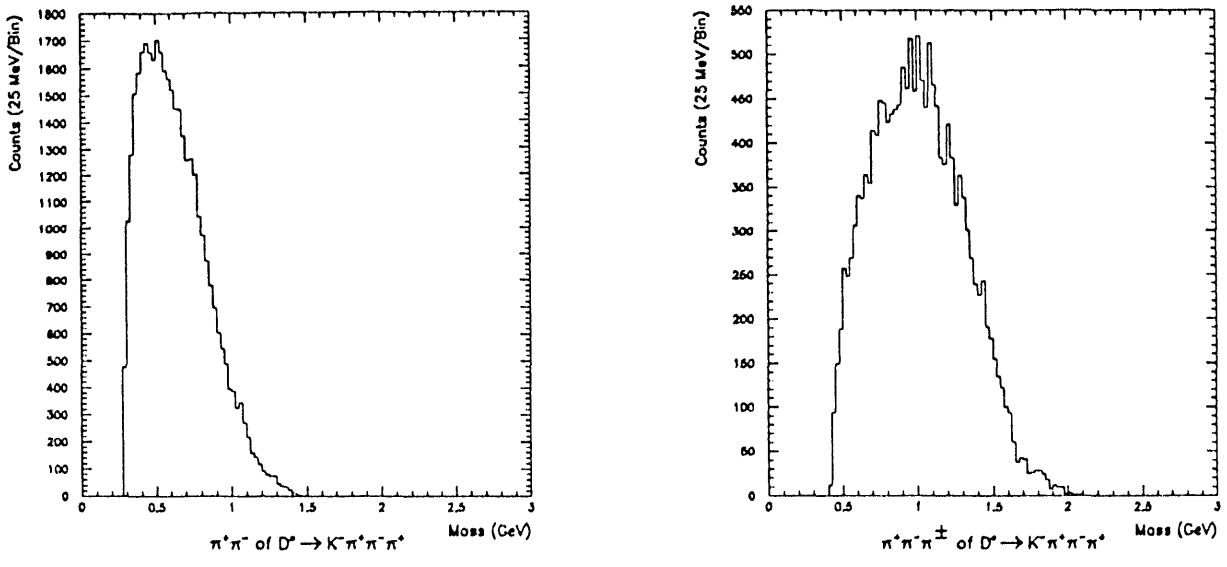

FIG. 12. A small sample of the neutral dipion combinations (a) and the 3π combinations (b) from the decay $D^0 \to K^-\pi^+\pi^+\pi^- + c.c.$.

B. E831 at FNAL

E831, an extension of E687, has been approved for the next fixed target run period at FNAL. It is hoped that this new run will allow the collaboration to fully reconstruct approximately 10^6 charm events. To achieve this level of charm statistics several upgrades to the current E687 detector will have to be undertaken.

1. Physics Motivations

With the proposed number of charm events it will be possible to do:

1. A high precision study of D semileptonic decays,

2. QCD studies of double D events,

3. Absolute branching fractions for D^0 decays,

4. $D^0/\overline{D^0}$ mixing,

5. CP violation,

6. Fully leptonic decays of the D^+,

7. Investigation of charm baryons and their lifetimes,

8. A search for rare and forbidden decays.

In addition to the charm physics, we will continue in our examinations of the vector meson states predicted by the standard quark model and for those states that lie outside this context, the exotics (see the E831 proposal [28]).

2. Upgrades of the Existing E687 Spectrometer

In order to achieve the anticipated number of charm events, it will be necessary to increase the photon flux delivered to the target and to also upgrade the E687 Spectrometer to handle the increased data rate.

- The higher flux of photons will be achieved, as follows:
  - E831 hopes that FNAL will be able to provide a more energetic proton beam – an increase in the 800 GeV/c proton beam to 900 GeV/c will increase the 350 GeV/c secondary electron flux by a factor of 1.86.
  - The flux will increase by a factor of ~ 3 by dropping the secondary electron beam energy from 350 GeV/c to 250 GeV/c. The relative background in the positron portion of this beam is also reduced, which would allow inclusion of the positron beam in generating the bremsstrahlung photon beam.
  - The target and lead radiator may themselves be changed, which would increase the number of interactions.
  - An increase in the number of protons in the initial beam, from 4×10^{12} to 6×10^{12}.

- With a higher flux of photons, sections of the detector will have to be modified to handle the increased interaction rates. These include:
  - The trigger counters will need to changed. The current trigger counters will not be able to handle the increased rate, especially from the increase of Bethe-Heitler pairs in the central region of the detector.
  - The tagging detector for the secondary electron beam will be upgraded to include more silicon strip detectors (oriented in both the vertical and 45° off the vertical directions) to locate the electron beam before it enters the radiator. This will assist the microstrip vertex detectors in ascertaining the photon direction.
  - The microstrip vertexing detector will need to be modified to handle the increased rates – hopefully with just electronics.
  - The Muon and PWC detectors will also need to be modified to handle the increased rates. The PWC's will in particular need to address the higher pair production rate in the central region.
  - The accuracy of the measurements which lead to the determination of the interacting photon energy will have to be improved. The profile of the secondary electron and positron beams will need to be known correctly in the higher luminosity environment. The method for measuring any non-interacting bremsstrahlunged photons will also need to be improved.
  - The Hadron Calorimeter will be upgraded and discussed in the the next section.

3. Hadron Calorimeter Upgrade

The Hadron Calorimeter (HC) for E831 will be converted from Iarroci tubes to scintillating tiles. The upgrade of the HC will satisfy the following requirements:

- The HC is to be an integral part of the 1st level trigger, which performs a fast sum of the energy seen in the HC, and requires at least 40 GeV be deposited in the HC

(to veto electron pair events). The HC needs to be capable of fast triggering, in order to decrease dead time and to handle the increased interaction rate. The decision rate will need to be 5 MHz, while the time of arrival for the trigger signal to the master gate must occur within a 300 ns time frame.

- The HC will need greater spatial resolution to detect showering neutral hadrons.
- The HC will incorporate an $E_\perp$ trigger, yielding an increase in the number of charm events relative to non-charm events.

The HC has been redesigned to accommodate the expected increased yield in charmed baryons – 10,000 Λ_c events alone are expected in the next set of runs [28]. The new HC will help distinguish the Σ^+ from the $\Lambda_c \rightarrow \Sigma^+\pi^+\pi^- + c.c.$ decays, with the $\Sigma^+ \rightarrow n\pi^+ + c.c.$

The University of Tennessee, along with some members of E831 (the Dip. di Fisica dell'Universita' and INFN, Pavia and FNAL), have been involved in the redesign of the HC.

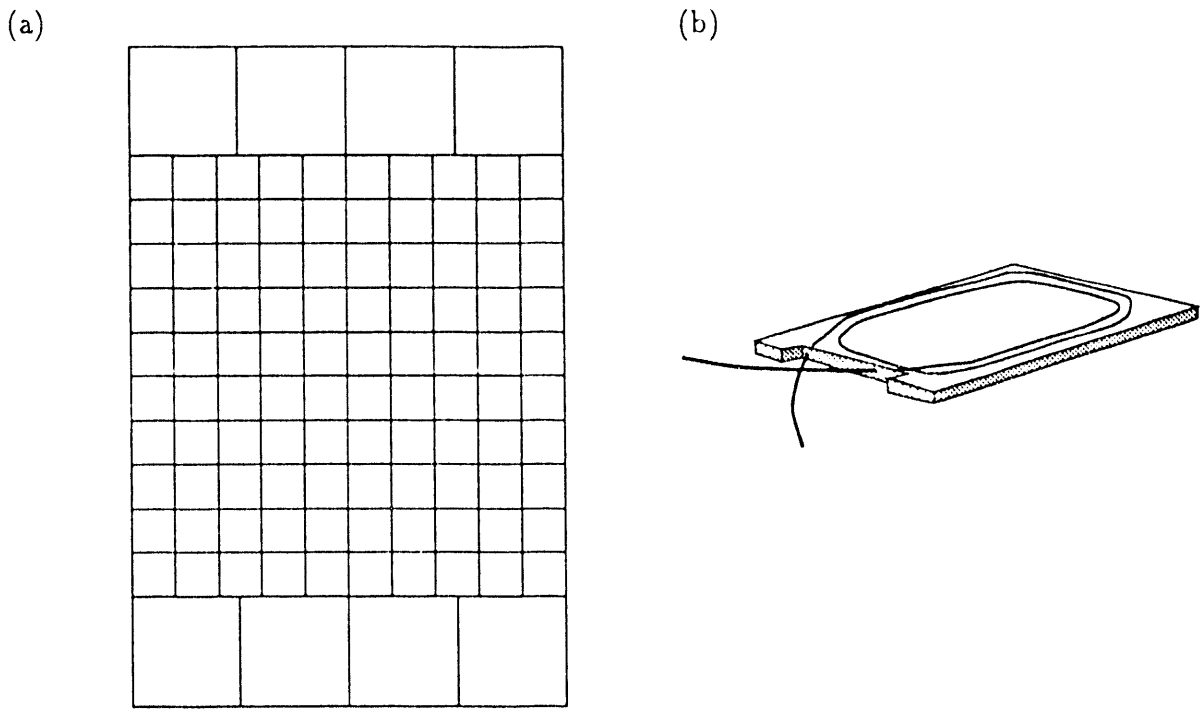

FIG. 13. (a) The segmentation of the scintillating tiles for the new HC. (b) An individual scintillating tile.

The HC will consist of 28 layers of $1\frac{3}{4}$" Fe followed by 0.6 cm scintillating tile with fiber readout. Each sampling layer will have 108 scintillating tiles arranged as shown in Figure 13(a). The tiles will probably be read out from both ends of scintillator (see Figure 13(b)). The 28 readout layers will be ganged into three longitudinal segments yielding a total of 324 channels of information.

The responsibilities of the groups involved with the rebuild of the HC have been delineated, with the University of Tennessee being responsible for the photomultipliers and their associated bases. In addition to the monetary support, the University of Tennessee will also supply logistical support at the appropriate time.

4. Neural Network Trigger

E831 will have more than twice the event rate than E687 had, and as such will require an efficient and robust trigger. In order to achieve such a trigger, several members of the collaboration have expressed an interest in exploring the possibility of using an artificial neural network (ANN). The ANN could in principle be used for determining the presence of neutral energy in the HC (neutrons), the presence of muons, and a more refined $E_\perp$ trigger [29]. Over the next year, simulations using actual E687 data will be carried out. If deemed feasible an ANN trigger could be built from a specially designed VLSI chip or from a modified commercially available INTEL chip. This work will be carried out in conjunction with Chuck Glover of Oak Ridge National Laboratory.

C. BC72: Light Quark Spectroscopy

The continuing analysis of BC72 has proven to be a substantive introduction into particle physics for young graduate students, who will subsequently work on FNAL experiments E687 and E831. From BC72 we have one paper that is to appear in Physical Review D [30], another that is in the review process [31] (Physical Review D), and finally one that we intend to submit later this year [32].

The data from BC72 continues to be fruitful for examining vector meson states. "Further Results from Charge Exchange Photoproduction" examines the charge exchange reaction $\gamma p \rightarrow n a_2^+(1320)$ and is to be published in Phys. Rev. D [30]. This work demonstrates that the reaction $\gamma p \rightarrow a_2^+(1320)n$ (see Figure 14) agrees with a one pion exchange mechanism [33].

(a) (b)

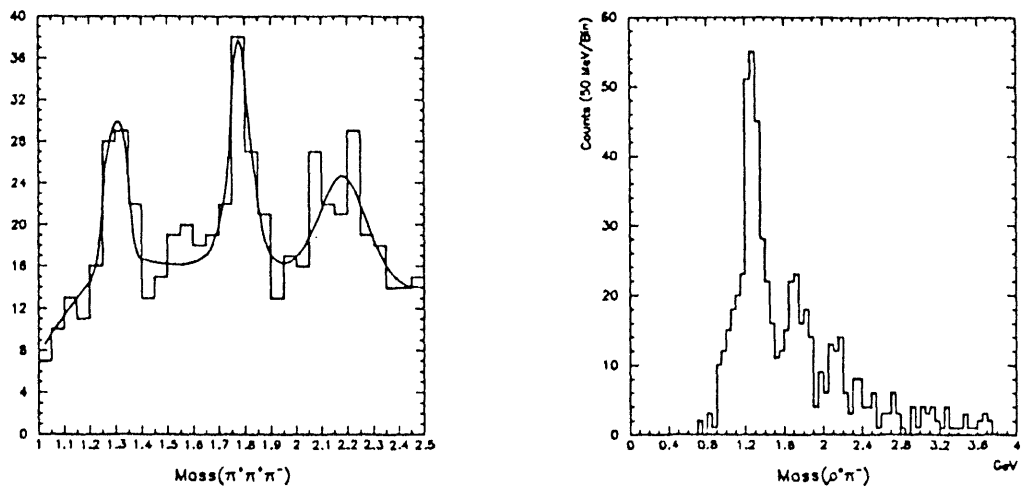

FIG. 14. (a) $\pi^+\pi^+\pi^-$ mass spectrum from the reaction, $\gamma p \rightarrow n\pi^+\pi^+\pi^-$, when either neutral dipion combination is a ρ^0 and when $|t'_{\gamma,3\pi}| < 0.12\,\mathrm{GeV}^2$ and (b) The $\rho^0\pi^-$ mass spectrum from the reaction, $\gamma p \rightarrow \Delta^{++}\rho^0\pi^-$ at $|t'_{\gamma,\rho^0\pi^-}| < 0.2\,\mathrm{GeV}^2$.

Since no evidence for the photoproduction of the $a_1^+(1260)$ was found, the only consistent conclusions (assuming the dynamics of $a_1(1260)$ and $a_2(1320)$ photoproduction to be the same) were shown to be that the $a_1(1260)$ has either an extremely large hadronic width or a mass somewhat less than 1260 MeV.

"Inelastic ρ^0 Photoproduction in the Reaction $\gamma p \rightarrow \rho^0\pi^+ n$" also examines the final state containing a neutron and three pions [31]. The $\rho^0(770)$ is found in this channel opposite an $N^* \rightarrow \pi^+ n$ (see Figure 15), and the data are consistent with the ρ^0 production being due to a double peripheral mechanism (Pomeron and pion exchange), which conserves s-channel helicity. The results compare favorably with calculations by Wolf [34], although a distortion

of the expected angular distributions occurs in the π^+n mass region 1.3 – 1.5 GeV/c^2. A similar phenomenon occurs in pion-induced N^* diffraction.

(a) (b)

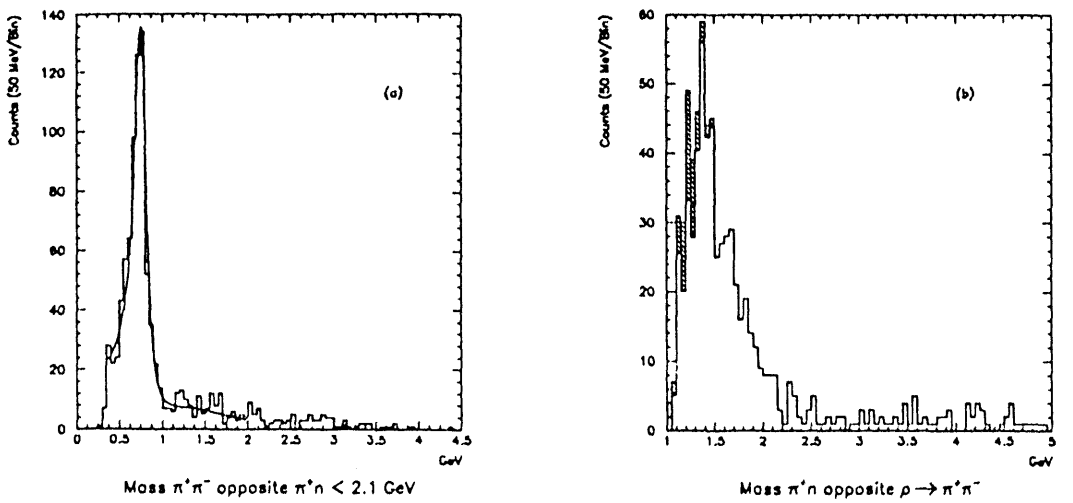

FIG. 15. (a) The $\pi^+\pi^-$ mass spectrum from the reaction, γp $\rightarrow \rho^0\pi^+$n, when $\mid t'_{\gamma,\pi^+\pi^-} \mid \leq 0.12$ GeV^2 and when $M(\pi^+$n$) < 2.1$ GeV and (b) the π^+n spectrum opposite ρ^0 production when $\mid t'_{\gamma,\pi^+\pi^-} \mid \leq 0.12$ GeV^2. The shaded portion represent the expected contributions from $\Delta^+\rho^0$ production.

The final state n$\pi^+\pi^+\pi^+\pi^-\pi^-$ is currently being examined for inelastic ρ^0 production and for charged $a_2(1320)$ – both of which appear to be present [32]. The latter appears to occur in the reaction γp $\rightarrow a_2^{\pm}(1320)\Delta^{(0)/(++)}$ where the $\Delta^{(0)/(++)}$ is an excited state of the $\Delta(1238)$. Since we have presented evidence in the past for the reaction γp $\rightarrow a_2^{\pm}(1320)\Delta^{++}(1238)$, the existence of this reaction is probably to be expected.

Finally, the π^0 channel (γp $\rightarrow$ p$\pi^+\pi^-\pi^0$) will be examined. Of particular interest will be the production of 1^{+-} states, namely the $h_1(1170)$. From the amount of neutral $b_1(1235)$ photoproduction that has been found previously and from theoretical ideas about the $\pi\gamma$ radiative widths of these states, the amount of $h_1(1170)$ photoproduction is rather tightly constrained.

D. SDC Collaboration

This past year our efforts within the Solenoidal Detector Collaboration have been concentrated on neural network calorimeter triggering, simulation of hanging file test data, and neutron backgrounds within the detector hall and detector components.

1. Neural Network Calorimeter Trigger

The original work [35], which effectively could be considered as zeroth order, on neural network triggers for the SDC detector had two major problems associated with it. These problems are:

1. The Artificial Neural Network, ANN, that was used was not optimized with regards to the number of hidden layers and the number of nodes in the hidden layers.

2. The tracks that were used for energy deposition in the calorimeter were not smeared by shower spreading within and across calorimeter towers and also did not account for calorimeter resolution.

Our efforts during this past year have been towards optimizing the size of the ANN and the inclusion of calorimeter effects.

The first task was to optimize the number of nodes in the hidden layer. The original ANN had 1000 nodes in the hidden layer. With a total of 960 input nodes this led to a total of $\sim 1,000,000$ weights that needed to be determined. Large amounts of computer time were needed to train an ANN of this size. Furthermore, even with a fairly large and robust data set for training such an ANN, it was difficult to ascertain that the network was not merely comparing the unseen data with a "memorized" training set.

A training set of 1500 events, containing equal numbers of two jet and min-bias events was generated using the default values of ISAJET for two jet and min-bias production. Table II shows the results of varying the number of hidden layer nodes from the original 1000 nodes to a low of 10 nodes.

TABLE II. Determining Network Size

	Percent Correct	
Hidden Layer Nodes	Minimum Bias	Two Jet
10	95.7%	94.9%
20	98.1%	94.0%
30	98.3%	89.4%
40	99.5%	88.6%
50	97.3%	92.2%
60	98.8%	90.3%
70	97.2%	87.5%
80	96.4%	92.3%
90	99.5%	86.7%
100	98.4%	91.2%
1000	99.5%	78.6%

As can be seen from Table II, for all hidden layer sizes the network was capable of identifying min-bias events very well. It is also evident that for two jet events the network performed better when the ANN had a smaller number of hidden layer nodes. It appears that a network with a small number of hidden layer nodes is capable of generalizing.

The second task concerning neural networks was the improvement of the realism of the input data to the ANN. To this end the energy of each track was smeared according to a variety of techniques. The basic technique was to distribute the energy of each track in a Gaussian fashion over a circle of radius 7 *cm* at a depth of 4 interaction lengths within the calorimeter. These energies were then accredited to the appropriate calorimeter tower. Various smearing techniques were utilized. The ANN that was used contained 10 hidden layer nodes. The results of various smearing techniques are shown in Table III.

TABLE III. Performance of Smeared Simulations

	Number Events	Events Identified	Percentage
Center Smear Approximation			
	Number Events	Events Identified	Percentage
Min-Bias Events	500	472	95.8%
Two Jet Events	500	487	97.4%
Intersection Smear Approximation			
	Number Events	Events Identified	Percentage
Min-Bias Events	500	483	96.6%
Two Jet Events	500	480	96.0%
Monte Carlo Approximation			
	Number Events	Events Identified	Percentage
Min-Bias Events	500	489	97.8%
Two Jet Events	500	485	97.0%

As can be seen the ANN performed well for all the smearing techniques used.

2. Hanging File Test Data Simulation

As part of the continuing effort to ensure the reliability of the predictive power of the CALOR89 code system, simulations were carried out and compared with the results from the Reconfigurable-Stack Calorimeter Test Measurements [36] - [37] which were conducted at Fermilab as part of the SDC calorimeter design effort. Previous comparisons of the results of the CALOR89 code system have largely been with calorimeter configurations which were uniform in their composition, *i.e.* the same absorber material throughout and the same thickness of absorber and thickness of scintillator throughout the calorimeter.

The initial comparisons were made on homogeneous configurations of lead-scintillator and iron-scintillator. Good agreement was obtained between the simulations and the measurements. Next, a non-homogeneous lead-scintillator configuration was simulated. In this configuration the lead was of different thicknesses in the two segments of the calorimeter. Here again good agreement was obtained between the CALOR89 predictions and the hanging-file measurements.

The next comparisons between the CALOR89 and hanging-file data was made on those configurations where the two segments of the calorimeter had different absorber materials. The electromagnetic segment had lead as the absorber while the hadron segment utilized an iron absorber. Here there was considerable disagreement between the simulations and the measurements. This disagreement was explored in detail. However, no resolution of the problem was found. It is difficult to imagine what could cause such disagreement when good agreement is obtained for other non-homogeneous configurations of all lead and for homogeneous configurations that contain iron. Attempts were made to obtain the raw hanging file data, so that we could try to independently reproduce the results that were supplied to us. However, considerable resistance to this was encountered.

3. Neutron Background Calculations

A problem that can severely affect the operating conditions of the SDC detector is the numbers of neutrons that are produced in the pp collisions. The effect of these neutrons will be to produce radiation damage, and thereby loss of light signal, in the scintillator tiles within the endcap and forward calorimeters. A further source of neutron background is neutron production resulting from beam-gas and beam scrapper interactions. These neutrons could affect the triggering rates of the muon chambers. Problems could also arise from the neutron activation of the materials used in the detector and beam shielding.

To attempt to answer the question of numbers of neutrons from pp collisions a series of calculations [39] were done using the CALOR89 system of simulation programs. Minimum-bias events from pp collisions at a center-of-mass energy of 40 TeV were generated using ISAJET. These events were then interfaced into the CALOR89 programs. As the computational time for event processing is directly proportional to the number of detector elements used, a simplified version of the SDC detector was used. As an example of this, the barrel calorimeter was reduced to just three elements: an electromagnetic calorimeter of homogenized lead and scintillator, a hadron calorimeter of homogenized iron and scintillator, and a second hadron calorimeter of homogenized iron and scintillator. The results of these calculations are given in [39].

REFERENCES

[1] Ted Barnes, private communication.

[2] "A Precise Measurement of the $D_s^{\pm}$ Meson Lifetime." By the E687 Collaboration (P.L. Frabetti, *et al.*), *Accepted in* Phys. Rev. Lett., (1993).

[3] "A Precise Measurement of the D^0 and D^+ Meson Lifetimes." By the E687 Collaboration (P.L. Frabetti, *et al.*), *Submitted to* Phys. Lett. **B**, (1993).

[4] "A Measurement of $\Gamma(D_s^+ \to \phi\mu^+\nu)/\Gamma(D_s^+ \to \phi\pi^+)$." By the E687 Collaboration (P.L. Frabetti, *et al.*), *Accepted in* Phys. Lett. **B**, (1993).

[5] "First Evidence of $\Omega_c^0 \to \Omega^-\pi^+$." By the E687 Collaboration (P.L. Frabetti, *et al.*), Phys. Lett. **B 300**, 190, 1993.

[6] "Analysis of the decay mode $D^+ \to \overline{K}^{*0}\mu^+\nu$." By the E687 Collaboration (P.L. Frabetti, *et al.*), Phys. Lett. **B 307**, 262, 1993.

[7] "Studies of $D\overline{D}$ correlations in High-Energy Photoproduction." By the E687 Collaboration (P.L. Frabetti, *et al.*), Phys. Lett. **B 308**, 193, 1993.

[8] "Measurement of the Lifetime of the Ξ_c^0." By the E687 Collaboration (P.L. Frabetti, *et al.*), Phys. Rev. Lett. **70**, 2058, 1993.

[9] "Measurement of the Mass and Lifetime of the Ξ_c^+." By the E687 Collaboration (P.L. Frabetti, *et al.*), Phys. Rev. Lett. **70**, 1381, 1993.

[10] "A Measurement of the Λ_c^+ Lifetime." By the E687 Collaboration (P.L. Frabetti, *et al.*), Phys. Rev. Lett. **70**, 1755, 1993.

[11] "Evidence of the Cabibbo-Suppressed decay $\Lambda_c^+ \to pK^-K^+$." By the E687 Collaboration (P.L. Frabetti, *et al.*), *To be published in* Phys. Lett. B, 1993.

[12] "High Energy Photoproduction of Charm Baryons," Proceeding of the XXVI International Conference on High Energy Physics, Dallas, Texas. August 6 - 12, 1992.

[13] "Rare Decay Modes of the D^0, D^+, D_s Charmed Mesons," Proceeding of the XXVI International Conference on High Energy Physics, Dallas, Texas. August 6 – 12, 1992.

[14] "Semileptonic Decays of Charm Mesons," Proceeding of the XXVI International Conference on High Energy Physics, Dallas, Texas. August 6 – 12, 1992.

[15] "Studies of Fully Reconstructed $D\overline{D}$ Events in High Energy Photoproduction," Proceeding of the XXVI International Conference on High Energy Physics, Dallas, Texas. August 6 – 12, 1992.

[16] "Charm Hadronic Decays in Photoproduction at Fixed Target," Proceeding of the Advanced Study Conference on "Heavy Flavours," Pavia, Italy. September 3 – 7, 1993.

[17] "Lifetime Measurements at Fixed Target," Proceeding of the Advanced Study Conference on "Heavy Flavours," Pavia, Italy. September 3 – 7, 1993.

[18] "Charm Semileptonic Decays at Fixed Target," Proceeding of the Advanced Study Conference on "Heavy Flavours," Pavia, Italy. September 3 – 7, 1993.

[19] K. Hikasa, *et al.*, Phys. Rev. D **45**, S1 1992.

[20] *Semi-Inclusive Production of Light Mesons by High Energy Photoproduction.* Gavin R. Blackett, Ph.D. thesis, University of Tennessee, May 1993.

[21] *Light-Quark Meson Photoproduction at a Mean Energy of 120 GeV/c.* Murali Pisharody, Ph.D. thesis, University of Tennessee, December 1993.

[22] Atkinson *et. al.* Z. Phys C **30**: 531 (1986). They have apparently observed the $\rho_3(1690)$ through its decay to $\eta\pi$ in central production.

[23] F.E. Close and Harry J. Lipkin. Phys. Rev. Lett., **41**(19), November 1978.

[24] S.I. Bityukov, *et al.* Sov. J. Nucl. Phys., **46**: 273 (1987).

[25] M. Bauer, B. Stech, and M. Wirbel. Z. Phys. C **34**: 103 (1987).

[26] A.N. Kamal and R.C. Verma. Phys. Rev. **D 45**, 982 (1992).

[27] J. Adler, *et al.* Phys. Rev. Lett., **64**(22) May, 1990; D. Coffman, *et al.* Phys. Rev. **D 45**, 2196 (1992).

[28] "A High Statistics Study of States Containing Heavy Quarks Using the Wideband Photon Beam and the E687 Multiparticle Spectrometer." By the Wideband Beam Photon Collaboration. FNAL Report, 1992.

[29] T. Handler, *et al.* Proceedings of the International Conference on Computing in High Energy Physics '92, (650) and references contained therein. C. Glover, *et al. ibid* (639).

[30] "Further Results from Charge Exchange Photoproduction." G.T. Condo, *et al.*, *To be Published in* Phys. Rev. D (1993).

[31] "Inelastic ρ^0 Photoproduction in the Reaction $\gamma p \rightarrow \rho^0 \pi^+ n$." G.T. Condo, *et al.*, *Submitted to* Phys. Rev. D (1993).

[32] "$a_2^{\pm}(1320)$ and ρ^0 Photoproduction in Association with $\Delta^{++}(1900)$." G.T. Condo, *et al.*, *To be Submitted to* Phys. Rev. D (1993).

[33] "Charge Exchange Photoproduction of the $a_2^-(1320)$ in Association with Δ^{++} at 19.3 GeV/c." G.T. Condo, *et al.*, Phys. Rev. **D 45**, 3317 (1990).

[34] G. Wolf, Nucl. Phys. **B 26**, 317 (1971).

[35] "Feasibility of Using Neural Networks as a Level 2 Calorimeter Trigger for Jet Tagging," Proceedings of the International Conference on Computing in High Energy Physics '92, Annecy, France, Sept. 21-25, 1992, CERN 92-07, p650.

[36] "Beam Tests of Composite Calorimeter Configurations from Reconfigurable-Stack Calorimeter," Nucl. Instr. and Meth., **A329** (1993) 50.

[37] "Study of Absorber Materials and Low-Z Cladding Layers from Reconfigurable-Stack Calorimeter," *To Be Submitted to* Nucl. Instr. and Meth.

[38] "Simulation of The Reconfigurable-Stack Test Calorimeter Experiments with CALOR89," *Submitted to* Nucl. Instr. and Meth.

[39] "Estimates of the Neutron Fluence for the SDC Detector," Nov., 20, 1992, SDC-92-354.

V. SLD

SLC and SLD had a very successful 1993 run during which more than 50,000 hadronic Z^0 decays were recorded on tape. Using a strained Gallium-Arsenide cathode beginning in April, the SLC electron beam had a (longitudinal) polarization consistently larger than 60% (~22% in 1992, ~45% with an Aluminium-Gallium-Arsenide cathode in the beginning of 1993).

The 1992 data sample of about 11,000 Z^0 decays with about 22% e^- polarization had allowed a measurement of the left-right asymmetry, giving a value for $\sin^2\theta_w$ derived therefrom of 0.2378 ± 0.044 (stat) ± 0.004 (sys)[1]; with the 1993 data sample we expect to reduce the error to ±0.0008 ± 0.0002, once the polarization, the main source of systematic error, is properly understood. The current value based on 1993 data is $\sin^2\theta_w = 0.2378 \pm 0.0056$. This is not a final number pending checks on the polarization measurement.

SLD/SLC Upgrades

Presently a major rebuilding of the damping ring vacuum chamber is underway. The new damping ring and improved final focus optics are expected to allow delivery of up to 200,000 Z^0's to SLD in 1994, and >250,000 Z^0's per year for the following years, such that SLD can expect a data sample of a million Z^0 decays. A proposal to extend the SLD Physics program for the next 4 years has been endorsed by the SLAC EPAC[2] along with a $2,000,000 upgrade of the SLD vertex detector to increase the acceptance,

improve the resolution and thus enhance the proposed measurement of B_s^0 mixing during the extended run for a total of 1 million Z^0's.[3]

Participation in Analysis Groups

Tennessee took heavy responsibility for shifts in the 1993 run with Kroeger, Weidemann, White, Cohn, Hart, Du, and Bugg. A total of 254 shift points were accumulated with 1 shift point ≈1 day shift. Besides providing 1 man year of shifts during the 1993 SLD run, we participated in and actively contributed to the most important SLD analysis groups and SLD planning activities

Luminosity--The analysis of the data from the Luminosity Monitor represents the major part of Sharon White's thesis which concentrates on radiative Bhabha production and comparison with theory and experiment. Her analysis of the 1992 luminosity and demonstration of a "G10" effect (local hardening of shower depending on arrangement of silicon and G10 boards) were presented to the collaboration at an analysis meeting on February 17, 1993. We have provided all full shower MC data for the Luminosity Monitor, a very time consuming process with a single event taking over 90 minutes of IBM 3090 time.

The larger data rate for the 1993 run made it impractical to keep all detector information for all Bhabha triggers available for re-analysis. Tennessee provided a fast filtering routine to allow writeout of LUM data for small-angle Bhabha events without

compromising the sample of radiative Bhabhas which was implemented in the SLD event filter.

Electroweak--The A_{LR} measurement mentioned above is clearly most important for SLD as SLC is the only collider providing polarized Z^0's.

We contributed to the analysis by EXPOSTAR[4] calculations of the corrections due to SLC running slightly off the Z^0 mass. We also now use the ZFITTER[5] Program from CERN for this purpose and related studies, among them prediction of the top mass.

B-Physics--The unique CCD-based vertex detector is one of the strengths of SLD and particularly useful in the analysis of B meson decays. Together with the known stability of the interaction point (IP), it allows tagging of B decays by requiring tracks of the decay products to originate away from the IP, rather than by the usual leptons tag with small efficiency.

Preliminary reports of measurements of the ratio of Z-decays into b-bbar decays to that into all hadrons, the left-right asymmetry for b-quarks, the flavor independence of the strong coupling constant α_s, and the charged multiplicity of b-events were submitted to the summer conferences (Lepton-Photon at Cornell, EPS in Marseille), and publications are in preparation.

A difficulty for Monte-Carlo (MC) studies of the vertices of longer-lived particles is that the standard Monte Carlo generators only provide the particle types and momen-

tum 4-vectors for the generated and decayed particles. We provided a general routine ("MCVTX") which inserts production and decay vertices into the SLD data structure for MC events, thus allowing vertex studies for any MC generator chosen.

Tau Physics--A separate subgroup studies tau events. For these studies, we provided KORALZ MC events[6] and supervised numerous re-reconstructions of these and tau data as the SLD reconstruction code improved over time. We reported our tau filtering and triggering efficiency studies to the collaboration at an analysis meeting on April 14, 1993.

The tau lifetime can be found by several methods using the vertex detector, and a note on it is in preparation. Several other tau studies are in progress. Most of them, however, become only viable with the additional statistics of the 1994 run.

QCD--One of the most active analysis groups has been the QCD studies group. Many QCD measurements are limited by systematic or theoretical errors, rather than statistical ones, so that SLD is not at a disadvantage due to its smaller data sample.

In addition to the papers mentioned under B-physics above, we also submitted one on jet handedness to the summer conferences. A paper on jet rates and a measurement of α_s[7] has just been accepted for publication by Phys. Rev. Lett., and one on the charged multiplicity of b-events[8] has just been submitted to the same journal.

As part of our participation in this group, we prepared the Monte-Carlo generator HERWIG5.7[9] to run with SLD code, so as to have a generator other than the

already used JETSET (Lund) for determining systematic (theoretical) errors. In cooperation with the Herwig authors, we upgraded SLD's HERWIG version to incorporate beam and gluon polarization effects.

Polarimeter Upgrade

Considering the importance of the polarization measurement for SLD, an upgrade of the Compton polarimeter to measure all three components of the electron spin has been proposed.[10] This would involve adding a detector for the back-scattered photons for which we propose the use of a silicon calorimeter using the silicon previously acquired for the first few layers of the SLD Medium-Angle Silicon Calorimeter (MASC). The feasibility of this measurement is currently being studied, in particular, the possibility of masking out the swath of synchrotron radiation generated by magnet bends following the Compton interaction point. This project may be one of the most crucial in the SLD upgrade. Since the proposed improved Compton polarimeter is similar to that Tennessee has prepared for E144, we plan to provide similar equipment for SLD.

REFERENCES

1. K. Abe, *et al.* (SLD Collaboration), "First Measurement of the Left-Right Cross Section Asymmetry in Z-Boson Production by e^+e^- Collisions," Phys. Rev. Lett 70, 2515 (1993).

2. SLD Collaboration, "Proposal for an Extension of the SLD Study of Polarized e^+e^- Collisions at the SLC," October 1993.

3. SLD Collaboration, "Proposal to Upgrade the SLD Vertex Detector," October 1993.

4. D. C. Kennedy and B. W. Lynn, Nucl. Phys. B322, 1 (1989); D. Levinthat, F. Bird, R. G. Stuart, and B. W. Lynn, "Global Analyses of e^+e^- Collision Data Near the Z^0...," CERN TH.6094/91.

5. D. Bardin, *et al.*, "ZFITTER, An Analytical Program for Fermion Pair Production in e^+e^- Annihilation," CERN TH.6443/92.

6. S. Jadach, B. F. L. Ward and Z. Was, "The Monte Carlo Program KORALZ V. 3.8 for Lepton or Quark Pair Production at LEP/SLC Energies," Comp. Phys. Comm. 66, 276 (1991).

7. K. Abe, *et al.* (SLD Collaboration), "A Study of Jet Rates and Measurement of α_s at the Z^0 Resonance," Phys. Rev. Lett., October 11, 1993.

8. K. Abe, *et al.* (SLD Collaboration), "Measurement of the Charged Multiplicity of $Z^0 \geq$ b-bbar Events," submitted to Phys. Rev. Lett.

9. G. Marchesini, B. R. Webber, M. H. Seymour, *et al.*, "HERWIG - A Monte Carlo Event Generator for Simulating Hadron Emission Reactions with Interfering Gluons," Comp. Phys. Comm. 67, 465 (1992).

10. C. Prescott, SLAC Memo (draft) of June 28, 1993.

11. A. W. Weidemann, ed., "The E-144 Collaboration Meeting - QED at Critical Field Strengths," SLAC, February 19-20, 1993.

12. K. Yokoya, "A Computer Simulation Code for the Beam-Beam Interaction in Linear Colliders," KEKE-Report 85-9, October 1985; T. Tauchi, K. Yokoya, and P. Chen, "Pair Creation from Beam-Beam Interaction in Linear Colliders," Part. Acc. 41, 29 (1993).

VI. E144 at SLAC

In fall 1992 we joined Princeton, Rochester and SLAC FFTB group to do a unique test of non-linear quantum electrodynamics by scattering 45 GeV electrons in the SLAC Final Focus Test Beam facility off photons from high power laser beam. The intense electric field from a 1 joule picosecond laser, enhanced in electron rest frame by relativistic factor γ ($\approx 10^5$), provides conditions where perturbation theory cannot be applied. Initiated by Princeton University, the experiment involves a three-year program of QED studies. University of Rochester has provided a very high power laser system operated at photon energy of 0.5 eV and 1 eV and Tennessee has constructed 3 silicon electromagnetic calorimeters for this experiment utilizing spare silicon already in hand either from SLD medium angle calorimeter or from SSC prototype.

Beam Test--In April 1993 we were, without much notice, given an opportunity to test a calorimeter in A line at SLAC. In 3 weeks we were able to assemble the calorimeter and electronics (borrowed from FNAL). Only 2.5 days were available to install the calorimeter and electronics in End Station A and to take data, but we nevertheless achieved rather complete results. Figure 1 shows the results of a typical 15 minute run. The peaks each correspond to a different number of 25 GeV electrons striking the calorimeter. The maximum number is about 24 and is limited by the beam intensity. The energy scale is in ADC counts with $\approx$10,000 counts/GeV. Figure 2 shows more clearly the high energy end of the spectrum while Figure 3 demonstrates linearity of

calibration up to 400 GeV. These results make apparent not only the quality of the calorimeter but also that the electron beam in the A line at SLAC is an outstanding facility for testing and calibrating EM calorimeters at high energy. There is no other facility in the world where a complete calibration with such a wide dynamic range can be done so efficiently.

FFTB Test--Figure 4 shows the downstream end of the Final Focus Test Beam (FFTB) facility including the interaction point for E144 and permanent magnets serving as magnetic spectrometers for positrons and electrons. The E144 electron and positron calorimeters are shown along with particle trajectories.

E144 is actually a two to three year program of experiments. We will look at the reaction

(1) $e^- + \omega \rightarrow e^- + e^+ + e^-$ Pair production (beamstrahlung)

(2) $e^- + n\omega \rightarrow e^- + \gamma$ (non-linear Compton Scattering)

(3) $\gamma + n\omega \rightarrow e^+e^-$ (e^+e^- mass spectrum 1 MeV to 6 MeV)

With sufficiently high laser power (electric field at IP) these processes involve multiphoton absorption and fields near the Schwinger critical field where perturbation theory is inadequate.

Our electron calorimeter and γ calorimeter were installed this fall for a test of the FFTB. The purpose of the test was to implement a scheme to measure beam spot size using a laser scheme of Shintake, *et al.* Since the E144 laser was not operative, our

calorimeter served as the primary tool to monitor the tuning of the FFTB beam. The system worked well although the electron calorimeter suffered appreciable radiation damage from low energy beam halo. Figure 5 shows a crude picture of the total energy deposited in the e calorimeter in a single pulse. It is clear that major background problems must be solved to permit the E144 reactions to be studied.

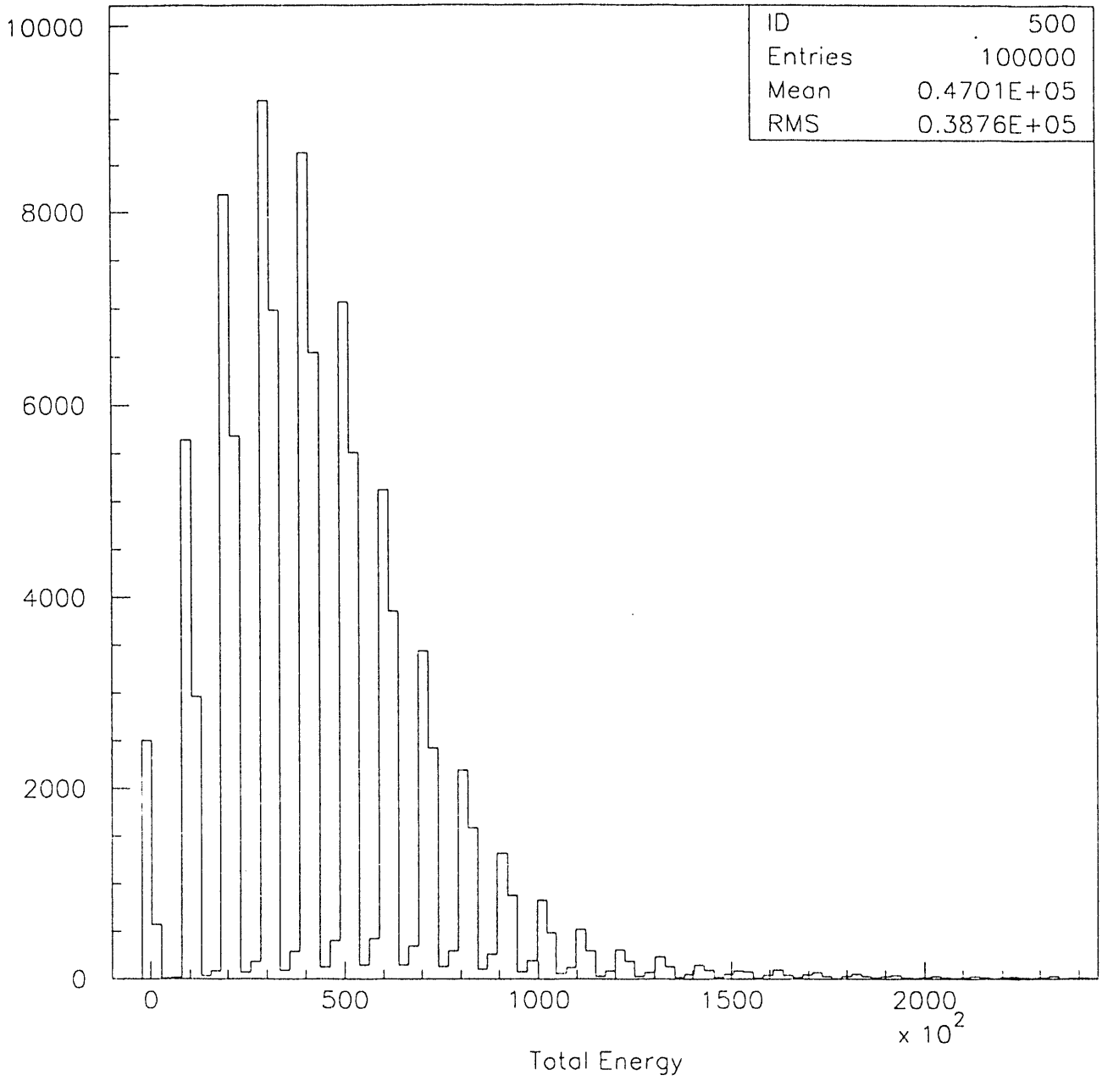
ID 500
Entries 100000
Mean 0.4701E+05
RMS 0.3876E+05
10000
8000
6000
4000
2000
0
0
500
1000
1500
2000
x 10^2
Total Energy

FIGURE 1

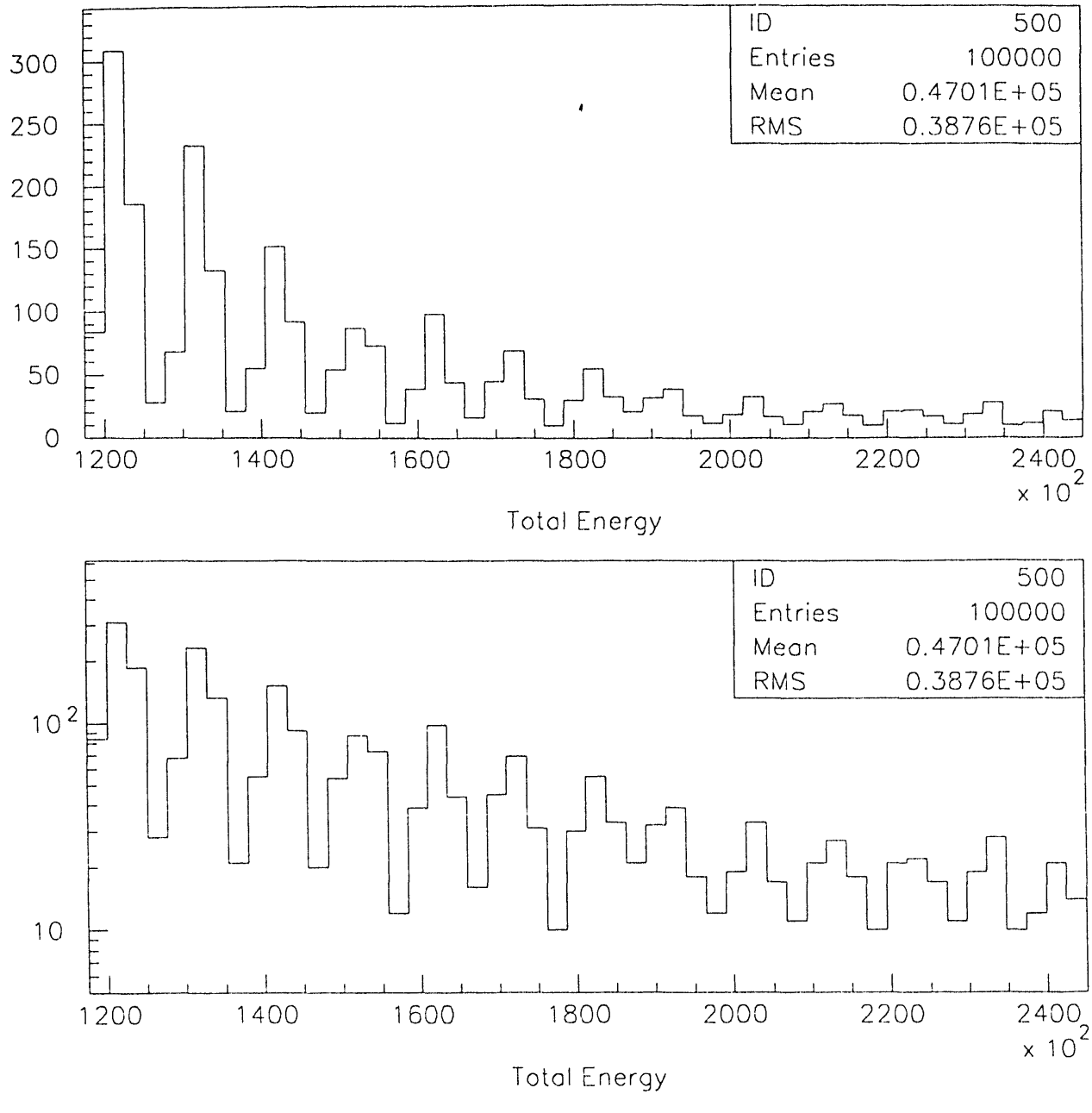
ID 500
Entries 100000
Mean 0.4701E+05
RMS 0.3876E+05
300
250
200
150
100
50
0
1200
1400
1600
1800
2000
2200
2400
x 10^2
Total Energy
ID 500
Entries 100000
Mean 0.4701E+05
RMS 0.3876E+05
10^2
10
1200
1400
1600
1800
2000
2200
2400
x 10^2
Total Energy

FIGURE 2

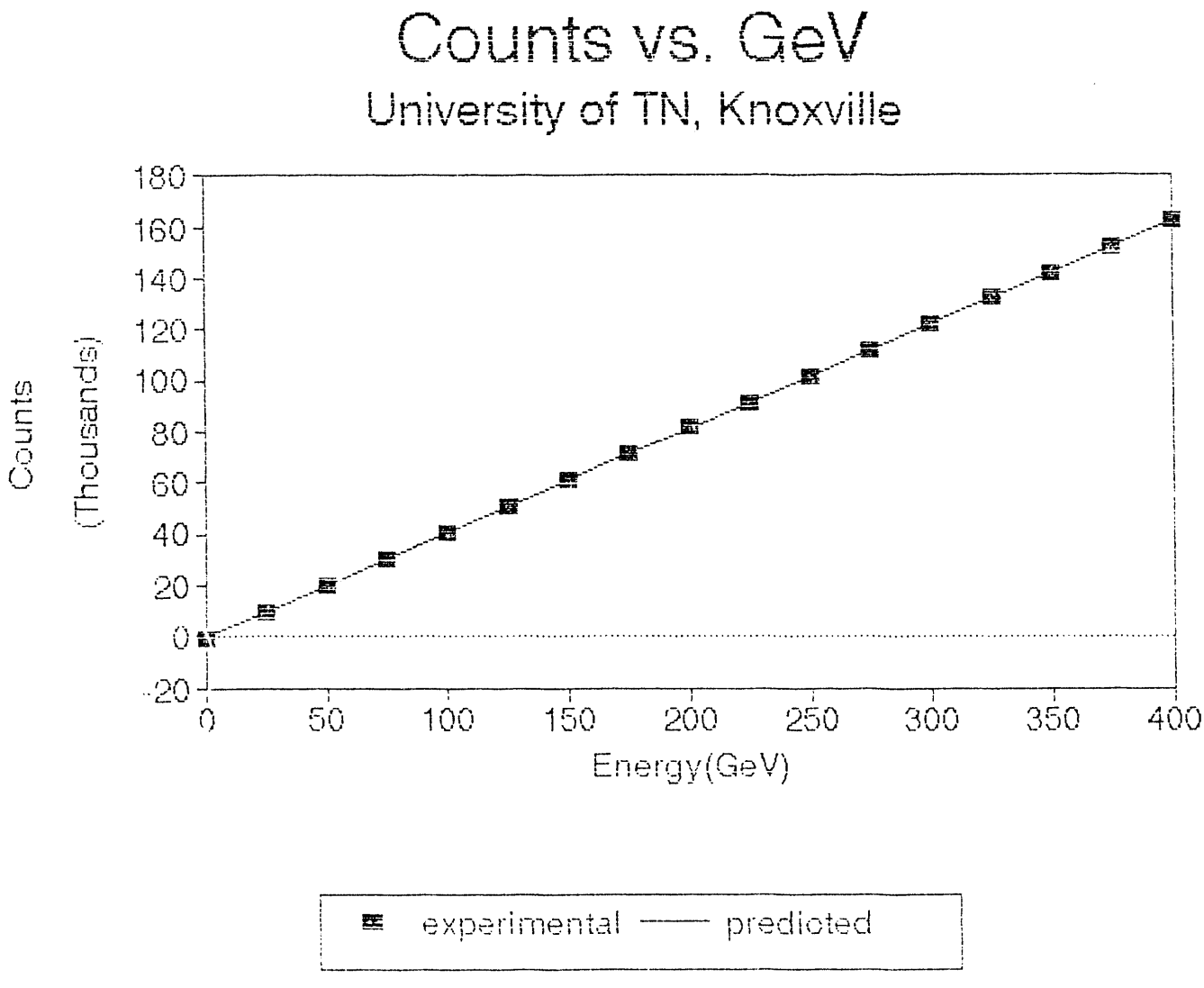
Counts vs. GeV
University of TN, Knoxville
Counts
(Thousands)
180
160
140
120
100
80
60
40
20
0
-20
0
50
100
150
200
250
300
350
400
Energy(GeV)
experimental
predicted

FIGURE 3

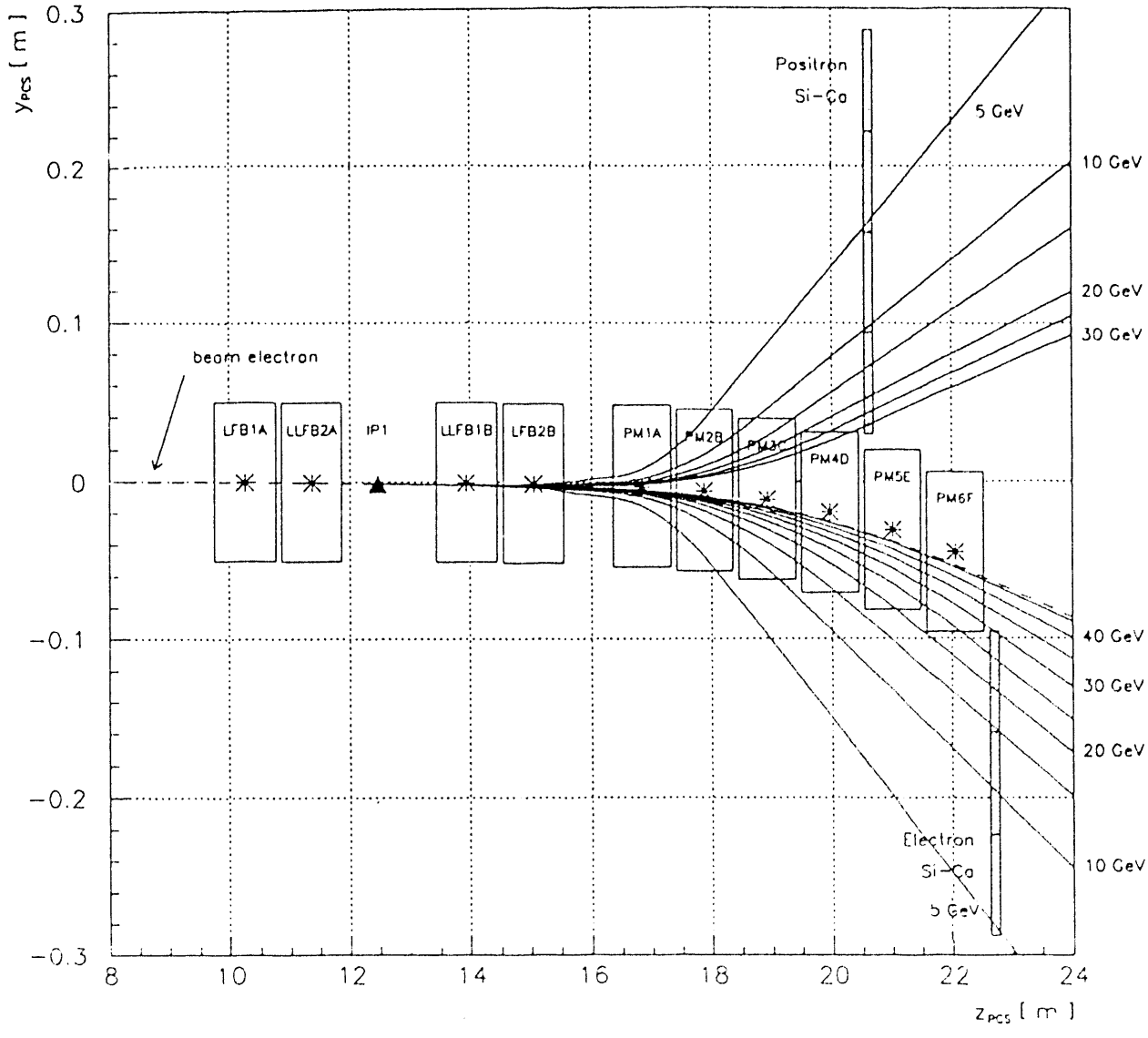

Figure 4 Trajectories of electrons and positrons through the FFTB dump magnets, assuming the 'hard edge' approximation for $B_x(y)$ (S1) in the permanent magnets PM1A to PM6F.

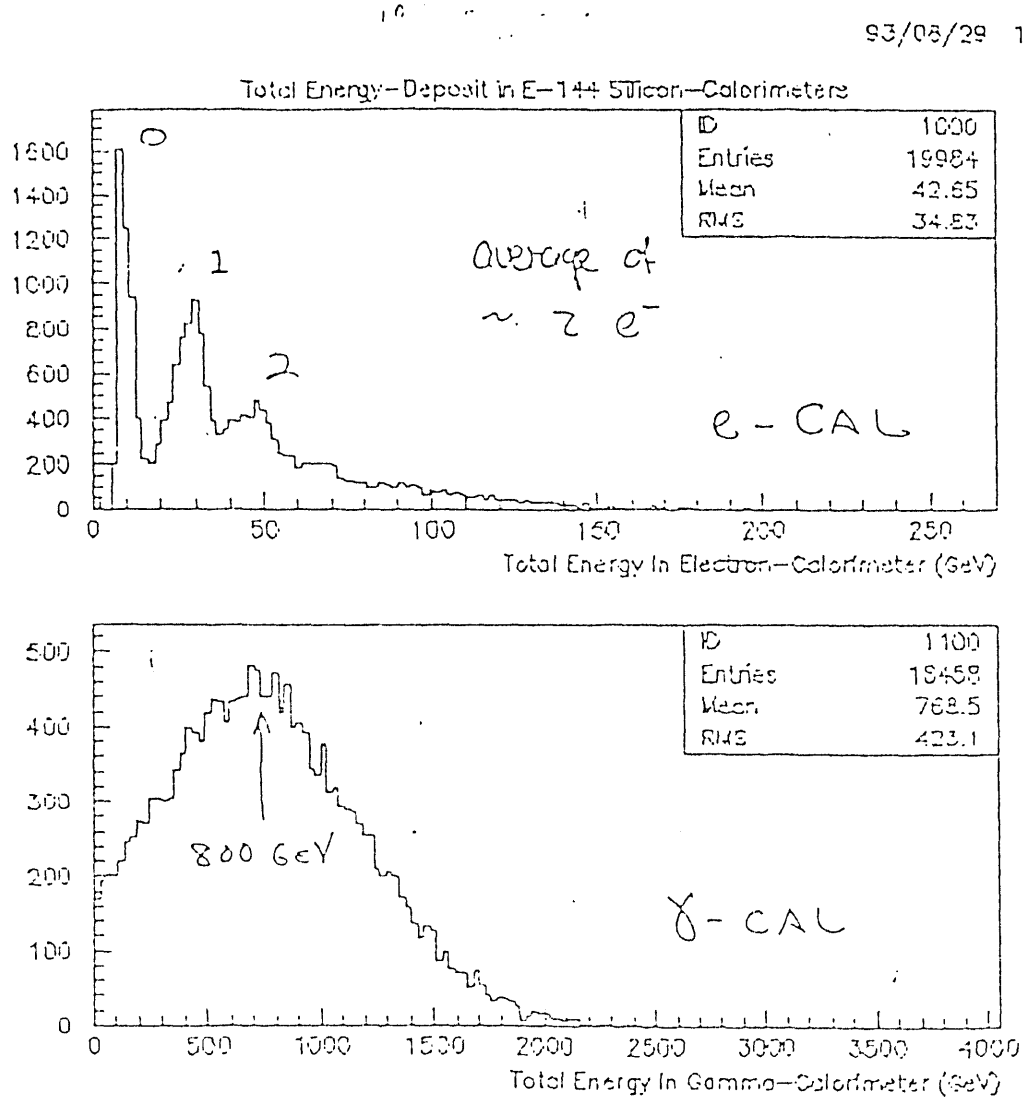
93/08/29 15.
Total Energy-Deposit in E-144 Silicon-Calorimeters
ID 1000
Entries 19984
Mean 42.65
RMS 34.83
0
1
2
average of ~ 2 e⁻
e - CAL
Total Energy in Electron-Calorimeter (GeV)
ID 1100
Entries 19458
Mean 768.5
RMS 423.1
800 GeV
γ - CAL
Total Energy in Gamma-Calorimeter (GeV)

FIGURE 5

VII. Radiation Hardened Silicon for Particle Physics Detectors

A. Model for Bulk Damage and Study of Surface Effects

SUMMARY

The objective of this program is to increase our knowledge of the basic mechanisms and defect configurations which create the radiation damage symptoms in Si detectors and to use this information to improve the radiation hardness of Si detectors. In this report, we review the current status of the radiation hardness program, the results of the past year, and our plans for continuing the program. Particular attention is given to the long term annealing effect which is causing considerable concern at the present time. This long term annealing effect, which has a time constant of many months after irradiation has stopped, consists of a rather large drift towards lower resistivity p-type material.

We have proposed a simple physical model for the effect which fits our recent data and the data of the LHC collaboration. This model assumes a slow evaporation of vacancies from the primary damage clusters which in turn allow the interstitial B to anneal back to its predamage substitutional state. We propose to continue our program to verify this model by doing more damage annealing tests at higher fluences with specially doped Si crystals and by doing tests on actual detectors made from these special materials.

We also outline a plan of research into the effects of oxygen on radiation damage with particular attention to the possibility of radiation damage related n-type layers near the surface of oxidized detectors.

INTRODUCTION and BACKGROUND

Silicon detectors are essential to elementary particle physics research for tracking arrays and would be the detectors of choice for sampling calorimeters, preradiators, luminosity monitors, etc., if the cost and radiation hardness were reasonable. The cost of replacing damaged silicon detectors will be high. Since some detectors will be located within the core of the magnet and the EM/Hadron detector systems, replacement may be impractical in some cases. Therefore, silicon detectors will need to have a life expectancy of many years in the presence of a high background of high energy neutrons. The neutron radiation damage problem is much worse at small forward angles and will dominate the question of what angular coverage can be provided by Si devices. Increasing the life expectancy of the silicon detectors even by a factor of two will be a valuable contribution.

The deleterious effects of bulk radiation damage show up as high leakage current and its associated noise, compensation level changes (resistivity and type), and charge collection problems. Therefore, we will briefly review these fundamental problems,

followed by a summary of the present state of knowledge about some of the more important defect states which may be responsible for the radiation damage symptoms.

Historically, there has been a large amount of research, development, and engineering design effort on the subject of improving the radiation hardness of silicon devices; a significant fraction of which is available in the open literature. However, the vast majority of this work focused on radiation effects at the surface of the device. This focus was justified by the fact that the devices of interest had very large surface to volume ratios and were therefore dominated by the surface effects caused by ionizing radiation. Although it is relevant to surface problems, particularly for tracking devices, this vast body of knowledge and technology is not adequate for radiation detectors with large sensitive depths where the radiation damage susceptibility may be dominated by bulk damage. The literature associated with this work is too extensive to cite individually; but a significant part of the published work in this field can be found in the IEEE Transactions on Nuclear Science and the IEEE Transactions and Conference Proceedings of conferences sponsored by the IEEE-NPSS Committee on Radiation Effects.

There is also a considerable body of knowledge in the literature[1,2,3,et.al.] relating to radiation damage centers in bulk semiconductor materials. However, most of and the best of this work has concentrated on using radiation damage as a tool to create new types of defect structures which could then be studied to gain improved understanding of solid state physics. Although this work provides excellent background knowledge for

the work described herein, there has been little previous attention given to the question of how this knowledge might be applied to improving the radiation damage resistance of the bulk material. Once again the literature is too extensive to cite individually, but an excellent overview can be found in the book cited as REF 1 and the works cited therein.

A third body of knowledge comes from research on annealing of defects in neutron transmutation doped silicon.[4,5,6] Although, the work cited in REF's 4,5,6 (and the references cited therein) has concentrated primarily on techniques for annealing and gettering the radiation damage caused by fast neutrons and the displaced transmuted Si/P, it also provides a good background of knowledge for this research.

The emergence of intense interest in silicon detectors for particle physics research has initiated a number of studies on radiation damage of silicon detectors.[7,8,9,10] Many of these studies have been reported at topical conferences or workshops and are not available in the open literature. The bulk of this work has been phenomenology focused on device leakage currents and depletion voltage changes, with little convincing evidence to establish the specific defect centers responsible for the GR current and compensation level changes.

We previously reported[11,12] on a study of the changes in compensation levels in Si resulting from fast neutron damage. This work concentrates on the effects of B and P (which are the major electrically active impurities in detector grade Si) and proposes a model to explain both first order effects from simple hydrogenic type defects like boron

and phosphorous and second and third order effects such as those caused by oxygen. Among other facts, this publication delineates the limits of potential usefulness of neutron transmutation doping for detector production. Perhaps more importantly, it shows that the original concentrations of P and B can be estimated by analysis of the curve of N (the net uncompensated impurity density) vs neutron fluence (Φ).

A major uncertainty associated with the completeness of existing detector radiation damage studies results from the fact that almost all of the experiments have been done on Si crystals from a common manufacturer using n-type material and some variations on the "Kemmer Process" for oxide passivation. If radiation hardness is the goal, the selection of n-type (P-doped) material is surprising since removal of active P by formation of E-centers (the P-Vacancy center) and by formation of interstitial P is very efficient and results in major spatial variations in the compensation level (see figures in REF 11). The historical use of n-type material results from the fact that the "single-pass" FZ material available from Wacker[13] and Topsil[14] tends to be n-type and because oxide passivation produces lower leakage currents on n-type material. The excess P which is responsible for the n-type doping can be removed by multiple float zone passes, but this would add significantly to the cost if existing FZ equipment designs and processes are used. None-the-less, such an approach may be appropriate in some applications, especially for drift chambers.

TECHNICAL CONSIDERATIONS

One problem associated with any device oriented discussion of "radiation damage" or "radiation hardness" is the fact that the definition of these terms is application specific. Consequentially, considerable care needs to be used in interpreting the relevance of radiation damage studies. As the short and intermediate term detector needs have become more well defined, our attention has focused more on the problems of tracking devices where both bulk and surface related damage play an important role.

Damage induced by ionizing radiation at the surface of the device can play a significant role even in large volume radiation detectors if it results in edge effects (at the edge of the junction) which cause excess leakage current or low breakdown voltage. However, it seems fairly well established that fast neutron induced bulk damage will remain a major problem. Therefore, this study will focus on bulk damage problems which result in charge trapping, compensation level changes, and generation current noise. The resulting knowledge will be directed towards perfecting radiation hardened detector grade Si and improved detector design. However, there are also important interactions between changes in the bulk properties and surface problems which will also be addressed.

Most of the radiation damage studies of silicon detectors have focused on the problem of excess current noise from GR current caused by radiation induced GR centers. In high luminosity machines with high repetition rates, the problems of charge

trapping and compensation level changes are more serious than leakage current for the following reasons[10]: Generation of leakage current by GR centers is a two step process requiring sequential thermionic emission and capture of both holes and electrons. In silicon (band gap of 1.1 eV) only GR centers near the center of the forbidden gap are efficient producers of GR current. The variation of current with temperature is of the form

$$I = I_0 e^{-E/kT}, \qquad \text{Eq. 1}$$

where T is the absolute temperature and E is the distance from the energy level of the GR center to the most distant band gap edge. As a consequence, the current is very temperature sensitive and even modest cooling can produce large reductions in current. Thus, in many systems, even modest cooling can reduce the leakage current noise problem to a manageable level in spite of considerable radiation damage.

The importance of leakage current noise also decreases rapidly as the amplifier shaping time is decreased to obtain improved time response from the detector system. For a two microsecond shaping time constant, the noise from 20 μA of radiation damage induced detector leakage is a relatively serious problem but at 20 nanoseconds shaping time the series noise from the preamplifier input will dominate. Thus, for fast detector systems, leakage current noise may not be the major problem and compensa-

tion level changes and charge trapping will become the dominate radiation hardness considerations.

The charge trapping problem may become worse as the operating temperature is lowered and as the amplifier shaping time is decreased until the point where the temperature gets so low that the traps remain frozen full. Therefore, in any particular application there may be an optimum operating temperature that balances the effects of leakage current noise and charge trapping. In applications which permit this type of optimization, both current and trapping radiation hardness will be important.

Radiation damage in high purity silicon occurs when scattering interactions result in the displacement of Si atoms from their normal site in the lattice. In the case of high energy neutrons, the energy transfer can be large enough to result in a cascade of interactions which tend to leave a dense cluster of damage. The primary radiation damage induced defect in bulk silicon is a silicon interstitial (Si_i) and a vacancy (V) which are referred to as a Frenkel Pair. Silicon radiation detectors with deep sensitive depths must be made from very high purity and very perfect crystals with electrically active impurities in the parts per billion or less range and non active defects in the parts per million or less range. In such high purity material, essentially all of the primary damage from fast neutrons, charged particles, etc. results from nuclear recoil reactions with the Si atoms with a resultant cascade of self interstitials and vacancies (Frenkel pairs). This being the case, one could reasonably ask how such material could possibly

be radiation hardened. The answer lies in the fact that neither the Si self interstitial nor an isolated vacancy are stable in a Si crystal.[15] The Frenkel Pair is not stable in Si and quickly disappears either by self annihilation (the majority of the time) or by interaction with some other defect. Si_i is very unstable and anneals athermally by ejection of an impurity from its substitutional site or by forming some type of complex. An isolated vacancy is stable only at cryogenic temperatures, so at room temperature it quickly disappears by interacting with some other defect. The resulting defect structures can involve other defects which were initially present in the crystal, pairing or clustering with other radiation induced defects or a combination of both mechanisms. It is these "secondary" sites that are responsible for many of the observed radiation damage effects. The end result should therefore be expected to be dependent on the original defects and their distribution, and therefore on the impurities and thermal history of the crystal. Consequently, the symptoms of radiation damage can be sensitive to small (ppm to ppb) concentrations of elemental impurities and structural defects which were present in the original crystal. Also to be considered are the primary damage cluster sites which may remain as small highly disoriented regions in the crystal (c.f., description of the Model of Terminal Clusters in REF 11).

An important part of our program is to systematically examine the impact of the most common defects (impurities & structural) on the radiation hardness of fast neutron damaged Si. Some of the impurities which may play an important role are P, B, O, C, N,

and H. Some potentially important structural defects are the divacancy, uncondensed vacancy clusters, swirls of vacancy clusters and extended complexes, and terminal radiation damage clusters. Dislocations, which are normally an excellent sink for vacancies and other defects, are not present in high quality, large diameter Si crystals.

The ubiquitous divacancy is near the center of the gap and is difficult to distinguish from the E-center which was mentioned above. Oxygen is known to be particularly active in the presence of free isolated vacancies such as those formed thermally at elevated temperature or formed by radiation damage. One reason why the integrated circuit industry has switched from Float Zone (**FZ**) crystal (low oxygen content) to Czochralski (**CZ**) crystal is because the oxygen in CZ material acts as an effective internal impurity getter during the thermal processing of LSI wafers. Oxygen is also responsible for the radiation induced A-center (oxygen-vacancy) which may act as an electron trap and for the formation of oxygen-vacancy pairs which act as shallow donors. H can be used to passivate radiation damage in bulk Si[16] but can also produce unwanted GR centers.[17]

Leakage Current: It has become rather common practice to characterize the leakage current of a damaged detector by the simple equation

$$I = I_0 + a_n \Phi \qquad \text{Eq. 2}$$

where I_0 and I are the currents before and after irradiation, Φ is the neutron fluence, and a_n is the "leakage current constant". The results of various investigators have shown values of a_n that vary by a factor of 2.[7] We do not think that agreement or lack of agreement in these previous numbers is that significant for the following reasons: (1) most of the deep depletion test devices were made from n-type FZ material, mostly from the same manufacturer, (2) most of the devices had similar high temperature processing histories, (3) different radiation sources were used, raising the issues of the effect of neutron energy distribution and dosimetry accuracy, (4) some of the studies did not make corrections for room temperature annealing effects and (5) the question of how these effects vary with temperature and with electric field applied during irradiation have not been adequately addressed.

More recent evidence[18] shows an abrupt change in the value of a_n when the Si passes from n-type to p-type as a result of radiation damage. This effect could be caused either by the fact that the recombination process becomes more efficient when the Fermi Level passes through mid-gap or/and by an increase in surface generated current when the Si at the oxide interface becomes depleted when the material changes to p-type.

No definitive or convincing evidence exists to identify the GR centers responsible for the leakage current problem. However, our work[11,12] together with other general evidence[18,19] permit some informed speculation about their origin. None of the known boron related states which result in deep levels near mid-gap are stable at room tempera-

ture. The phosphorous-vacancy pair (E-Center) forms a stable deep level in the gap; however, according to our work,[11] formation of E-centers should saturate well below neutron fluences of 10^{13} cm^{-2}. Since the linear behavior of Eq. 2 continues to higher fluences, it would appear that the E Center is not the dominate factor in the leakage current problem. Of the known centers which might be involved, this leaves the divacancy, oxygen-vacancy complexes, and primary terminal damage clusters (highly disordered damage clusters at the primary interaction origin) as prime suspects. The complex nature of the self annealing time constants makes us suspect the slow breakup of terminal damage clusters may be involved.

Compensation Level Changes: Radiation damage induced changes in compensation level will cause changes in depletion voltage, field strength distribution, and conductivity type.

The depletion depth (sensitive depth) of a partially depleted Si detector is given by,

$$W = a\, V^{1/2}\, |N|^{-1/2}, \quad N = N_d - N_a, \qquad \text{Eq. 3}$$

where, W is the depletion depth, V is the applied bias voltage, N_d is the density of donor centers and N_a is the density of acceptor centers.

Since the equation for the resistivity of Si is of the form,

$$\rho = b\,N^{-1}, \qquad \text{Eq. 4}$$

Eq. 3 can be expressed as,

$$W = c\,[V\,\rho]^{1/2}\,. \qquad \text{Eq. 5}$$

The value for b, and therefore c, depends on the mobility of the electron or hole, as the case may be, and therefore is different for p-type material and n-type material. Confusion from this difference will not occur if we talk about N and Eq.3 rather than ρ. Measurement of the resistivity of the material or measurement of the capacitance voltage characteristics of a diode can determine N but not N_d or N_a. However, we have shown[11] that progressive measurements of N vs Φ can be analyzed to obtain values for the original concentrations of P and B, i.e., N_d and N_a.

If W is fixed, and we set a practical operating limit on V, there will be a range of N over which a totally depleted device is possible. For W of 400 μm and V of 250 volts, the upper useful limit on N is 10^{12} cm^{-3}. Within this range, it does not matter in principal whether the material is n-type or p-type if all that is required is simple depletion of the device. Calorimeter pad detectors fall into this simple category; however, some device

designs, e.g. drift detectors, require uniform electric fields in a known direction and will therefore be very sensitive to changes in the compensation level induced by radiation damage. Bias voltages of higher than 250 volts and sensitive depths of less than 400 μm are of course possible and we will use these values only as examples of the practical limit.

Previous reports of measurements at BNL, CERN, Tennessee, and Hamburg were in contention about whether Si did actually invert to p-type as a result of neutron damage. Measurements at BNL with p^+np^+ structures and the sign of accumulated charge on MOS structures indicated that the Si remains n-type. Our measurements of conductivity type using our cryogenic probe indicated that the material did convert to p-type.

Measurements, at Hamburg and CERN, of the saturation of the pulse height for short range alpha particles incident on the front and rear contacts indicated that the material type did invert. Capacitance-voltage characteristics, which are a good way to determine N in undamaged Si whose resistivity is not too high, were measured by both groups. Not surprisingly, both groups found anomalous behavior which was frequency dependant. There are many practical and fundamental considerations which limit the usefulness of C-V measurements at these very high resistivity levels.[12]

It is now generally agreed that the material does change to p-type with sufficient neutron damage. However, the reasons for the earlier anomalous results have not been

resolved. One phenomenon which would explain both sets of results would be a thin n-type layer at the surface of the device while the bulk of the material was p-type. One possible cause for such a layer could be the formation of oxygen-vacancy complex donors[11] in an oxygen rich surface layer. The temperature and gas ambient during thermal oxidation of the wafers are in the range where significant quantities of oxygen may diffuse into the surface during detector fabrication. Formation of such layers could have important effects on device performance, particularly for tracking devices, through several mechanisms. Formation of an n-type layer under the oxide could affect edge leakage current and voltage breakdown. It could also have a major impact on the inter-electrode capacitance and leakage on tracking detectors. Formation of n-type layers under the detector contacts (where the oxide layer has been removed) would convert the structure from $p^+\nu n^+$ or $p^+\pi n^+$ to $p^+n\nu nn^+$ or $p^+n\pi nn^+$; (ν and π are conventionally used to represent very high resistivity p-type and n-type material respectively). Such a change in structure could have important effects on device performance.

We believe REF 11 settles the issue about type conversion in bulk material which has not been enriched with oxygen as a result of oxide passivation, but confirmation of the presence or absence of n-type layers remains an important issue.

It is well known that the formation, annealing, and spatial drift characteristics of some defects in Si are affected by electric field, free charge carrier density (leakage current), temperature, and the rate of introduction of free vacancies and self interstitials

(i.e., radiation damage rate). Therefore, at some point studies will need to be extended to determine the possible influence of these other variables.

Long Term Compensation Level Annealing: Recently, the problem of "reverse annealing" has become a major concern because the experimental data suggest that the long term changes in the compensation level of neutron damaged Si was much larger than previously thought based on data taken shortly after damage. The term "reverse annealing" needs some explanation. In earlier work at the University of Hamburg, it was observed that changes in the depletion voltage drifted partially back towards their original value during short intervals of the order of weeks. This effect was understandably characterized as annealing with the presumption that the damage was somehow reversing itself. It was later discovered that this trend reversed itself and ΔN eventually became much worse than immediately after the irradiation (with a time constant of many months).[18] This trend towards lower p-type resistivity even after irradiation is stopped has disturbing implications. The CERN collaboration concerned with LHC apparently considers this to be a very serious problem and has devised detailed scenarios and forecasts to predict the implications of "reverse annealing."[19] Some of these plans require the detectors to be cooled during beam-off periods.

We agree with the potential seriousness of the problem, but are uncomfortable with the term "reverse annealing" since we think its implications confuse what is actually happening. Therefore, we will refer to this problem as long term annealing. Previous

data on the long term annealing problem were obtained primarily by extrapolations of the shapes of capacitance-voltage characteristics to estimate the depletion voltage.[18-19] We have confirmed the existence of long term annealing towards more p-type material by independent measurements of resistivity and conductivity type changes for a number of Si samples with different origins and original characteristics. These results are summarized in Figures 1 through 8 and in Table 1.

Before proceeding with a discussion of the figures and table, we will describe a simple model we have developed to explain the long term annealing effect. In our earlier work, we developed a model[11] to explain the radiation damage induced changes in N. In summary, this model assumed that changes in donor (P_s) and acceptor levels (B_s) were caused by the interaction of damage induced vacancies (V) and Si self interstitials (Si_i) with the donors and acceptors. In the case of P, a vacancy can pair with P to form an E center which is no longer a shallow donor or a Si_i can eject P to an interstitial site where it is no longer a donor. In the case of B, the B-V center anneals below room temperature, so although it may be formed continuously during irradiation, it will anneal immediately. However, N_a can be reduced by the interaction of B_s and Si_i to form B_i. This model successfully fits our previous data and provides a method for determining the starting values of P_s and B_s.

We can extend this model to cover the observed long term annealing by making the simple assumption that the primary damage clusters are somewhat unstable at room

temperature and continue to evaporate vacancies over a long time period. These mobile vacancies can then find interstitial B atoms and return them to their substitutional state. This thermal break up of damage clusters to provide free vacancies is consistent with the observation that neutron damage in Ge detectors may be undetectable until after the device has been warmed up and recooled.

There are a number of simple ways that the credibility of this model can be checked. They are as follows:

♦ The magnitude of the annealing effect should be proportional to the B_s concentration in the crystal. Table 1 suggests that this is indeed the case.

♦ The reaction should be of second order since the rate of V generation is time dependant and the reaction rate also depends on the remaining concentration of B_i. The Univ. of Hamburg has made measurements that confirm a second order reaction.

♦ The effect should saturate at large neutron fluences. Figure 8, suggests that such saturation does occur.

♦ The total long term annealing effect, when saturated at large fluences, can not exceed the total B concentration in the crystal. The maximum density of B required to explain the high fluence results in Table 1 is $N_a = 4x10^{12}$ cm^{-3} a value which is not inconsistent with previous estimates of B levels in FZ crystals.

If this model proves to be correct, it has important implications since it not only makes it possible to quantitatively predict the size of the effect, but also provides the direction to a solution for minimizing the effect.

The samples shown in Figures 1-7 were all exposed to a fast neutron fluence of $1.4 \times 10^{13} cm^{-3}$. Figures 1 and 2 correspond to two low resistivity p-type FZ starting crystals that were expected to have a relatively high B content. Figure 3 corresponds to a high resistivity n-type FZ starting crystal and Figure 4 to a high resistivity p-type starting crystal. Figures 5-7 correspond to high resistivity p-type multi-pass FZ crystals.

Table 1 compares the results for the samples illustrated in Figures 1-7 and the results on detectors from REF 18. N_B is the B concentration estimated by the technique described in REFs 11 & 12. N_B calculations for 526-1, 1048-2 and 118-2 have not been completed yet. N_1 corresponds to the value of N in the period of a few weeks to one month after irradiation which is a good baseline where short term effects have subsided but long term annealing effects are still small. N_∞ corresponds to N after long term annealing is complete, i.e., after more than 12 months.

RESEARCH OBJECTIVES

The objective of this program is to increase our knowledge of the basic mechanisms and defect configurations which create the radiation damage

symptoms in Si detectors and to use this information to improve the radiation hardness of Si detectors.

Our long range goals include: the problems of leakage current generation centers which affect detector noise; charge trapping and mobility problems which deteriorate signal size and pulse rise time; and compensation level changes which affect depletion voltage, electric field distributions and surface leakage currents or breakdown problems. These studies need to be extended to included the effects of electric field, leakage current and detector operating temperature during radiation damage.

Our priority ranked goals are:

1) To check the validity of our model by extending our measurements on long term annealing of N to larger fluences and to detectors made from the special materials shown in the upper part of Table 1.

2) To verify the model which we use to determine the original concentrations of P and B in the crystal by measuring N vs Φ. We plan to do this by making damage studies on the special crystals which we have already prepared for this process (including NTD doped crystals where we accurately know the added P content).

3) To verify the presence or absence of n layers caused by the combination of radiation damage and the presence of oxygen rich surface layers generated during oxide passivation of the detector.

4) To investigate the effect of the surface depletion layer, that occurs under the oxide coating when the substrate switches from n- to p-type, on the inter-electrode capacitance and conductance in tracking detectors.

(5) To complete the study on compensation level changes by studying the effects of oxygen, vacancy swirls, nitrogen, carbon and hydrogen. We already have special crystals with swirls and elevated nitrogen.

(6) To extend our current work to include charge trapping centers and charge carrier mobility problems.

(7) To identify the nature of the dominate GR centers which are responsible for the leakage current and if they are vacancy related, to see how they are affected by the concentration of oxygen, etc..

(8) To study dynamic effects from fluence rate, electric field, etc.. . . .

RESEARCH PLAN

We plan to compare the fast neutron radiation damage characteristics of several sources of silicon crystal made by different manufacturing process and containing different defects and impurities. A pragmatic study of the properties of radiation damaged detectors is a good way to make sure important effects are not overlooked. However, the interpretation of the underling reasons for the detector related symptoms is sometimes difficult. Our program is unique in that we study the properties of the

material itself rather than simply trying to infer these properties from device performance. It is also unique because we intentionally study materials with different origins, crystal growing techniques and known defect levels to gain a better understanding of the radiation damage process. However, we are also cognizant of the advantages of studying actual detectors and IntraSpec, Inc. is now in a position to polish, oxidize, and fabricate detectors from special Si crystals in our own facilities. We intend to use this capability in parallel with our other measurements to study the long term N annealing problem. In fact, we have already produced oxidized wafers from some of the special materials shown in Table 1 and sent them to the University of Hamburg for collaborative study. The resulting detectors have been irradiated and are now undergoing annealing studies in Hamburg.

In addition to the detector assembly clean room facilities and conventional techniques for characterizing the performances of Si detectors which are available at the University of Tennessee, we plan to employ the following specialized measurement and Si processing technologies available at IntraSpec, Inc. (ISI): (1) a cryogenic thermoelectric probe which can be used to distinguish between very high resistivity p and n type material. We have previously used this instrument to delineate p and n type regions in the same Si crystal at the >200 K ohm-cm ($< 10^{11}$) level,[12] (2) a resistivity probe to profile Si resistivity at the > 200 K ohm-cm level, (3) instrumentation for measuring room temperature Hall coefficients at very high resistivities, (4) contactless technique for

measuring charge carrier lifetimes, (5) variable frequency three-terminal small-signal capacitance measurements, (6) clean room and furnace facilities for oxide growth, crystal heat treatment and specialized detector fabrication, (7) technology for adding P dopant by neutron transmutation doping.

The ORELA facility at Oak Ridge National Laboratory (ORNL) will continue to be used as a 1 MeV fast neutron source to induce radiation damage. The reactor at North Carolina State University will be used as a thermal neutron source for neutron transmutation addition of controlled levels of P doping. The Deep Level Transient Spectroscopy (DLTS) equipment at ORNL is available for this project if needed.

We plan to add capability for: (1) low temperature Hall coefficient measurement, (2) isochronal annealing studies to identify defects by their annealing temperature, and (3) temperature dependance of leakage current to help identify the sources of GR leakage current.

REFERENCES

1. S. T. Pantelides - Ed., **Deep Centers in Semiconductors - A State-of-the-Art Approach,** Gordon & Breach Science Publishers, New York (1986): QC 611.6.D4 D418

2. R. R. Hasiguti - Ed., **Lattice Defects in Semiconductors**, University of Tokyo Press, Tokyo.

3. D. S. Billington and J. H. Crawford, **Radiation Damage In Solids**, Princeton Univ. Press (1961).

4. R. D. Larrabee - Ed., **Neutron Transmutation Doping of Semiconductor Materials**, Plenum Press, New York.

5. J. M. Meese - Ed., **Neutron Transmutation Doping in Semiconductors**, Plenum Press, New York (1978): QC 611.6.D6 I57

6. J. Guldberg - Ed., **Neutron-Transmutation-Doped Silicon**, Plenum Press, New York (1980): QC 611.6.06 I57

7. M. Hasegawa et al, **Nucl. Inst. & Methods**, A277 (1989), 395-400.

8. E. Fretwurst et al, **Nucl. Inst. & Methods**, A288 (1990), 1-12

9. E. Beuville et al, **Nucl. Inst. & Methods**, A288 (1990), 68-75

10. John Walter, unpublished proceedings of L* workshop, Oak Ridge National Laboratory, September, 1989

11. I. Tsveybak, et al, **IEEE Trans. Nucl. Sci.**, Vol39, No. 6 (1992), 1720-1729

12. J. Walter, et al, Invited Paper at the 1993 Spring Meeting of **The Materials Research Society**, to be published in the proceedings

13. P. Dreier, **Nucl. Inst. & Methods**, A288 (1990), 272-277

14. Personal communication, Karsten Nielsen

15. G. Watkins, THE LATTICE VACANCY IN SILICON, Chapter 3 of S. T. Pantelides - Ed., **Deep Centers in Semiconductors - A State-of-the-Art Approach,** Gordon & Breach Science Publishers, New York (1986): QC 611.6.D4 D418

16. S. T. Estreicher, **SERI Workshop On The Role Of Point Defects/ Defect Complexes In Silicon Device Fabrication,** Aug 30-31,1990

17. T. Ciszek, Personal communication

18. R. Wunstorf, Doctoral Thesis, University of Hamburg, 1992 (in German)

19. E. Fretwurst, et al, Contribution to the Int. Symp. on Development and Applications of Semiconductor Tracking Detectors, Hiroshima, Japan, May 1993, to be published in **Nucl. Inst. and Methods**

FIGURE CAPTIONS

FIGURE 1: LONG TERM ANNEALING OF COMPENSATION IN FAST NEUTRON DAMAGED SILICON WITH HIGH B CONCENTRATION (wafer 1090-78)

FIGURE 2: LONG TERM ANNEALING OF COMPENSATION IN FAST NEUTRON DAMAGED SILICON WITH HIGH B CONCENTRATION (wafer 526-1)

FIGURE 3: LONG TERM ANNEALING OF COMPENSATION IN FAST NEUTRON DAMAGED HIGH RESISTIVITY N-TYPE SILICON (wafer 1048-2)

FIGURE 4: LONG TERM ANNEALING OF COMPENSATION IN FAST NEUTRON DAMAGED HIGH RESISTIVITY P-TYPE SILICON (wafer 118-02)

FIGURE 5: LONG TERM ANNEALING OF COMPENSATION IN FAST NEUTRON DAMAGED MULTI-PASS FZ SILICON (wafer FZH-Q1-3 #2)

FIGURE 6: LONG TERM ANNEALING OF COMPENSATION IN FAST NEUTRON DAMAGED MULTI-PASS FZ SILICON (wafer FZH-Q1-3 #5)

FIGURE 7: LONG TERM ANNEALING OF COMPENSATION IN FAST NEUTRON DAMAGED MULTI-PASS FZ SILICON (wafer FZH-4A-3 #8)

FIGURE 8: SATURATION IN THE LONG TERM ANNEAL OF COMPENSATION LEVEL IN RADIATION DAMAGED DETECTORS (after Fretwurst, et. al.)

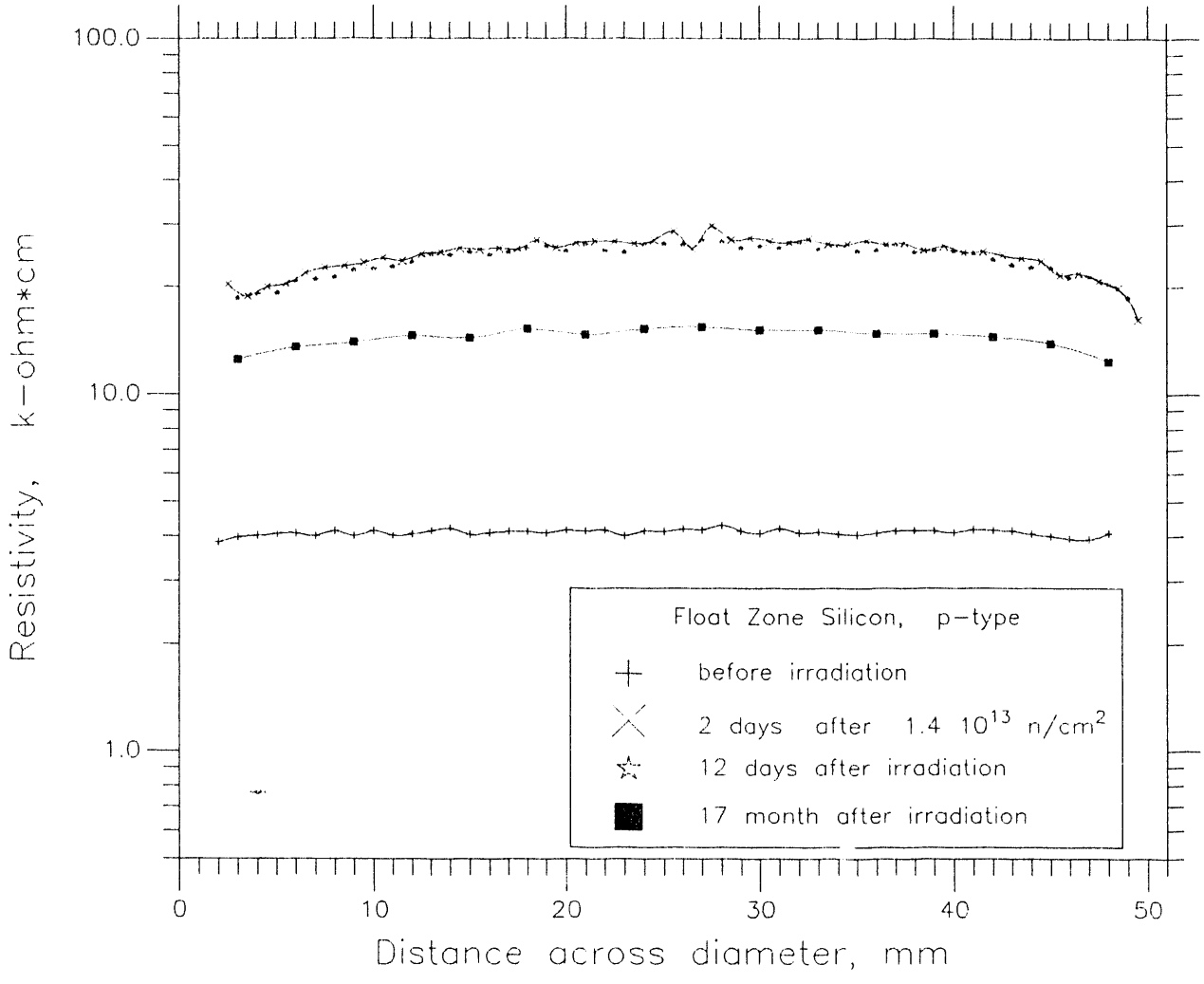

FIGURE 1: LONG TERM ANNEALING OF COMPENSATION IN FAST NEUTRON DAMAGED SILICON WITH HIGH B CONCENTRATION (wafer 1090-76)

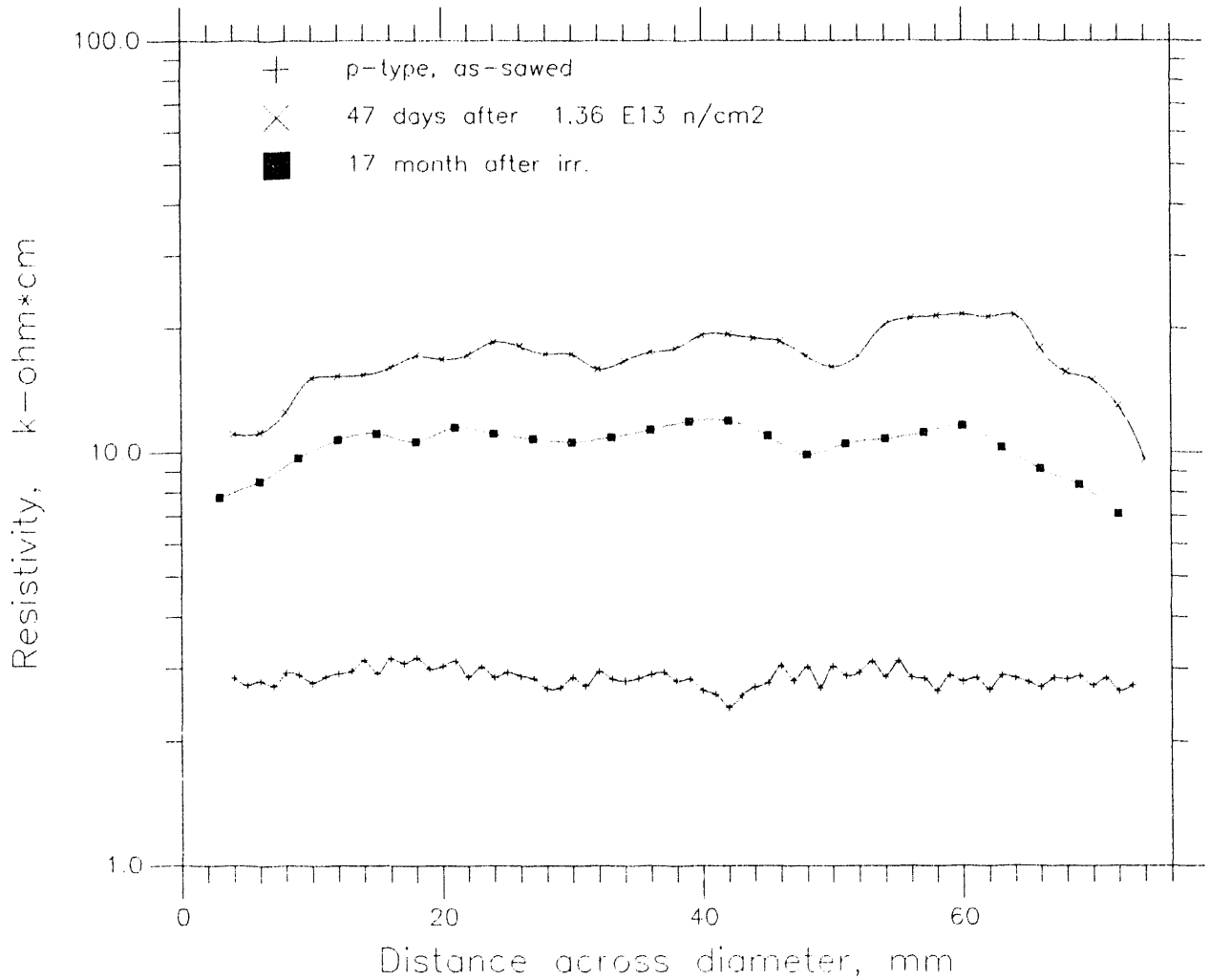

FIGURE 2: LONG TERM ANNEALING OF COMPENSATION IN FAST NEUTRON DAMAGED SILICON WITH HIGH B CONCENTRATION (wafer 526-1)

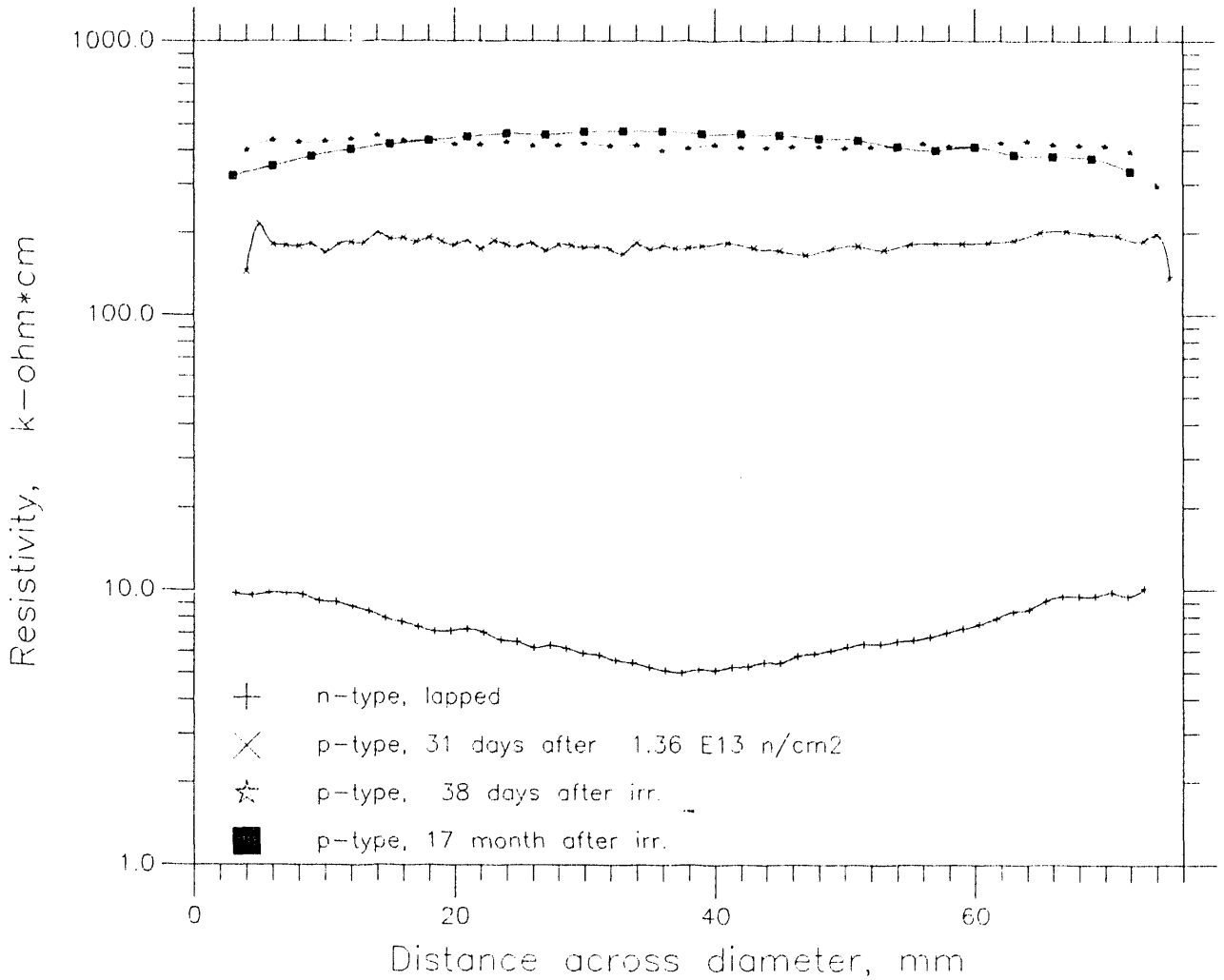

FIGURE 3: LONG TERM ANNEALING OF COMPENSATION IN FAST NEUTRON DAMAGED HIGH RESISTIVITY N-TYPE SILICON (wafer 1048-2)

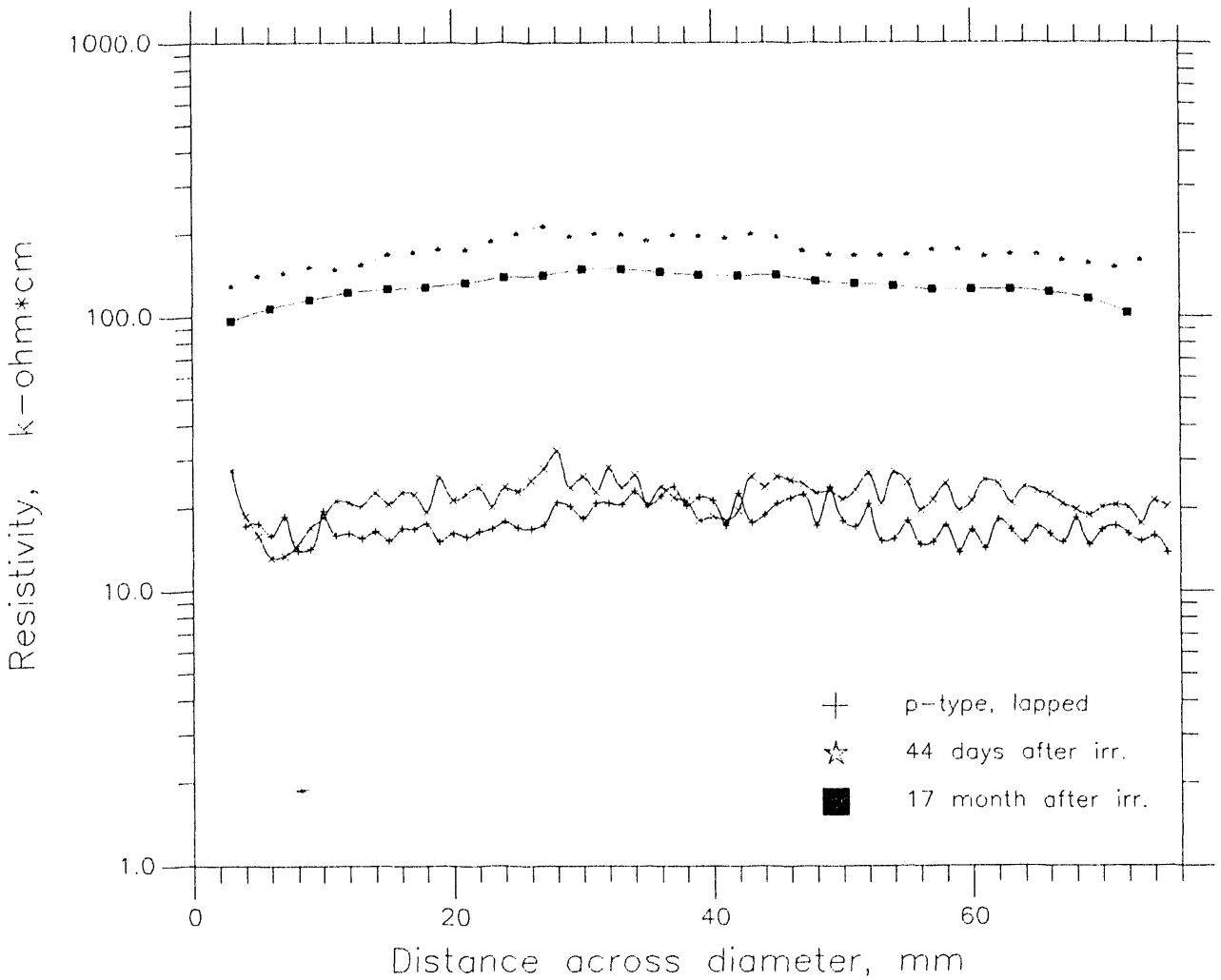

FIGURE 4: LONG TERM ANNEALING OF COMPENSATION IN FAST NEUTRON DAMMAGED HIGH RESISTIVITY P-TYPE SILICON (wafer 118-02)

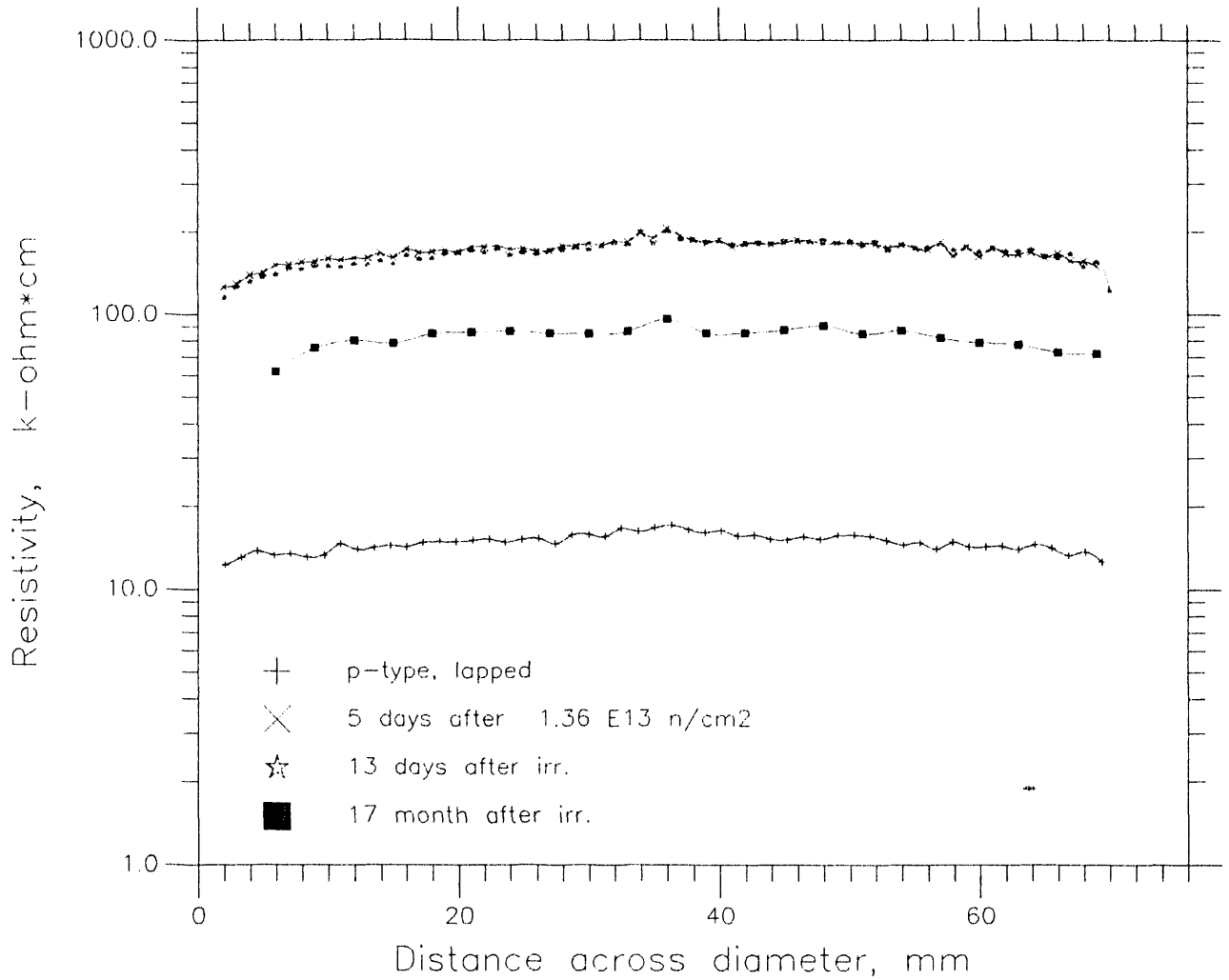

FIGURE 5: LONG TERM ANNEALING OF COMPENSATION IN FAST NEUTRON DAMAGED MULTI-PASS FZ SILICON (wafer FZH-Q1-3 #2)

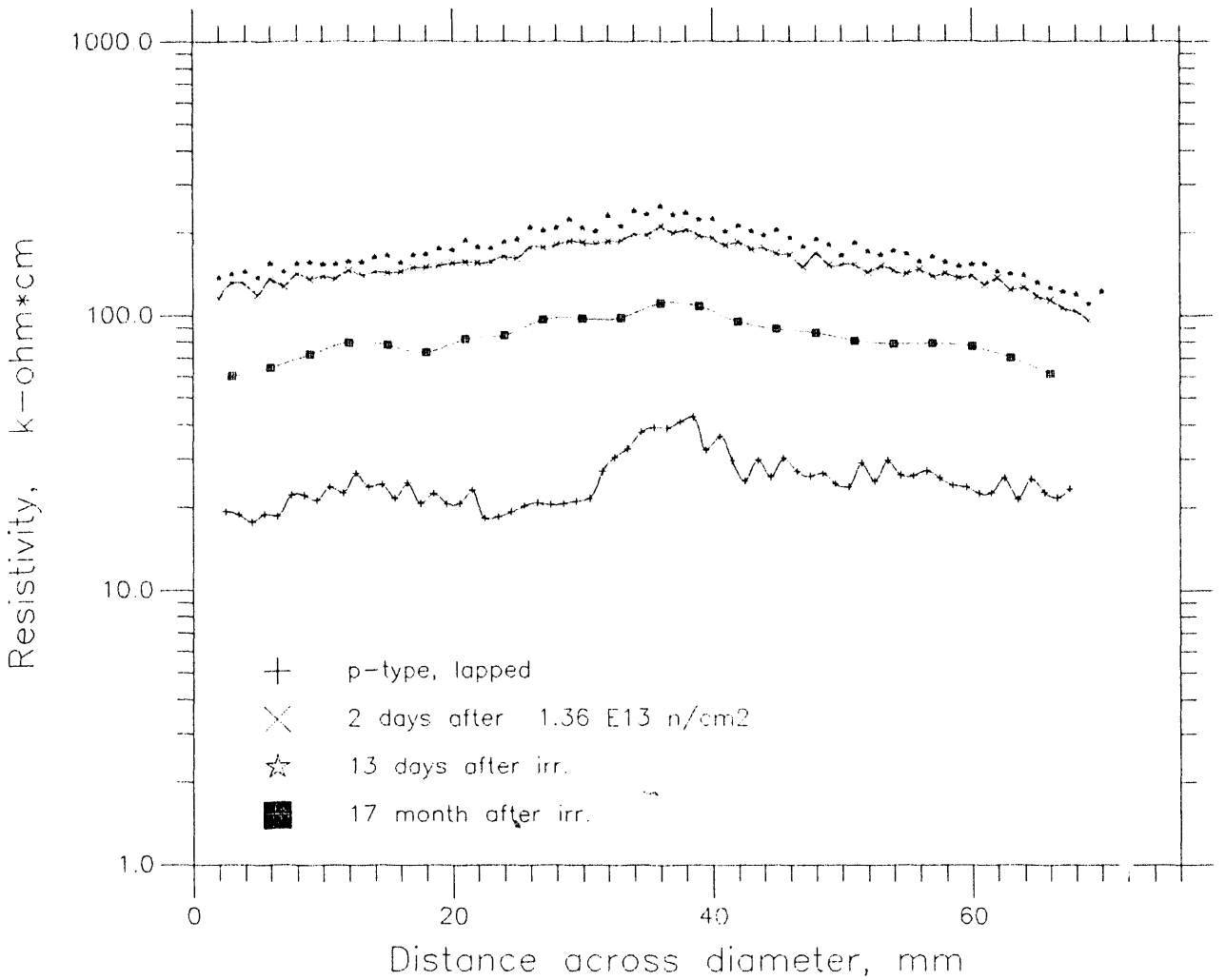

FIGURE 6: LONG TERM ANNEALING OF COMPENSATION IN FAST NEUTRON DAMAGED MULTI-PASS FZ SILICON (wafer FZH-Q1-3 #5)

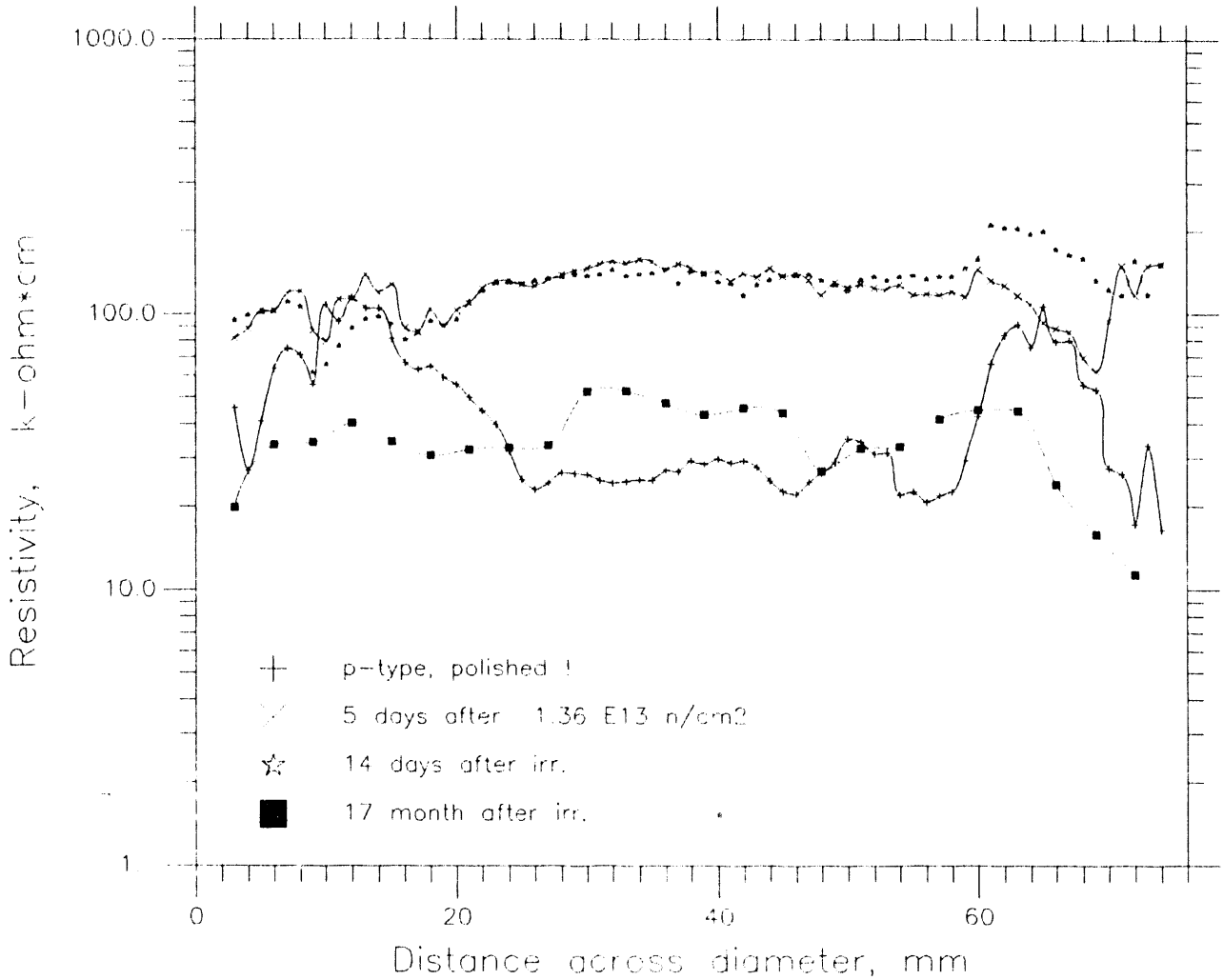

FIGURE 7: LONG TERM ANNEALING OF COMPENSATION IN FAST NEUTRON DAMAGED MULTI-PASS FZ SILICON (wafer FZH-4A-3 #8)

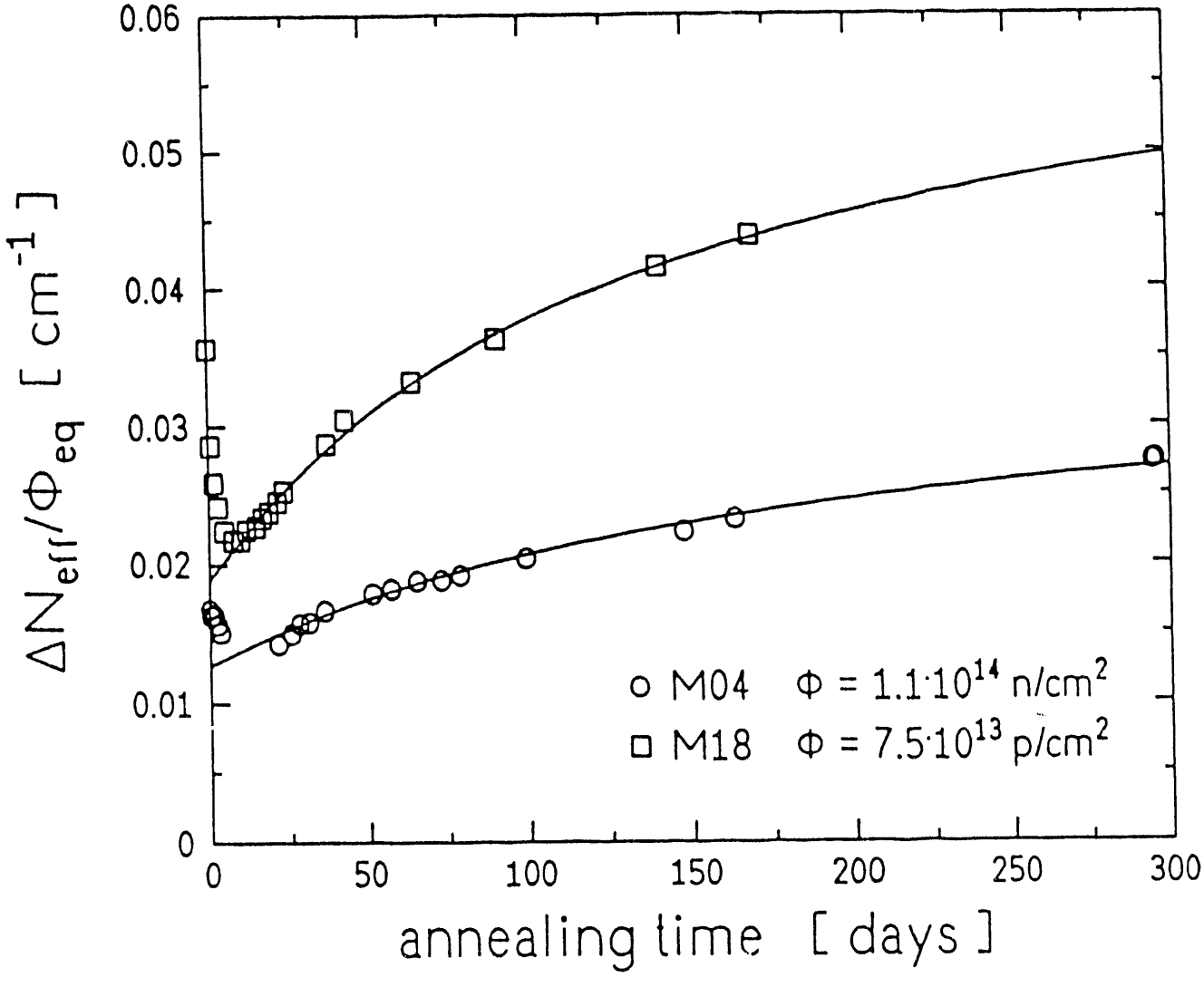

FIGURE 8: SATURATION IN THE LONG TERM ANNEAL OF COMPENSATION LEVEL IN RADIATION DAMAGED DETECTORS (after Fretwurst, et. al.)

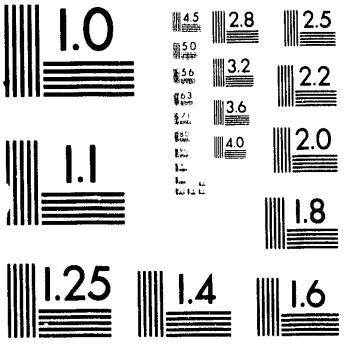
1.0
4.5
5.0
5.6
6.3
2.8
3.2
3.6
4.0
2.5
2.2
2.0
1.8
1.1
1.25
1.4
1.6

2 of 2

	Starting Material								
	ρ kOhm cm	N $10^{11}cm^{-3}$	N_B $10^{11}cm^{-3}$	Φ $10^{13}n/cm^2$	Annealing Temperature °C	N_1 $10^{11}cm^3$	N_∞ $10^{11}cm^{-3}$	$N_\infty-N_1$ $10^{11}cm^{-3}$	$(N_\infty-N_1)/\Phi$ cm^{-1}
Detector Grade Silicon Wafer:									
1090-76	4.1	-31.5	44	1.4	23	-4.9	-8.5	-3.6	-0.026
526-1	2.8	-46.4	-	1.4	23	-7.3	-10.9	-3.6	-0.026
1048-2	9.7	4.5	-	1.4	23	-0.7	-0.3	0.4	0.003
118-2	21.0	-6.2	-	1.4	23	-0.7	-0.9	-0.2	-0.002
FZH-Q1-3#2	16.5	-7.9	16	1.4	23	-0.7	-1.5	-0.8	-0.006
FZH-Q1-3#5	39.0	-3.3	12	1.4	23	-0.6	-1.2	-0.6	-0.004
FZT-4A-3#8	27.2	-4.8	23	1.4	23	-0.9	-2.3	-1.9	-0.014
Silicon Detectors*:									
901G16	8.5	5.2	-	2.1	isochronal 20-200	-	-	-6.3	-0.030
911G36	8.7	5.0	-	2.9		-	-	-8.1	-0.028
912G16	8.0	5.5	-	3.1	21	10.5	-18.6	-8.1	-0.026
M18	10.6	4.1	-	7.5 (p)	25	-18.0	-37.5	-19.5	-0.026
912G15	8.1	5.4	-	8.7	21	-23.5	-44.4	-20.9	-0.024
M04	13.3	3.3	-	11.0	25	-16.5	-29.7	-13.2	-0.012

Table 1: Comparison of the Long Term Annealing Effect in the Net Impurity Concentration N for Different Detector Grade Silicon Wafers and Silicon Detectors after Radiation Damage.

(Net impurity concentration N_1 about 1 month after irradiation, and N_∞ for the wafer 17 month resp. for the detectors about 12 month after irradiation; negative values refers to a surplus of acceptors, p-type material; N_B is the boron concentration)

*after E. Fretwurst et al., Contribution to the Int. Sym. on Development and Application of Semiconductor Tracking Detectors, Hiroshima, Japan, May 1993 (to be publ. in Nucl. Instr. & Meth.)

B. MATERIAL CHANGE IN SILICON THROUGH GAMMA EXPOSURE

I. Introduction

Material changes in Silicon (Si) targets due to exposure to high energy (gamma, γ) photons are studied in this research project. When Si is exposed to high energy photons, certain nuclear reactions take place resulting in the formation of new stable and radioactive isotopes.

Most of the isotopes that are produced as a result of high energy γ-rays interaction with Si are unstable and decay by the emission of certain characteristic γ-rays. Identification of unstable isotopes is accomplished using High Resolution Gamma Spectroscopy techniques. By combining information about γ-energies and half-lives, the isotopes can be identified and their production rates then determined. However, production rates of stable isotopes formed as photons interact with Si are evaluated using resistivity measurements.

II. Gamma Exposure

Exposure of the Si samples to γ-radiation was performed at the Oak Ridge Linear Accelerator (ORELA) of Oak Ridge National Laboratory (ORNL). Design characteristics of the ORELA are a maximum of 50 kW at an electron (e-) energy of 180 MeV with pulse rates up to 800/sec. Actual exposures of Si samples were performed at a 150 MeV beam.

The experimental setup is shown in Figure 1. After the main beam is activated, a bending magnet is used to deflect the beam in the direction of the target route, yielding 2 pulses/sec to the experimental setup. The target that receives the beam consists of a 2 Radiation Length (RL) (0.81 cm thick) Tantalum (Ta) target. The interaction of the primary beam with the Ta target results in the creation of a mixed radiation field which contains both γ-rays and e-'s. Separation of γ-rays and e-'s is achieved by allowing this mixed radiation field to pass through the magnetic field of another magnet. Because of the magnetic effect, e-'s are bent 90° downward and are no longer effectively participating in this experiment. The magnet is placed in a 20 cm long container of water to stop neutrons that may be generated.

On the other hand, the γ-ray beam is allowed to pass to the target assembly where it interacts with Si samples. These samples are placed on an X-Y scanner and/or at a fixed position 49.5 cm away from the Ta target. To prevent the interference of background γ-radiation, lead bricks are used to shield the beam line (as indicated in Figure 1). To determine the size of the γ-beam, Nickel (Ni) foils are placed in front of the Si samples; the activated Ni foils are then placed on polaroid film. The

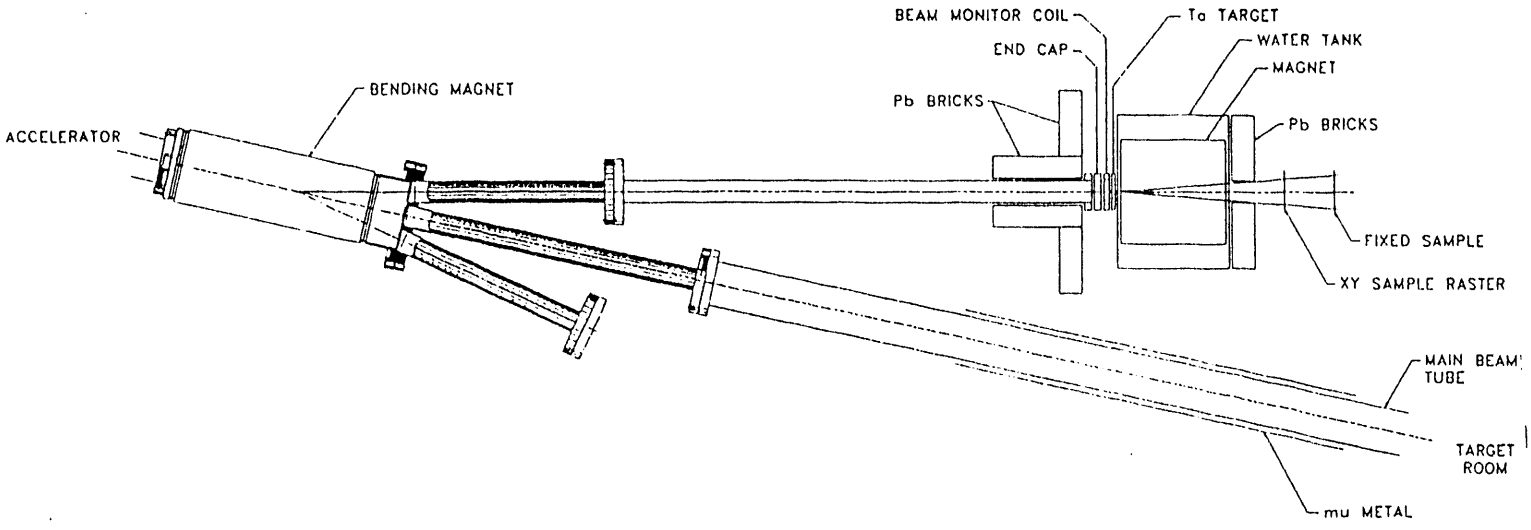

EXPERIMENT LAYOUT PLAN

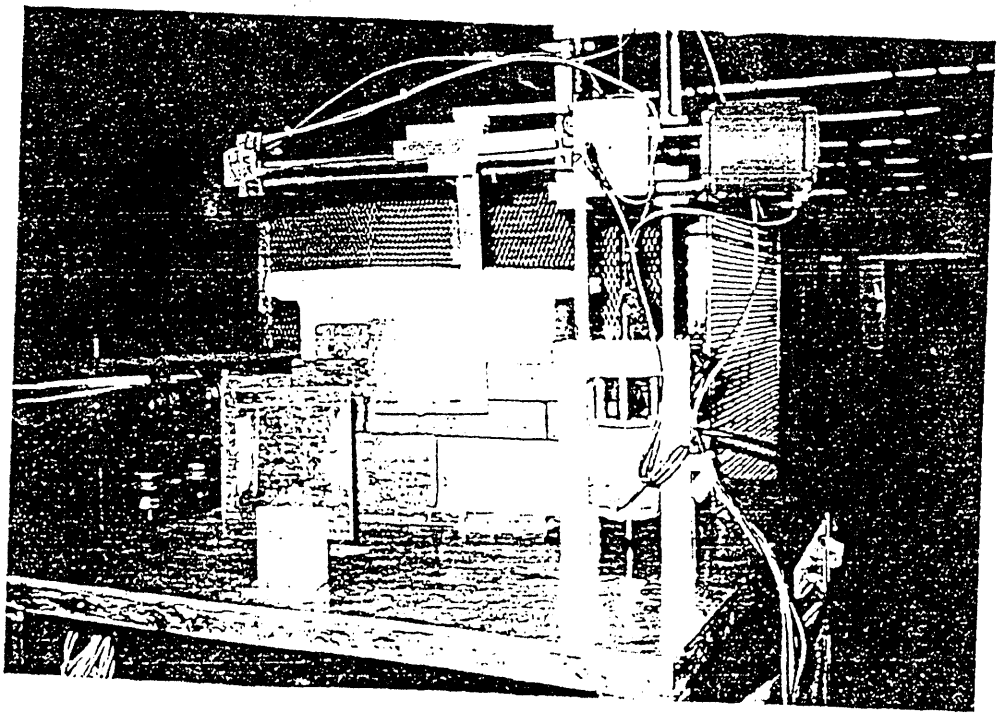

Figure 1

polaroid picture (Figure 2) shows the size of the beam, which is approximately 7 cm by 5 cm. The beam was about 1 cm to the right of the center.

Figure 2

The γ-spectrum produced by the incident 150 MeV e-'s on the Ta target (calculated by Dr. T.A. Gabriel at ORELA) is illustrated in Figure 3.

III. Material Change in Silicon

Interaction of γ-radiation with nuclei of Si yield several products, some of which are stable isotopes while others are unstable (radioisotopes). Major nuclear reactions that are of significant importance for this research are identified in Table 1. The stability status of product isotopes (i.e., stable or unstable) together with the half-life of radioactive isotopes are also included in Table 1.

^{28}Si (γ, p) ---> ^{27}Al (stable)
^{29}Si (γ, p) ---> ^{28}Al (unstable) $T_{1/2}$ (half-life): 2.3 minutes
^{30}Si (γ, p) ---> ^{29}Al (unstable) $T_{1/2}$: 6.6 min.

^{28}Si (γ, 2p) ---> ^{26}Mg (stable)
^{29}Si (γ, 2p) ---> ^{27}Mg (unstable) $T_{1/2}$: 9.5 min.
^{30}Si (γ, 2p) ---> ^{28}Mg (unstable) $T_{1/2}$: 21 hours

^{28}Si (γ, n) ---> ^{27}Si (unstable) $T_{1/2}$: 4.2 seconds ---> ^{27}Al (stable)
^{29}Si (γ, n) ---> ^{28}Si (stable)
^{30}Si (γ, n) ---> ^{29}Si (stable)

^{28}Si (γ, 2n) ---> ^{26}Si (unstable) $T_{1/2}$: 2.1 sec. ---> ^{26}Al (unstable) $T_{1/2}$: 7.4 x 10^4 years
^{29}Si (γ, 2n) ---> ^{27}Si (unstable) $T_{1/2}$: 4.2 sec. ---> ^{27}Al (stable)
^{30}Si (γ, 2n) ---> ^{28}Si (stable)

28Si (γ, np) ---> ^{26}Al (unstable) $T_{1/2}$: 7.4 x 10^4 yrs.
^{29}Si (γ, np) ---> ^{27}Al (stable)
^{30}Si (γ, np) ---> ^{28}Al (unstable) $T_{1/2}$: 2.3 min.

^{28}Si (γ, α) ---> ^{24}Mg (stable)
^{29}Si (γ, α) ---> ^{25}Mg (stable)
^{30}Si (γ, α) ---> ^{26}Mg (stable)

^{28}Si (γ, αn) ---> ^{23}Mg (unstable) $T_{1/2}$: 12.1 sec. ---> ^{23}Na (stable)
^{29}Si (γ, αn) ---> ^{24}Mg (stable)
^{30}Si (γ, αn) ---> ^{25}Mg (stable)

^{28}Si (γ, αp) ---> ^{23}Na (stable)
^{29}Si (γ, αp) ---> ^{24}Na (unstable) $T_{1/2}$: 15 h.
^{30}Si (γ, αp) ---> ^{25}Na (unstable) $T_{1/2}$: 60 sec. ---> ^{25}Mg (stable)

^{28}Si (γ, αnp) ---> ^{22}Na (unstable) $T_{1/2}$: 2.6 yrs.
^{29}Si (γ, αnp) ---> ^{23}Na (stable)
^{30}Si (γ, αnp) ---> ^{24}Na (unstable) $T_{1/2}$: 15 h.

Table 1. Production of Al, Mg, and Na due to interaction of high energy γ-rays with Silicon.

In these reactions, each radioisotope decays by the emission of γ-rays with certain characteristic energies. Measurements of γ-spectra were performed by Dr J.K. Dickens using a High Purity Germanium - based γ-spectroscopy system at ORELA. A typical spectrum that is obtained using this technique is shown in Figure 4.

The rate of production of radioisotopes is calculated by using the following decay equation:

$$N(t) = N_o e^{-\ln 2 t/T_{1/2}},$$

where: $T_{1/2}$ = Half-lives
N_0 = Initial number of Nuclei
$N(t)$ = Number of Nuclei at time t

In calculating rates of isotopic production, exposure and counting times are taken into consideration. The calculated production rates are listed in Table 2.

ISOTOPE	PRODUCTION RATE (1/sec)
^{27}Al	1.55×10^7
^{28}Al	5.77×10^5
^{29}Al	2.38×10^5
^{27}Mg	1.07×10^4
^{28}Mg	1.55×10^3
^{22}Na	6.83×10^4
^{24}Na	2.25×10^4

Table 2.Rates of Production

Impurities in Si atoms cause changes in resistivity if impurities cause shallow energy levels in the band structure. Therefore, resistivity measurements can be utilized to evaluate the production of the stable isotopes that could not be detected by γ-spectroscopy. However, since some of the elements produced are unstable with extremely short half-lives (e.g. ^{27}Si with $T_{1/2}$ of 4.2 sec which decays to the stable ^{27}Al), their production rates cannot be obtained with neither γ-spectroscopy nor resistivity measurements. On the other hand, elements with extremely long half-lives (e.g., ^{26}Al with a half-life of 7.4×10^5 yrs) cannot be detected by the γ-spectroscopy method, but their presence contributes to resistivity changes. However, in the case of Magnesium, its production could not be evaluated by resistivity measurements because Mg has no shallow energy level in the band gap. Aluminum (Al) production is calculated using resistivity measurements because the change in impurity concentration, ΔN_{eff} (directly measured by resistivity) represents the production of Al. ΔN_{eff}, Al production respectively, is calculated from resistivity measurements using:

$$N_{eff} = \frac{1}{q_o \, \mu_n \, \rho}, \quad \mu_n = 1427 \, \frac{cm^2}{V.s},$$

for n-type conductivity and

$$N_{eff} = \frac{1}{q_o \, \mu_p \, \rho}, \quad \mu_p = 480 \, \frac{cm^2}{V.s}.$$

for p-type conductivity.

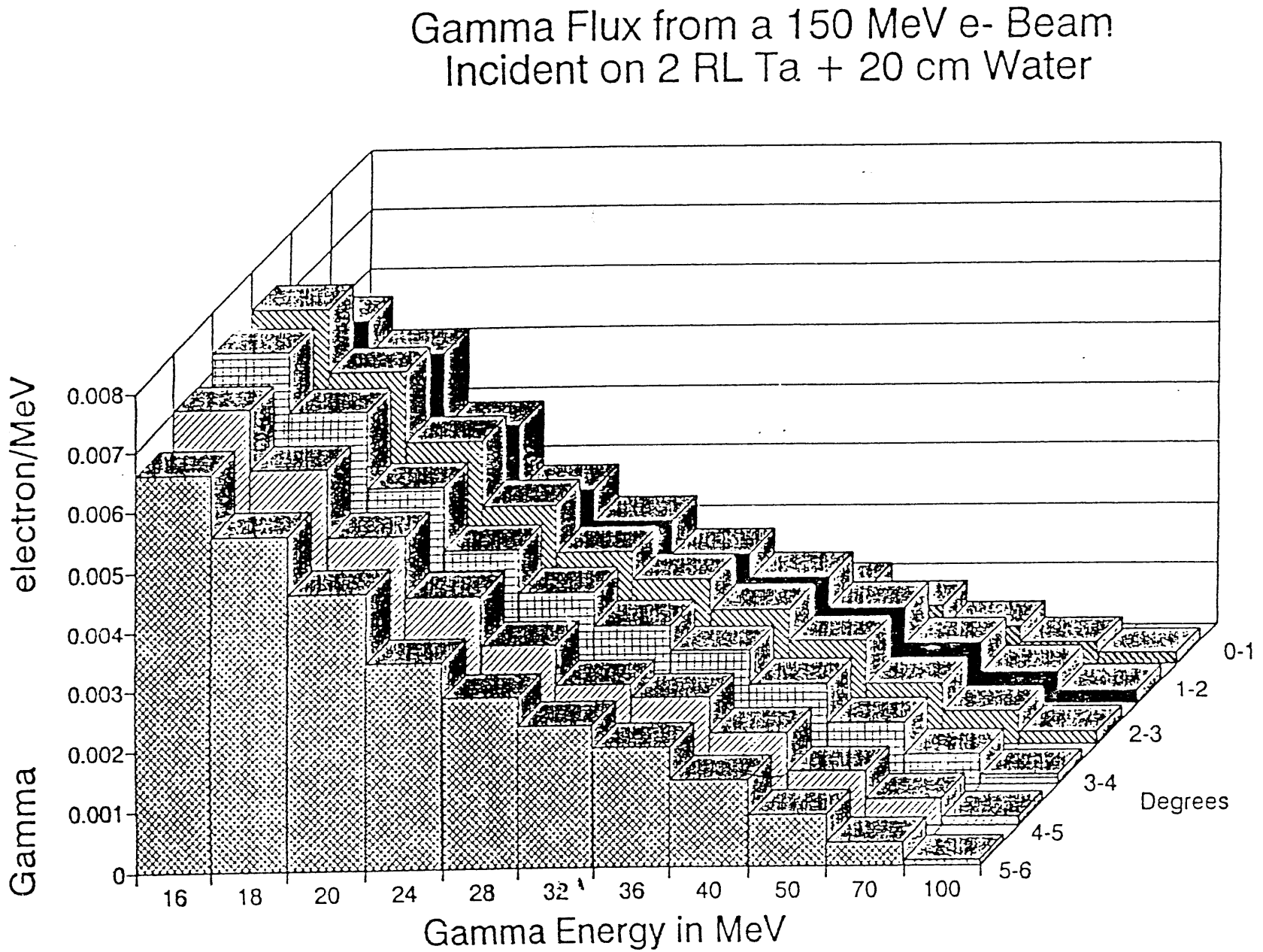
Gamma Flux from a 150 MeV e- Beam
Incident on 2 RL Ta + 20 cm Water
Gamma electron/MeV
0.008
0.007
0.006
0.005
0.004
0.003
0.002
0.001
0
16
18
20
24
28
32
36
40
50
70
100
Gamma Energy in MeV
0-1
1-2
2-3
3-4
4-5
5-6
Degrees

Figure 3

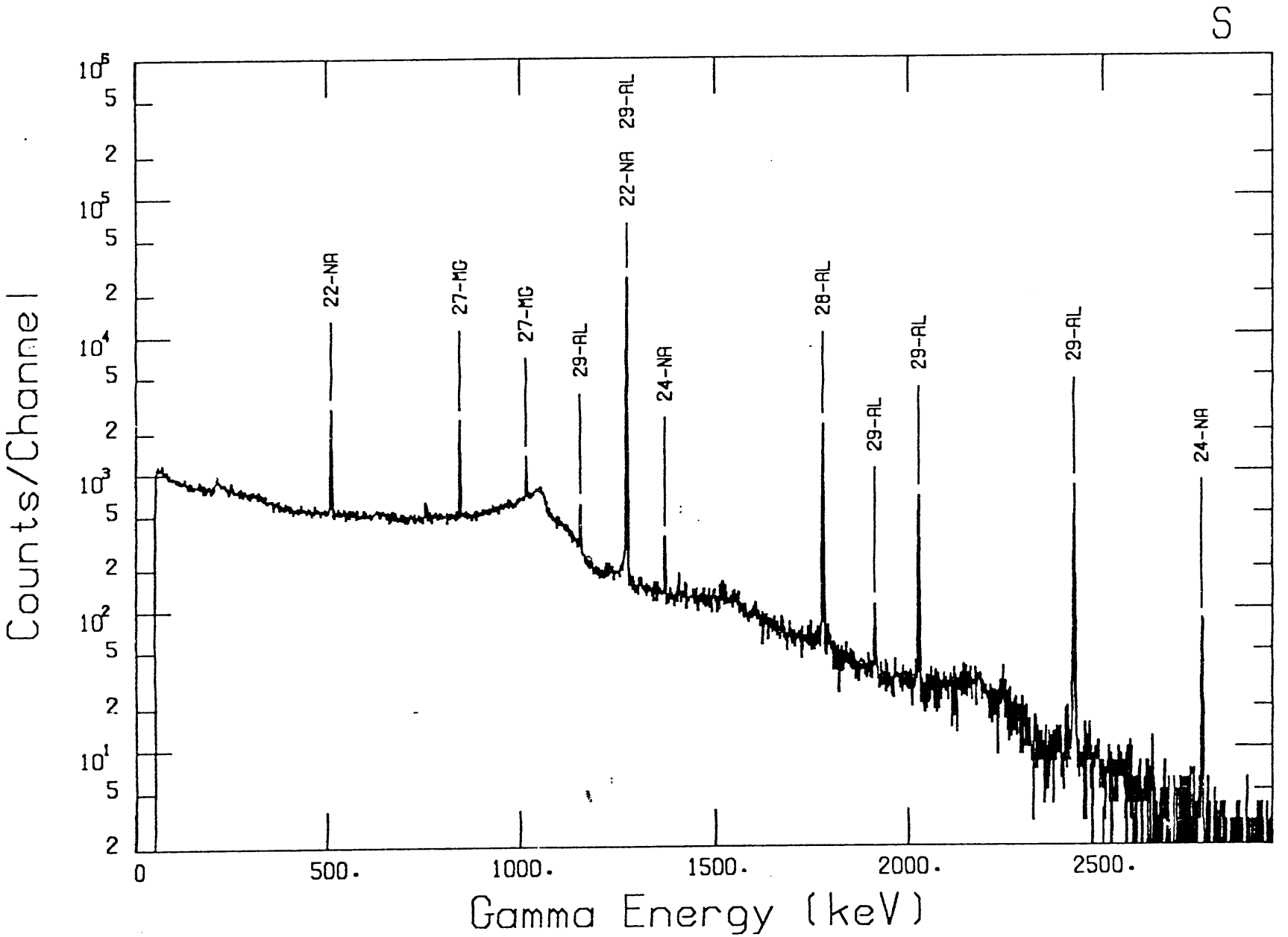
S
Counts/Channel
Gamma Energy (keV)
0
500.
1000.
1500.
2000.
2500.
22-NA
27-MG
27-MG
29-AL
22-NA
29-AL
24-NA
28-AL
29-AL
29-AL
29-AL
24-NA

Figure 4

Conductivity type of the Si was measured before and after exposure; the initial conductivity was n-type for the Si placed on the scanner and at the fixed position. However, after exposure, the sample on the scanner was mixed type (both n and p), while the sample at the fixed position was still n-type. Changes in resistivity, hence changes in ΔN_{eff}, are shown in Figure 5 for a Si sample placed on the scanner and in Figure 6 for a Si sample in the fixed position. Resistivity measurements were performed using the four-point probe method at IntraSpec, Inc., Oak Ridge, Tennessee.

IV. Conclusion

In conclusion, after exposure to γ-rays, material changes in Si do occur and other different isotopes are formed, ranging from ^{22}Na to ^{29}Al. The rates and amounts of production for these various isotopes are evaluated with the aid of High Resolution Gamma Spectroscopy and resistivity measurements.

V. Acknowledgement

The author would like to thank all the accelerator operators at ORELA for their co-operation and all the personnel at ORELA who helped obtain the final results. Furthermore, Many thanks to the staff and management of IntraSpec, Inc. for allowing the author to use their facilities, and for giving the author the chance to conduct such an interesting research and acquire valuable experience in the field of semiconductors. Also, the author would like to give a very special thanks to Dr. Renate Wunstorf whose help and advise made this research much more meaningful and interesting; without her support, it would have been difficult to complete this research in such a short time. This research project was financially supported through the Southeastern Universities Research Association for the summer of 1993.

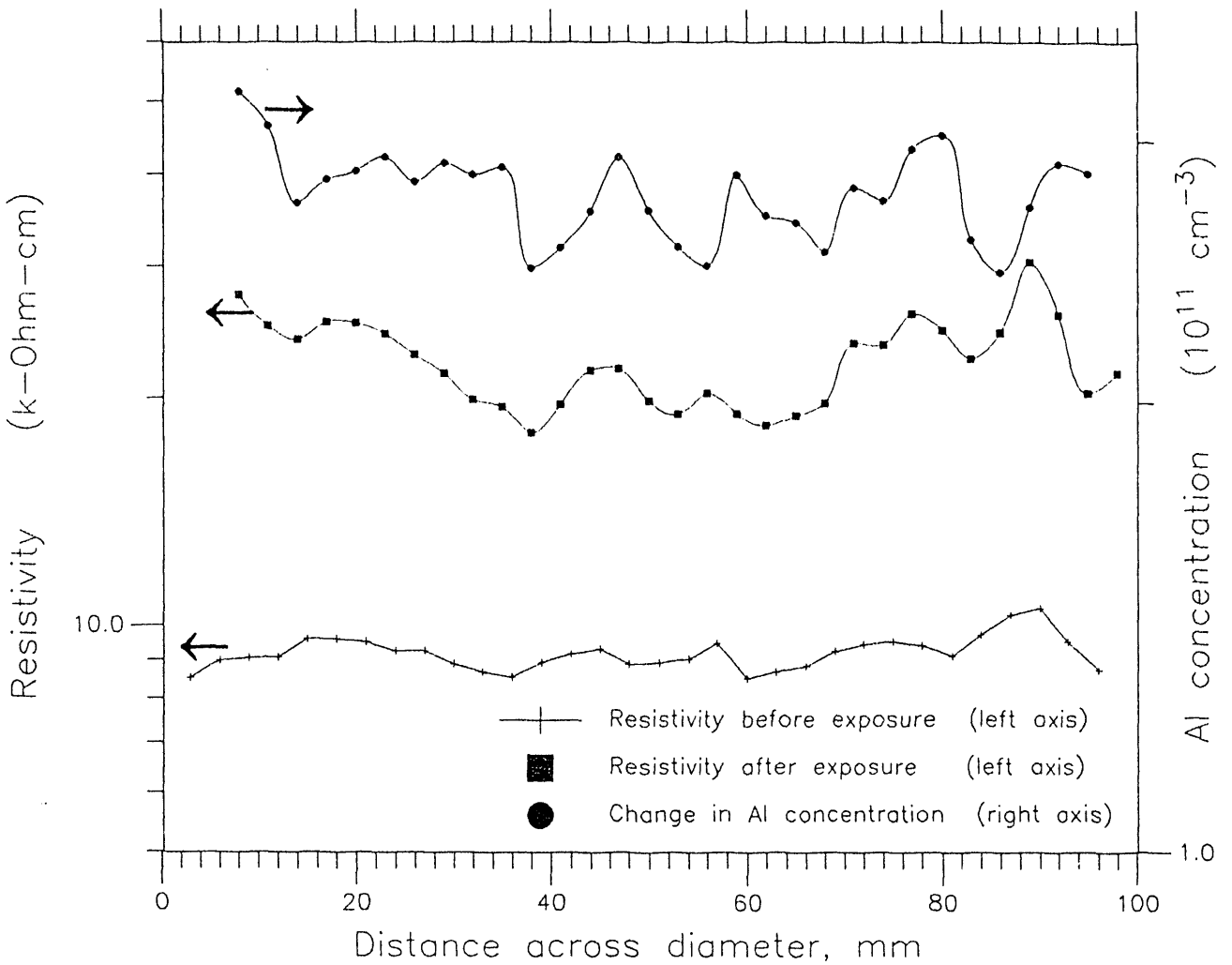

Silicon Sample on Scanner

Figure 5

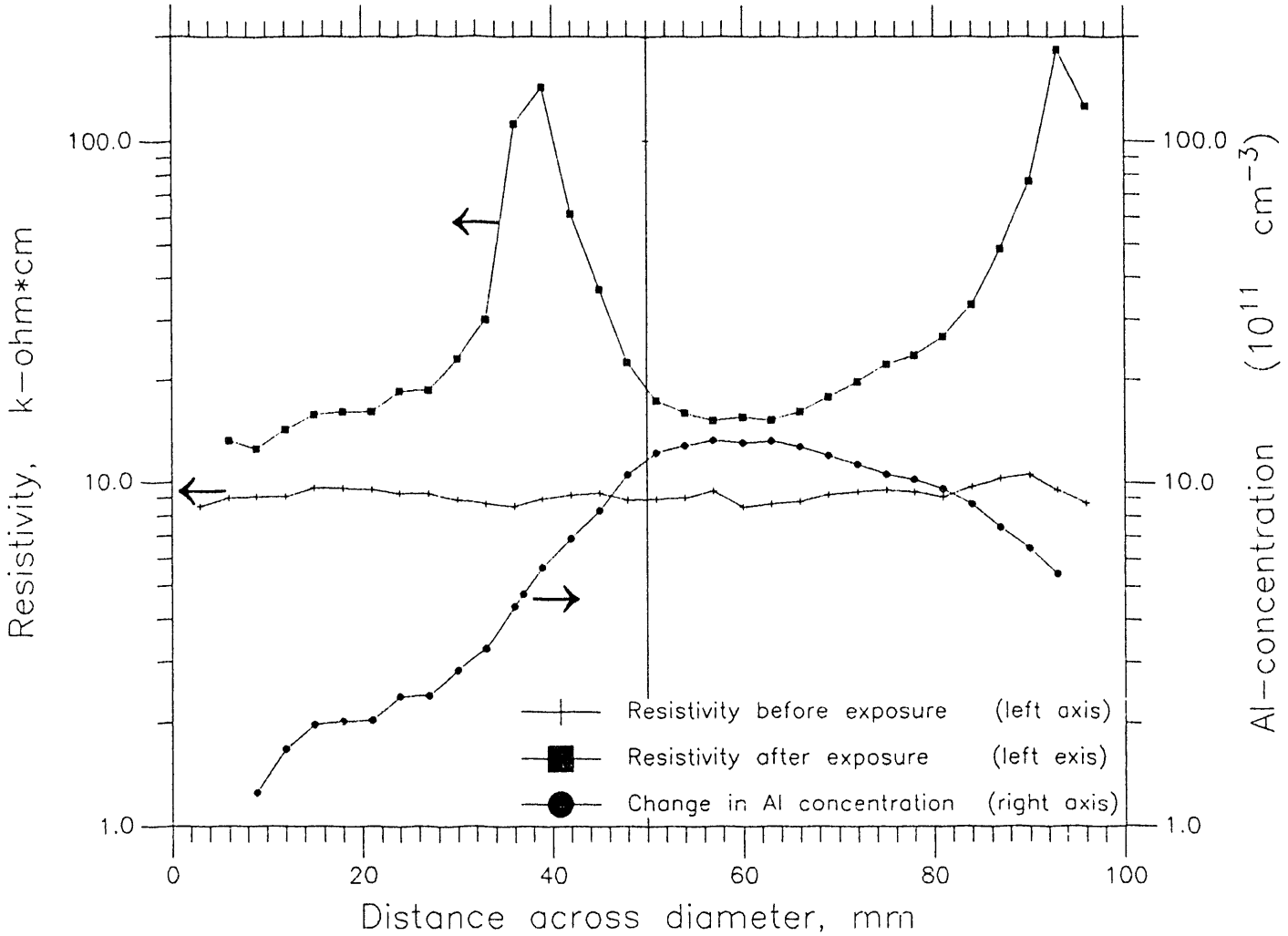

Silicon Sample on Fixed Position

Figure 6

TASK A

Publication List

1. "First Measurement of the Left-Right Cross Section Asymmetry in Z Boson Production by e^+e^- Collisions," (K. Abe, *et al.*, SLD Collaboration), Phys. Rev. Lett. 70, 2515 (1993).

2. "A Measurement of α_s from Jet Rates at the Z^0 Resonance," (K. Abe, *et al.*, SLD Collaboration), Phys. Rev. Lett. 71, 2528 (1993).

3. "First Measurement of the Left-Right Asymmetry in Z-Boson Production," (K. Abe, *et al.*, SLD Collaboration), Mod. Phys. Lett. A8, 2237 (1993).

4. "A Preliminary Measurement of $R_b = \frac{\Gamma(Z^0 \to b\bar{b})}{\Gamma(Z^0 \to hadrons)}$ at SLD," (D. Su, *et al.*, SLD Collaboration), Particles and Fields 92, Batavia, Illinois, November 1992.

5. "Measurements of Spin-Sensitive Quantities in Hadronic Decays of Z^0 Bosons Produced in e^+e^- Annihilations," (P. N. Burrows, *et al.*, SLD Collaboration), 10th International Symposium on High Energy Spin Physics, Nogoya, Japan, November 1992.

6. "Studies of QCD B-Physics and Jet Handedness at SLD," (P. N. Burrows, *et al.*, SLD Collaboration), XXVIII Rencontre de Moriond: QCD and High Energy Hadronic Interactions, Les Arcs, France, March 1993.

7. "SLD Results from the Study of Polarized Z^0 Produced at the SLC," (M. Piccolo, *et al.*, SLD Collaboration), Les Rencontres de Physique de la Vallée d'Aoste: Results and Perspectives in Particle Physics, La Thuile, March 1993.

8. "Tohoku 1.4m Holographic Bubble Chamber," (T. Kitagaki, E. L. Hart, and E-745,782 Collaboration), Conference on the Bubble Chamber and Its Contributions to Particle Physics, CERN, Geneva, Switzerland, July 1993.

9. "Studies of Hadronic Event Structure and Comparisons with QCD Models at the Z^0 Resonance," (B. Adeva, *et al.*, L3 Collaboration), Z. Phys. C55, 39 (1992).

10. "Determination of α_s from Hadronic Event Shapes Measured on the Z^0 Resonance," (O. Adriani, *et al.*, L3 Collaboration), Phys. Lett. B284, 471 (1992).

11. "Measurement of Inclusive η Production in Hadronic Decays of the Z^0," (O. Adriani, *et al.*, L3 Collaboration), Phys. Lett B286, 403 (1992).

12. "An Improved Measurement of B^0-$\bar{B}^0$ mixing in Z^0 Decays," (O. Adriani, *et al.*, L3 Collaboration), Phys. Lett. B288, 395 (1992).

13. "A Test of Quantum Electrodynamics in the Reaction $e^+e^- \rightarrow \gamma\gamma(\gamma)$," (O. Adriani, *et al.*, L3 Collaboration), Phys. Lett. B288, 404 (1992).

14. "Inclusive J Production in Z^0 Decays," (O. Adriani, *et al.*, L3 Collaboration), Phys. Lett. B288, 412 (1992).

15. "Measurement of the $e^+e^- \rightarrow b\bar{b}$ and $e^+e^- \rightarrow c\bar{c}$ Forward-Backward Asymmetries at the Z^0 Resonance," (O. Adriani, *et al.*, L3 Collaboration), Phys. Lett. B292, 454 (1992).

16. "Determination of the Number of Light Neutrino Species," (O. Adriani, *et al.*, L3 Collaboration), Phys. Lett. B292, 463 (1992).

17. "Isolated Hard Photon Emission in Hadronic Z^0 Decays," (O. Adriani, *et al.*, L3 Collaboration), Phys. Lett. B292, 472 (1992).

18. "Searches for Non-minimal Higgs Bosons in Z^0 Decays," (O. Adriani, *et al.*, L3 Collaboration), Phys. Lett. B294, 457 (1992).

19. "A Measurement of τ Polarization in Z^0 Decays," (O. Adriani, *et al.*, L3 Collaboration), Phys. Lett. B294, 466 (1992).

20. "High Mass Photon Pairs in $\ell^+\ell^-\gamma\gamma$ Events at LEP," (O. Adriani, *et al.*, L3 Collaboration), Phys. Lett. B295, 337 (1992).

21. "Search for Isosinglet Neutral Heavy Leptons in Z^0 Decays," (O. Adriani, *et al.*, L3 Collaboration), Phys. Lett. B295, 371 (1992).

22. "Search for Anomalous Production of Single-Photon Events in e^+e^- Annihilations at the Z Resonance," (O. Adriani, *et al.*, L3 Collaboration), Phys. Lett. B297, 469 (1992).

23. "Radiation and Solvent Effects on Wavelength Shifting Fibers Used with Liquid Scintillators," (K. G. Young, *et al.*), Radiat. Phys. Chem. 41, 215 (1993).

24. "Determination of Quark Electroweak Couplings from Direct Photon Production in Hadronic Z Decays," (O. Adriani, *et al.*, L3 Collaboration), Phys. Lett. B301, 136 (1993).

25. "Search for Non-minimal Higgs Bosons in Z^0 Decays," (O. Adriani, *et al.*, L3 Collaboration), Z. Phys. C57, 355 (1993).

26. "A Search for the Neutral Higgs Boson at LEP," (O. Adriani, *et al.*, L3 Collaboration), Phys. Lett. B303, 391 (1993).

27. "Search for a Z′ at the Z Resonance," (O. Adriani, *et al.*, L3 Collaboration), Phys. Lett. B306, 187 (1993).

28. "Measurement of $\Gamma_{b\bar{b}}/\Gamma_{had}$ from Hadronic Decays of the Z," (O. Adriani, *et al.*, L3 Collaboration), Phys. Lett. B307, 237 (1993).

29. "Determination of the Effective Electroweak Mixing Angle from Z Decays," (O. Adriani, *et al.*, L3 Collaboration), Phys. Lett. B309, 451 (1993).

30. "Further Results from Charge-Exchange Photoproduction," (G. T. Condo, *et al.*), Phys. Rev. D48, 3045 (1993).

31. "Precise Measurement of the $D_s^{\pm}$ Meson Lifetime," (P. L. Frabetti, *et al.*, E687 Collaboration), Phys. Rev. Lett. 71, 827 (1993).

32. "Inelastic ρ° Photoproduction in the Reaction $\gamma p \to \rho^\circ \pi^+ n$," (G. T. Condo, *et al.*), submitted to Phys. Rev. D, July 1, 1993.

33. "A Measurement of $\Gamma(D_s^+ \to \phi\mu^+\nu)/\Gamma D_s^+ \to \phi\pi^+)$," (P. L. Frabetti, *et al.*, E687 Collaboration), Phys. Lett. B313, 253 (1993).

34. "Studies of $D\bar{D}$ Correlations in High Energy Photoproduction," (P. L. Frabetti, *et al.*, E687 Collaboration), Phys. Lett. B308, 193 (1993).

35. "Analysis of the Decay Mode $D^+ \to \bar{K}^{*0}\mu^0\nu$," (P. L. Frabetti, *et al.*, E687 Collaboration), Phys. Lett. B307, 262 (1993).

36. "First Evidence of $\Omega_c^0 \to \Omega^- \pi^+$," (P. L. Frabetti, *et al.*, E687 Collaboration), Phys. Lett. B300, 190 (1993).

37. "Evidence of the Cabibbo-Suppressed Decay $\Lambda_c^+ \to pK^-K^+$," (P. L. Frabetti, *et al.*, E687 Collaboration), FERMILAB-Pub-93/183-E, July 1993; to be published in Phys. Lett. B, 1993.

38. "Measurement of the Lifetime of the Ξ_c^0," (P. L. Frabetti, *et al.*, E687 Collaboration), Phys. Rev. Lett. 70, 2058 (1993).

39. "Measurement of the Λ_c^+ Lifetime," (P. L. Frabetti, *et al.*, E687 Collaboration), Phys. Rev. Lett. 70, 1755 (1993).

40. "Measurement of the Mass and Lifetime of the Ξ_c^+," (P. L. Frabetti, *et al.*, E687 Collaboration), Phys. Rev. Lett. 70, 1381 (1993).

41. "Charged Particle Track Reconstruction Using Artificial Neural Networks," (Charles Glover, *et al.*), Proceedings of the International Conference on Computing in High Energy Physics '92, Annecy, France, September 21-25, 1992, CERN 9207, p.639.

42. "Feasibility of Using Neural Networks as a Level 2 Calorimeter Trigger for Jet Tagging," (Thomas Handler, *et al.*), Proceedings of the International Conference on Computing in High Energy Physics '92, Annecy, France, September 21-25, 1992, CERN 9207, p.650.

43. "Estimates of the Neutron Fluence for the SDC Detector," (P. K. Job, *et al.*), SDC-92-354, November 20, 1992.

44. "Semileptonic Charmed Meson Decays," (G. Bellini, *et al.*, E687 Collaboration), Proceedings of the XXVI International Conference on High Energy Physics, Dallas, Texas, August 6-12, 1992.

45. "Simulation of the Reconfigurable-Stack Test Calorimeter Experiments with CALOR89," (P. K. Job, *et al.*), submitted to Nucl. Instr. and Meth. (1993).

"Research in Theoretical High Energy Physics"

PROGRESS REPORT TO DEPARTMENT OF ENERGY

DOE DE-FG05-91ER40627

TASK B

Bennie F. L. Ward

Progress Report

TASK B

B. F. L. Ward

The research in Task B during 1992-1993 focussed on the further development and application of our new YFS (Yennie-Frautschi-Suura) Monte Carlo approach[1] to $SU_2 \times U_1$ radiative corrections in the Z° physics scenarios at the SLC and LEP. In addition, more progress was made on the application of perturbative QCD methods to heavy quark decay physics in the context of B-Factory high energy e^+e^- collider physics. There was some progress on manifestly gauge invariant covariant (closed) string field theory.

Specifically, during 1990-1991, we completed the implementation of our YFS[1] Monte Carlo procedure to the processes $e^+e^- \rightarrow f\bar{f} + n\gamma$, $f = \mu, \tau$, neutrino, quark, to the level of .1% accuracy. Thus, the LEP and SLC collaborations all have implemented the respective YFS2 Fortran program which allows them to simulate ,in the presence of detector cuts, the effects of multiple photon radiation on an event-by-event basis; the respective multiple photon 4-vectors are included in the list of final particle 4-vectors with no restriction on their number for the first time ever in $SU_2 \times U_1$ radiative correction simulations. Additionally, we succeeded in integrating this YFS2 calculation

into the pure electroweak corrections program KORALZ in version KORALZ3 [2], so that for the first time one may study the interplay of pure electroweak effects on the one hand with multiple photon effects on the other hand,on an event-by-event basis. This program KORALZ3 is now in use by all LEP and SLC collaborations (for SLC, this is the SLD Collaboration) and has been useful in the respective $f\bar{f} + n(\gamma)$ final states physics analyses, $f \neq e$. It has been demonstrated that the various pure weak libraries in KORALZ3 (one by W. Hollik, one by D. Bardine et al. and one unsupported library by R. Stuart) agree within .3% on the absolute normalization of the cross section near the Z° resonance in e^+e^- annihilation so that, for the present at SLC and LEP, we have an adequate knowledge of the respective pure weak effects. We must improve on this agreement in the not-too-distant future, in view of the current Z° production rate at LEP and the expected long term rate at the SLC.

Indeed, we are in the process of making an independent check of the pure weak libraries by Hollik, Stuart and Bardine et al. as they are implemented in KORALZ3. This we are doing in collaboration with Prof. Jadach in Krakow, Poland, with possible further collaboration from Prof. Zralek in Silesia, Poland. We have made substantial progress in our check and we hope to report more on this progress soon. Here, we may note that recently, using our results on the interplay of pure weak corrections and QED, we resolved the issue operationally of the gauge invariance of the renormalized Z° rest mass [3]. This shows that the mass measured at LEP/SLC for the Z° is in fact gauge invariant.

Recently, we have introduced [4] the new YFS Monte Carlo event generator YFS3, which treats for the first time $n(\gamma)$ final state multiphoton radiation in $e^+e^- \rightarrow f\bar{f}$

+ n(γ), with $\underline{f \neq e}$. We are currently implementing it into the SLC/LEP experimental activities and refining its precision tag as dictated by the LEP(/SLC) data. Such final state radiation data afford new roads for Standard Model tests.

Indeed, the L3 Collaboration recently observed[5] an accumulation of high γγ mass events in $e^-e^+ \rightarrow \ell\bar{\ell} + 2\gamma$ where the photons are at wide angles with respect to the charged particles near the γγ mass 60 GeV. Working with us, they used our YFS3 calculation to conclude that the probability that their observation was a fluctuation of the expectations from QED was ~.1%. The current situation[6] is that all LEP collaborations have collectively seen 15 such L3-type events and YFS3 predicts 9. The probability of a fluctuation is now a few % and more data are needed to clarify the situation. Our YFS3 calculation is thus an important part of this exciting analysis of a possible new phenomenon at LEP in Z° physics.

Concerning the basic luminosity process $e^+e^- \rightarrow e^+e^- + n\gamma$ at low angles, we recall that we had implemented, during 1989-1990, our BHLUMI Monte Carlo YFS program[7] at SLC and at LEP, so that indeed the higher order corrections to the luminosity were known to 1%. This result already played a significant role in controlling the systematic error on the measurement of the luminosity at SLC and LEP and, hence, it made a significant contribution to the 1989 MkII discovery that the number of massless neutrino generations is 3 (this MkII finding was immediately corroborated by ALEPH on using our BHLUMI program to calculate the higher order corrections to their luminosity). Thus, we feel that our YFS methods were brought to the level of implementation which was sufficient for the 1989-early 1990 scenario in bhabha scattering at low angles. However, for the current and long term SLC-LEP

objectives, we needed to carry this level of accuracy on the bhabha luminosity process to the .2% and below .1% regimes, respectively.

Accordingly, Prof. Jadach and the PI, working with Drs. Z. and E. Was, have established [8] an $0(\alpha)$ baseline description of the luminosity cross section so that it is understood in absolute normalization from both an analytic and Monte Carlo standpoint at the .1% level. This, we expected, would then allow us to check our Monte Carlo methods for BHLUMI for their absolute normalization to the .2% level by 11/1/90 and to below .1% ultimately with the corresponding improvement in the baseline description to the below .1% regime; we explained this in detail in our 1991-1992 renewal proposal.

And, indeed, during 1990-1991, we developed[9] two independent $0(\alpha^2)$ LL YFS exponentiated Monte Carlo's for the higher order corrections to the SLC/LEP luminosity so that, in a CERN Theory Division Seminar by Jadach in 12/90, we already presented a procedure[9] for correcting $O(\alpha)$ Monte Carlo luminosity simulations for higher order effects which was accurate to .2% on the pure bremmstrahlung and to .3% for the total luminosity. In addition, we developed, for the first time, analytic improved naive exponentiated formulae[10] for the luminosity process accurate to a technical precision of .02% so that we could check the normalization of BHLUMI 1.13 to .15%. Finally, to obviate the need of using two different MC simulations in the complicated software management environment of a LEP/SLC collaboration, we developed[9] BHLUMI 2.00 as a single, YFS MC solution to the luminosity problem at SLC/LEP with a total precision of .25%, including an allowance for pairs, vacuum polarization uncertainty, etc. For reference, the 1992 best experimental error from LEP on the luminosity measurement was ALEPH's .5%. Thus, we were providing, during 1992, a sufficiently

accurate simulation; we emphasized in our 1992 Progress Report that we would to improve this in the near future, when ALEPH installs and calibrates its new luminosity monitor. (This improvement is in progress.)

In fact, BHLUMI 2.01, recently published in Ref. 10, is now in use at LEP [11] for the analyses of the 1991-1992 LEP data (BHLUMI has always been used at MkII and SLD for data analysis). This means that during 1991-1992, we have succeeded with the implementation and acceptance of BHLUMI 2.01 as the basic luminosity data analysis radiative corrections simulator at LEP as a replacement of the Berends-Kleiss-Hollik generator BABAMC [12], which had been the standard data analysis luminosity generator at LEP since 1989-(BHLUMI was previously only used for the higher-order corrections to BABAMC at LEP, as we have explained; now, it is the program which generates the events which are passed through the long LEP detector simulations. This has greatly improved the understanding of these detectors' responses so that it has facilitated the precision tag of ~.5% which ALEPH reached with its original luminosity monitor. Thus, this represents a major achievement for the DOE's investment in Task B.) Recently,[13] using BHLUM2.01 and its new luminosity monitor, ALEPH has reached .32% precision on its luminosity. Thus, BHLUMI continues in 1993 to open the way to higher precision Z° physics.

What we should emphasize as one our most important successes is our work between SLAC and CERN during the period April, 1989 - September, 1989, as we described in detail in our renewal proposal for 1990-1991. During this period, we and our collaborators resolved discrepancies in KORALZ3 libraries and in the luminosity calculations so that these calculations were in a usable state for the SLC and LEP turn-

on's (our higher order bhabha work made the $N_\nu = 3$ discovery possible). We continued this commuting approach between SLAC and CERN during 1990 and 1991 - in the former case, working directly with physicists in both places, we were able to formulate and develope the benchmark $O(\alpha)$ process simulation[9] for the crucial luminosity problem and in the latter case, we were able to arrive at the desired .25% accuracy for our BHLUMI (YFS) calculation using this benchmark. In addition, our interactions with Drs. Locci (ALEPH) and Komamiya (OPAL) allowed us to start the implementation of our wide-angle YFS bhabha MC event generator BHLUMI 3.0, which we had made available to the SLD Collaboration at SLAC (it has already been used in analyzing the initial SLD engineering data (1991) and is now being used, in a new polarization version 3.01, on the 10^4 20% beam polarization Z° data sample (1992) and on the recent 5×10^4 60% beam polarization Z° data sample (1993)). During 1991-1992, we continued our commuting approach between SLAC and CERN and thereby made the important acceptance and implementation of BHLUMI 2.01 at LEP possible. Further, we made BHLUMI 3.0 available to OPAL and continued to interact with that Collaboration in its implementation and use at LEP. Similarly, during 1992-1993, our SLAC-CERN commuting arrangement allowed us to assist L3 with the use of YFS3, to prepare for our .05% version of BHLUMI and to interface properly BHLUMI3.01 to SLD/LEP, and to participate effectively in the SLAC B-Factory activities. These achievements at CERN were only possible because I was able to work directly with the members of the CERN EWMC Working Groups, and my collaborators Drs. Jadach, Richter-Was, and Was, as we explain in our proposal for 1990-1991 and as we review in our 1991-1992, 1992-1993, 1993-1994 and 1994-1995 proposals.

We have recently[14] made progress in understanding the possible meaning of the value $N_\nu = 3$, where N_ν is the number of massless neutrino generations. We interpret this as evidence for an $SU(3)^f$ family symmetry which breaks at a scale ~ 100 TeV. The attendant association of the C-K-M matrix with $SU(3)^f$ mixing interactions then gives the prediction for m_t in terms of $\alpha \equiv V_{cb}/V_{ub}$ and the light quark masses m_q, q = u,d,s,c,b (the respective formula is given in Ref. [14] and in our 1992-1993 renewal proposal). The recent CLEO-ARGUS results for α then allow us to conclude with 95% confidence that

$$67.8 \text{ GeV} \lesssim m_t \lesssim 127.9 \text{ GeV}.$$

This result is extremely interesting from the standpoint of the CDF Standard Model limit $m_t > 113$ GeV. Perhaps, top will be discovered soon!

We should note that with Dr. Zhang, our former post-doc, and with our collaborators in Cracow, Poland, Prof. Jadach's Group, we have succeeded[15] in obtaining an analytic result for the important Z° physics total differential distribution in $e^+e^- \to \bar{\mu}\,\mu + 2\gamma$. This result and its generalizations have been used to carry our YFS2 FORTRAN simulations beyond the .1% precision regime in Z° physics. We began a similar analysis for the process $e^+e^- \to e^+e^- + 2\gamma$ with our former post-doc, Dr. S. Lomatch. We had a preliminary[16] formula for the real bremsstrahlung process $e^+e^- \to e^+e^- + 2\gamma$ at SLC/LEP energies and, with Dr. S. Yost, we our replacement for Dr. Lomatch, we have recently completed[17] the calculation of 2γ emission part of $\overline{\beta}_2$ for the bhabha process and moved the theoretical uncertainty on the bremsstrahlung process in BHLUMI to the below .1% regime as desired. Working with Prof. Jadach, Dr. Yost and I have recently[18] checked to

normalization of YFS3 in the L3 high mass $\gamma\gamma$-event acceptance region to be better than 20%, as needed.

Continuing with our effort to reach the below .1% regime of precision for BHLUMI 2.01, we recently finished with our post-doc M. Skrzypek the calculation[19] of new formulae for the pairs production effect in the Bhabha scattering luminosity process at SLC/LEP. We are currently in the process of implementing this calculation in BHLUMI[20] so that the soft pairs four-vectors will be available to the experimentalists in the final particle list. This soft pairs effect represents an important step on the way to below .1% precision luminosity simulations.

With the advent of ~60% beam polarization at SLD and an attendant Z° physics sample of 5 x 10^4 produced therewith, Prof. Jadach and I recently looked[21] into the role of A_{LR} in high precision Z° physics to see what effect SLD could have in that physics. We find that A_{LR} does provide a view on the $O(\alpha)$ electroweak corrections, as given in our KORALZ3.8 program from Hollik and from Bardine et al. as described above, which yields new information beyond what is available at LEP. Thus, we encourage the SLD to collect as many high polarized beam Z°'s as possible and we hope the DOE will support both the SLD and us as we help them analyze these Z°s.

In the area of QCD methods in heavy quark decay physics, we recently[22] analyzed the decay $B \rightarrow \psi/JK_+^*$ from the standpoint of the luminosity requirement for CP violation studies at a SLAC-LBL-LNL-type B-Factory. We find that, in three relativistically invariant models, the CP even decay final state is dominant so that, indeed, this decay can be used for CP violation studies at a SLAC-LBL-LNL-type B-Factory. The attendant reduction in luminosity required is ~ 2.5. In fact, our result for

the Lepage-Brodsky theory prediction for this decay is in agreement in detail with recent measurements by ARGUS[23].

And, recently, following further preliminary work by ARGUS[24], we analyzed[25] the decays $B \to \chi_c K_s$ as possible further new modes for CP violation exploration at the SLAC-LBL-LLNL Asymmetric B-Factory device. We find agreement with the ARGUS results $B(B \to \chi_c X) = (1.05 \pm .35 \pm .25)\%$ and $B(B \to \chi_c K^+) = (.19 \pm .13 \pm .06)\%$ and that the ratio of CP odd to CP even final states is ~.38, so that, indeed, such modes as $B \to \chi_c K_s$ can be used to further reduce the required luminosity in the SLAC B-Factory project. (Just how much it is reduced requires more analysis.)

Continuing our study of new modes for exploration of CP violation in a B-Factory of the SLAC-LBL-LNL asymmetric variety, we have recently developed[26] a benchmark analysis of the decays $D \to \pi\pi$, KK for testing how well one might hope to predict a mode like $B \to \pi\pi$, where isospin considerations have recently been advanced for removing the unwanted penguin-type contributions in the measurement of the unitarity triangle angle α. What we find is that our methods, based on Lepage-Brodsky theory, allow us to predict $\Gamma(D \to K^+K^-)/\Gamma(D \to \pi^+\pi^-) \simeq 2.00$, $\Gamma(D \to K^+K^-) \simeq .561\%$, $\Gamma(D \to \pi^+\pi^-) \simeq .280\%$, to be compared with the ARGUS-CLEO results $2.42 \pm .42$, $.46 \pm .06\%$, $.210 \pm .031\%$ respectively. Hence, it seems that 25% knowledge of $B \to \pi\pi$ rates and ratios of rates might be possible with our methods and we are currently effecting this.

Indeed, with our success in the development of the relevant quantitative methods in $D \to \pi\pi$, K K, we turned recently to the analysis of the interplay between penguins and the CKM CP violating phase with an eye toward measuring the unitarity triangle

angle α in $B \rightarrow \pi\pi$ in the proposed SLAC-LBL-LNL Asymmetric B-Factory device. Our results[27] show that $B \rightarrow \pi^+\pi^-$ is resilient to penguins and that α is generally measurable at the ~25% level in this mode; we find that $B \rightarrow \pi^\circ\pi^\circ$ is strongly affected by penguins and only Gronau-London type penguin trapping methods could make it useful most probably in a study of α. Our rates for $B \rightarrow \pi^+\pi^-$ and $B \rightarrow \pi^\circ\pi^\circ$ depend on the allowed variation of the CKM parameters as reported by the 1992 PDG Data Listings for example but are consistent with recent CLEO limits (See P. Drell, in 1992 Rochester Conf., Proc., ed. J. Sanford (AIP, N.Y., 1993), for example) and with a recent penguin-less analysis by A. Sczepaniak et al. (Phys. Lett. B243, 287 (1990)).

Finally, during 1992-1993, we had a small amount of time to devote to our quantum gravitation research. The recent result[28] is a solution for the ground state of string theory in the open string case. We used the methods of the operator field to show that the tachyon is really absent in the true spectrum of the theory. After discussion with Prof. M. E. Peskin of SLAC, we have extended[29] the first paper in Refs. 28 to address several questions which are not discussed therein. We may now hope to incorporate this result into our earlier results[28] for the manifestly gauge invariant closed string field theory to arrive at a sound physical framework from which to study the true spectrum of the heterotic string theory of Gross et. al. eventually. We must emphasize that, while we made a small amount progress toward this end, our pre-occupation with SLC-LEP physics research will not allow us to devote very much time to string theory, however. And, this is as it should be.

Finally, it is appropriate to report that, on March 20, 1991, we were awarded Texas National Research Laboratory Commission grant number RCFY9101 for applying our

YFS methods developed in TASK B to higher order radiative corrections to SSC physics processes. On January 15, 1992, this award was renewed for a second year; in February, 1993, it was extended for a third year. These awards were major achievements for the research in TASK B and we feel that this successful application of the work developed in Task B shows that the DOE's investment therein was and is well-placed. (For reference, we list recent preprints from our SSC physics activity in [30].) We hope it encourages the DOE to continue to expand its support for Task B so that even larger applications will be possible, such as the support of Dr. G. Siopsis' OJI proposal, for example.

References

1. S. Jadach and B. F. L. Ward, Phys. Rev. D38, 2897 (1988); ibid. 39, 1472 (1989); Phys. Lett. B220, 611 (1989); Comp. Phys. Commun. 56, 351 (1990).
2. See D. Bardine et al., report of the LEP100 Monte Carlo Working Group, in LEP100 Yellow Book, ed. G. Altarelli (CERN, Geneva, 1989); CERN-TH-5994/91, Computer Phys. Commun., 1991, in press.
3. B. F. L. Ward, IC/91/161; Nucl. Phys. B (Proc. Suppl.) 29A, 253 (1992), Phys. Lett. B296, 209 (1992).
4. S. Jadach and B. F. L. Ward, Phys. Lett. B274, 470 (1992).
5. O. Adriani et al., Phys. Lett. B295, 337 (1992).
6. G. Coignet, in Proc. 1993 Lepton-Photon Symposium, 1993, in press.
7. S. Jadach and B. F. L. Ward, Phys. Rev. D40, 3582 (1989).

8. B. F. L. Ward, talk to CERN Th. Division, 8/17/90; S. Jadach et al., Phys. Lett. B253, 469 (1991).

9. S. Jadach et al., Phys. Lett. B260, 438 (1991); Phys. Lett. B268, 253 (1991); Phys. Rev. D44, 2669 (1991).

10. S. Jadach et al., Comp. Phys. Commun. 70, 305 (1992).

11. See H. Meinhard, Proc. 1992 Rochester Conf., ed. J. R. Sanford (AIP, New York, (1993) p. 687.

12. F. A. Berends, R. Kleiss, and W. Hollik, Nucl. Phys. B304, 712 (1988).

13. J. Rander, talk presented at CERN, May, 1993.

14. B. F. L. Ward, UTHEP-89-1202; IL Nuovo Cimento 105A, 1313 (1992).

15. S. Jadach et al., Phys. Rev. D42, 2977 (1990).

16. S. Lomatch et al., unpublished.

17. S. Jadach, B. F. L. Ward and S. Yost, UTHEP-92-0601; Phys. Rev. D47, 2682 (1993).

18. S. Jadach, B. F. L. Ward and S. Yost, to appear.

19. S. Jadach, M. Skrzypek and B. F. L. Ward, UTHEP-92-0701; Phys. Rev. D47, 3733 (1993); UTHEP-93-0301.

20. S. Jadach, M. Skrzypek and B. F. L. Ward, to appear.

21. S. Jadach and B. F. L. Ward, UTHEP-93-0101, 1993.

22. B. F. L. Ward, invited talk at the SLAC B-Factory Workshop, June, 1990; ICTP preprint 1990 IC/90/271, Proc. SLAC B-Factory Workshop, ed. D. Hitlin (SLAC, Stanford, CA, 1991), p. 123; Phys. Rev. D45, 1544 (1992); UTHEP-91-0102.

23. H. Schroder, 1990 Rochester Conf., Proceedings, (S. E. Asia Th. Phys. Assoc. et al., Singapore, 1991).

24. H. Albrecht et al., DESY-91-077, July, 1991.

25. B. F. L. Ward, in Proc. 1992 SLAC B-Fact. Workshop, in press; UTHEP-92-0502; Phys. Rev. D47, 2832 (1993).

26. B. F. L. Ward, talk presented at the 1991 SLAC B-Factory Workshop, June, 1991; UTHEP-91-0901; UTHEP-92-0702; Phys. Rev. Lett. 70, 2533 (1993).

27. B. F. L. Ward, UTHEP-93-0201; UTHEP-93-0902, in press in Proc. 1993 Heavy Flavors Symposium, ed. D. MacFarland, to appear.

28. B. F. L.Ward, UTHEP-90-0101; UTHEP-89-0101; IL Nuovo Cimento 105A, 603 (1992); ibid. 106A, 309 (1993).

29. B. F. L. Ward, UTHEP-91-0601.

30. D. DeLaney, S. Jadach, Ch. Shio, G. Siopsis and B. F. L. Ward, "Multiple Photon Effects in p p Scattering at SSC Energies," UTHEP-92-0501; Phys. Lett. B292, 413(1992); ibid. B302, 540 (1993); "Multiple Photon Effects in Fermion-(Anti-) Fermion Scattering at SSC Energies," UTHEP-92-0101; Phys. Rev. D47, 853 (1993); "Renormalization Group Improved Exponentiation of Soft Gluons in QCD," UTHEP-93-0401.

reprints + preprints removed; conf papers cycled separately. ds

DATE FILMED

2/10/94

END